Plant traits and carbon storage in freshwater wetlands

By

Saras M. Windecker
ORCID: 0000-0002-4870-8353

Submitted in total fulfilment
of the requirements of the degree of
Doctor of Philosophy

September 2019

School of BioSciences
Faculty of Science
The University of Melbourne

© Saras M. Windecker, 2019.

Abstract

Freshwater wetlands are an important part of the global carbon cycle due to their role in sequestering carbon in the soil. Despite covering less than 8% of global land area, freshwater wetlands are significant reservoirs of soil carbon due to long-term storage in the soil. Soil carbon stocks are high because wetlands are highly productive and can have low rates of decomposition. Plant communities capture carbon during photosynthesis and deposit it as litter. My thesis broadly examines the influence of vegetation communities on soil carbon storage across a range of scales, from the landscape down to the leaf.

To examine the relative contribution of vegetation to carbon stock on a landscape-wide scale, I modelled carbon density of soil cores collected in 100 inland wetlands across Victoria, Australia. I determined that the nonlinear relationship of carbon with soil depth varies between wetlands, which has important implications for extrapolating carbon density necessary in wide-scale comparisons. Using a hierarchical model with continuous spatial data, I found that we could predict soil carbon stock using these globally available datasets and that intermediate inundation was a strong predictor for high soil carbon stock.

At the wetland level, plants take up carbon dioxide during photosynthesis and contribute to soil carbon through deposition of litter. Litter quality, such as nitrogen level, affects how much litter material remains in the soil and for how long. Leaf economics spectrum theory suggests that a range of functional traits correlate along a spectrum of nutrient level that can be used to generalise litter quality. Despite relevance to a range of ecosystem processes including decomposition, direct measures of carbon composition of litter are not included among the economics spectrum traits. To test the generality of the trait correlations to carbon composition, I measured seven traits of litter in 29 wetland plant species: litter area per mass, dry matter content, nitrogen content, carbon content, and relative composition of hemicellulose, cellulose, and lignin. I tested thermogravimetric analysis, an analytic technique for estimating these carbon components. To replace proprietary software currently used in the modelling step of this estimation technique, I developed an open-source statistical R package called 'mixchar'. In general, species invested predominantly in either lignin- or cellulose-based tissue, and variation in this division was not correlated with variation in the other morphologic and chemical traits.

Decomposition of litter impact long-term storage of carbon in the soil and is driven by litter quality. I conducted a mesocosm decomposition experiment of 29 wetland plant species, and evaluated the predictive performance of functional traits related

to both nitrogen level and carbon complexity. I prepared a series of Bayesian decay models to test which traits affected rate of overall decay. I evaluated the models by comparing the cross-validative predictive performance on a new species. I found that trait models that include both litter nitrogen and carbon characteristics ranked among the best at predicting decomposition. However, differences among trait models were marginal, suggesting perhaps no single 'best' model for litter decomposition rate based on traits alone. My research improves our understanding of how plants contribute to soil carbon, from the scale of a leaf to the wider landscape, and clarifies how plants decay in wetlands and contribute to carbon storage in wetland soils.

Declaration

This is to certify that:

(i) the thesis comprises only my original work towards the PhD except where indicated in the Preface,

(ii) due acknowledgement has been made in the text to all other material used,

(iii) the thesis is fewer than 100 000 words in length, exclusive of tables, maps, bibliographies and appendices.

Saras M. Windecker
September, 2019

Preface

This thesis has been supported through various collaborations within the Quantitative and Applied Ecology Group (School of BioSciences, University of Melbourne), the Blue Carbon Lab (Centre for Integrative Ecology, Deakin Ecology), and external collaborators, detailed below. To facilitate journal publications throughout and subsequent to my PhD candidature, Chapters 2–5 are written as independent studies and therefore include detailed introductions and discussions in their own right. This will produce some unavoidable repetition in the chapters. I have written these chapters using the collective first-person plural "we", consistent with academic publishing practice. Appended to this thesis is a published paper associated with Chapter 2 led by Paul Carnell and a book chapter led by Jane Catford. Chapter contributions to the thesis and collaborator input were:

Chapter 2

Windecker, S.M., Carnell, P.E., McColl-Gausden, E., Vesk, P.A., Catford, J.A., Macreadie, P.I. (in prep) Drivers of soil carbon storage in freshwater wetlands of south eastern Australia.

Contributions: SW, PC, & PM conceived the ideas and designed methodology; SW and PC collected the data; SW & EMG analysed the data; SW led the writing of the manuscript. All authors contributed critically to the drafts.

Chapter 3

Windecker, S.M., Trevathan-Tackett, S.M., Golding, N., Catford, J.A., Macreadie, P.I., Vesk, P.A. (in prep) Decoupling plant economics traits and biomass carbon composition in wetland litter.

Contributions: SW, PV, JC, PM, and STT conceived the ideas and designed methodology; SW collected the data; SW, PV, and NG analysed the data; SW led the writing of the manuscript. All authors contributed critically to the drafts.

Chapter 4

Windecker, S.M., Vesk, P.A., Trevathan-Tackett, S.M., Golding, N. (in review) mixchar: An R package for the deconvolution of thermal decay curves.

Contributions: SW, PV, and STT conceived the ideas and methodology; SW and NG created the package; SW led writing of the manuscript. All authors contributed

critically to the drafts.

Chapter 5

Windecker, S.M., Golding, N., Catford, J.A., Sanchez, P., Camac, J.S., Vesk, P.A. (in prep) Understanding variation in litter decomposition in a multispecies mesocosm.

Contributions: SW, PV, and JAC conceived the ideas and designed methodology; SW and PS collected the data; SW, PV, NG, and JSC analysed the data; SM led the writing of the manuscript. All authors contributed critically to the drafts.

Support

My PhD candidature was generously supported by a University of Melbourne International Research Scholarship, a Melbourne International Fee Remission Scholarship, the Australian Research Council Centre of Excellence for Environmental Decisions, and the Holsworth Wildlife Reseach Endowment & The Ecological Society of Australia.

The entirety of this thesis can be reproduced with the data and R code available on Github https://github.com/smwindecker/thesis/. In order to aid in the reproducibility of this work, I wrote the code in a *remake* framework (FitzJohn, 2015). This allows others to reproduce the data preparation, analysis, visualisation steps, in addition to the final pdf document by calling `remake::make()` in R.

Publications

(i) Carnell PE, **Windecker SM**, Brenker M, Baldock J, Maque P, Brunt K, & Macreadie PI. 2018. Carbon stocks, sequestration, and emission of wetlands in south eastern Australia. Global Change Biol. 2018;00:1–12.

(ii) Catford JA, Roberts J, Capon SJ, Froend RH, **Windecker SM**, & Douglas MM. 2017. Wetland vegetation of inland Australia. *Australian Vegetation* (ed. D.A. Keith), 3rd edition. Cambridge University Press, p. 490-515.

Acknowledgements

I would like to begin by thanking my PhD supervisors, Peter Vesk, Jane Catford, and Peter Macreadie, as well as my committee chair Mick McCarthy, for their guidance, patience, and overall contribution to my development as an academic. PV, you went above and beyond as my primary supervisor in supporting me during some very difficult periods. I admire you immensely and aspire to support a student in the future in the same way you supported me.

A lot of life happens during a PhD. Besides my academic support, what stands out to me is the incredible community of personal support I received from my supervisors, my labs, and my friends and family.

To my wonderful mentors and friends at QAECO, I could not have done this without you. Casey, Esti, Hugh, and Michelle, you were the best room to join and I feel so lucky for your friendship and guidance those early days. Reid, Els, Tash, Simon, David, and Will, thank you for being my mentors and friends. Jian, Payal, Holly, and Carolyn, thank you for getting me through it at the end.

I was very lucky to be part of two fantastic labs during my candidature. Thank you to my colleagues and friends at the Blue Carbon Lab, especially Stacey, Paul, and Carolyn for inspiring me, teaching me, and doing way too much fieldwork with me...

I received invaluable mentorship during my PhD. Thank you Nick for believing in me, teaching me, and giving me so many learning opportunities. I attribute many of the skills I'm most proud of gaining during my PhD to your mentorship. Thank you Jimmy Camac, for teaching me, getting excited about nerdy code with me, and inspiring me in my research.

I would like to thank my fieldwork volunteers Abbey Kinnish, Kelsey Johnson, Francesca Dina, Madeline Brenker, and Urtzi Enriquez Urzelai, and especially Paula Sanchez who watched over my experiment when I had to leave the country during some ill-timed visa exile.

I received funding from a variety of sources that allowed me not only to conduct my fieldwork, lab analysis, and greenhouse experiment, but also to attend conferences, short courses, and lab visits. Thank you to the Australian Government, the Australian Research Council Centre of Excellence for Environental Decisions, the Lifeworks Foundation via the University of Melbourne Botany Foundation, the School of Biosciences, and the Holsworth Wildlife Research Endowment. Thank you to Alain Zuur and Elena Ieno for your Bayesian statistics course and Richard McElreath for Statistical Rethinking - I learned so much from you. Thank you to Hans Cornelissen for hosting me for two months at the VU.

Thank you to Gregoire Freschet, Daniel Falster, and Will Cornwell for illuminating discussions about traits and decomposition. To two anonymous reviewers who provided valuable feedback on this thesis. And to Nick Tierney, Miles McBain, and Mathew Ling for coding inspiration and companionship, and for the opportunities to grow with organisations such as ROpenSci and the Melbourne Open Research Network.

Thank you to my adoptive family here in Melbourne, Francisca Fuenzalida and Walter Bishop, for supporting me at home this last year, and these final days (and for some wicked graphic design), and to my family back home in the US for supporting me from afar.

Contents

List of Figures

List of Tables

1
General Introduction

1.1 Overview: soil carbon in wetlands

Wetlands are some of the most productive ecosystems on the planet. They provide valuable ecosystem services such as water filtration, flood mitigation, and carbon sequestration. Best estimates suggest that wetlands account for more than 30% of soil carbon storage (Bridgham et al., 2006), despite covering less than 5% of the earth's surface (Davidson, 2014; Mitsch & Gosselink, 2007). Wetland systems play an important role in soil carbon sequestration because they are highly productive ecosystems and experience low rates of decay. Tidal ecosystems accumulate more carbon per unit area than freshwater wetlands due to saline conditions that inhibit decomposition rates (Chmura et al., 2003; Ewers Lewis et al., 2018; Macreadie et al., 2017), but despite their slower rate of accumulation, freshwater wetlands are estimated to hold as much as ten times more carbon than tidal wetlands (Nahlik & Fennessy, 2016) due to their comparatively wider extent.

In this thesis I explore the role of plant communities in storing carbon in freshwater wetlands. Plants affect soil carbon primarily through their litter, by depositing organic carbon acquired in photosynthesis (De Deyn, Cornelissen & Bardgett, 2008). Long-term storage of litter-derived carbon in wetlands depends on the rate and extent to which it is decomposed (De Deyn, Cornelissen & Bardgett, 2008; Prentice et al., 2001). I examine the contribution of vegetation at a range of scales, from landscape-wide to leaf tissue.

In the following sections of this chapter I summarise our current understanding of how wetlands store carbon and the role of plant communities in general. I briefly review traits associated with litter quality that are used to generalise how plants contribute to carbon stored in soil. Following this, I explore approaches that researchers have used to estimate these traits and how they affect decomposition rates. I then present the aims and outline of my thesis.

1.2 How do wetlands store carbon?

Carbon storage rates in freshwater wetlands vary among and within wetlands (Pearse et al., 2018) due to high variation in biota and inundation conditions found across sites (Mitra, Wassmann & Vlek, 2005; Mcleod et al., 2011). Wet areas in the landscape are often highly productive, adding significant biomass to the system in the form of litter. In addition to high productivity of locally-derived ('autochthonous') carbon, externally-derived dissolved and particulate organic matter ('allochthonous' carbon) flows into the wetland from the surrounding water catchment area (Mitsch & Gosselink, 2007). Wetlands exist geomorphically in low parts of the landscape and therefore are hydrologically connected with their surroundings, receiving inflows of water from rainfall or riverbank flooding (Mitsch & Gosselink, 2007). This can lead to high levels of inundation which promotes conditions under which soil organic matter experience low rates of decay. Despite the importance of inundation regime and geomorphology, research suggests that these environmental predictors may act on carbon storage primarily through their effects on plant communities (Manning et al., 2015).

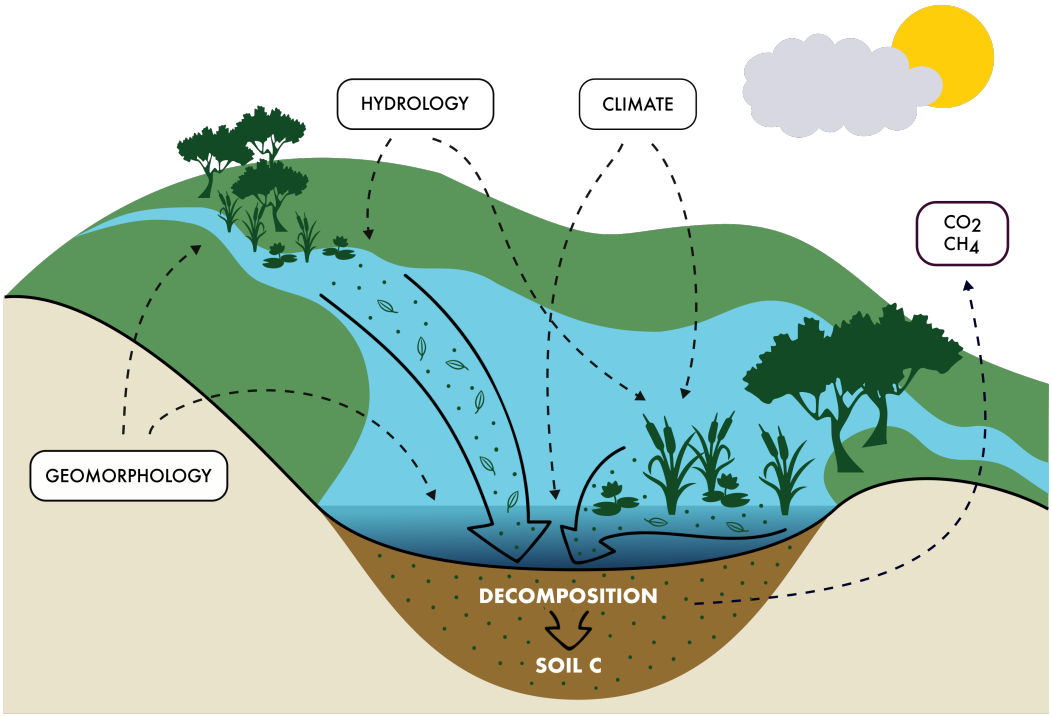

Figure 1.1: Conceptual model of the drivers of soil carbon storage in inland wetlands. Soil organic carbon density depends on relative rates of carbon import through deposition of primary production litter and carbon export via soil microbial and microfaunal respiration during decomposition. Primary production is typically high in wetlands, because water is availabile to stimulate plant growth. The degree to which a wetland is an effective sink for carbon depends on the size and condition of its catchment and the flow and consistency of its hydrologic connectivity. Inundated conditions can promote anoxic conditions ideal for limited litter decomposition. Plant communities are both indicators of these underlying hydrogeomorphic conditions and also direct drivers of soil carbon themselves, due to the amount and quality of their litter.

1.2.1 Variability among wetlands

Existing studies contradict one another with respect to how exactly hydrogeomorphology and vegetation interact to affect carbon storage. Depressional wetlands may store more carbon than river-fed wetlands, but this effect might be dependent on climate (Bernal & Mitsch, 2012, 2013). Hydrogeomorphology may not be relevant at all (Marín-Muñiz, Hernández & Moreno-Casasola, 2014), nor might inundation alone (Villa & Mitsch, 2015).

Some recent large-scale studies have begun to address these discrepancies, but each has still relied upon broad classifications of wetland type (Nahlik & Fennessy, 2016; Carnell et al., 2018). These classifications generally cluster wetlands imprecisely for purposes of studying carbon storage. The U.S. Army Corps of Engineers uses the Brinson classification system (Brinson, 1993), which separates wetlands by geomorphology, water supply, and water flow. This multifaceted approach contrasts with the Corrick

and Norman scheme common among research agencies in Victoria, Australia, which combines inundation and vegetation categories into classes such as 'deep freshwater marsh' and 'shallow herbland' (Corrick & Norman, 1980). Categorising carbon storage by these broad and inconsistent criteria might mask finer scale variability in the actual drivers of carbon storage. Well-supported models using globally available spatial data, such as conducted for coastal wetlands (Sanderman et al., 2018), is needed for freshwater wetlands.

1.3 What is the role of plant litter?

Studies in diverse systems have identified the correlation between local plant community and carbon stock (Orwin et al., 2010; Manning et al., 2015; Bernal & Mitsch, 2012; Fornara & Tilman, 2008, 2012). There are many potential explanations for the precise mechanism by which plants drive carbon storage. The physical structure of plants can slow flow and trap exogenous material (Kramer-Walter et al., 2016). Root traits are also important due to effects such as priming, in which labile soil organic matter speeds up decomposition of more recalcitrant carbon (Guenet et al., 2010). However, it is well-established that long-term storage of litter-derived carbon in wetlands depends in large part on the rate and extent to which it is decomposed (De Deyn, Cornelissen & Bardgett, 2008; Prentice et al., 2001). Decomposition in plant communities is regulated by complex interactions between oxygen availability, water levels, soil pH, ambient nutrient availability, and the composition of microbial and macroinvertebrate decomposer communities (Rejmánková & Houdková, 2006). However, site level studies and global syntheses point to the outsize importance of litter quality on mass loss rates across diverse biomes worldwide (Cornwell et al., 2008; Zhang et al., 2008; Liao et al., 2008; Valéry, Bouchard & Lefeuvre, 2004).

1.3.1 Functional trait approach

Although the balance between soil carbon stabilisation and destabilisation is impacted by processes other than decomposition, chemical recalcitrance is the dominant mechanism controlling long-term carbon stability in the soil (Krull, Baldock & Skjemstad, 2003). Chemical recalcitrance of litter can be approximated with a range of functional traits (Cornwell et al., 2008; Freschet, Aerts & Cornelissen, 2012b; Manzoni et al., 2012). Trait-based ecology promises that easy-to-measure and widely available morphological and physiological attributes of species can be used to generalise about the impact that shifts in plant community composition have on ecosystem function (Lavorel & Garnier, 2002; Suding et al., 2008; Westoby & Wright, 2006; Díaz et al., 2007; Violle et al., 2007). Traits that impact ecosystem function would allow us to look beyond our exact study system and compare across ecosystems and in changing environments (Garnier et al., 2004). Community-weighted mean trait values have been used to explain ecosystem-level variations in plant production, decomposition, photosynthesis, respiration, and microbial composition (de Vries et al., 2012; Díaz et al., 2007; Garnier et al., 2004; Grigulis et al., 2013). Functional trait research is the least

well developed in wetlands (de Bello et al., 2010), however, interest and discussion of wetland –specific considerations is growing (Moor et al., 2017).

Covariation in functional traits

Covariation among traits defines a 'plant economic spectrum' of trait variation, for example, nearly three-fourths of the total variation of key leaf traits is described by a single axis in multidimensional trait space (Wright et al., 2004). Originally described in leaves, it has since been described in wood (Chave et al., 2009), roots (Roumet et al., 2016), and across multiple plant organs (Freschet, Aerts & Cornelissen, 2012a; Reich, 2014). This spectrum purports to identify coordinated species-level strategies for nutrient uptake, water use, and also carbon cycling (Reich, 2014).

Functional traits related to litter quality

Economic spectrum theory suggests that fast-growing, herbaceaous species are evolutionarily adapted for resource acquisition and therefore allocate carbon to photosynthetically active structures with high nitrogen content; these plant structures are often shed on an annual or basis and are more easily decomposed (Reich, 2014; Aerts & Chapin, 2000). Slow-growing species adapt to conserve resources and therefore trade-off more efficient photosynthetic tissue for lower quality tissue with higher concentrations of carbon, including recalcitrant forms that do not easily decompose (Reich, 2014; Garnier et al., 2004; Manning et al., 2015). However, the wide variety of plant forms in wetlands (Fig. 1.2) raises questions about the universality of the plant economic spectrum concept in those systems (Moor et al., 2017).

Empirical work has concluded that a range of economic spectrum traits as well as carbon compounds correlate with overall decomposition rate of leaf and/or plant litter in general: (i) carbon, nitrogen, or carbon to nitrogen ratio (Britson, Wardrop & Drohan, 2016; Cornelissen et al., 2001; Cornwell et al., 2008; Cornwell & Weedon, 2014; Freschet, Aerts & Cornelissen, 2012a), (ii) lignin or lignin to nitrogen ratio (Britson, Wardrop & Drohan, 2016; Cornwell et al., 2008; Freschet, Aerts & Cornelissen, 2012a,b; Jackson, Peltzer & Wardle, 2013; Zhang et al., 2008; Makkonen et al., 2012), (iii) specific leaf area or leaf mass area (Cornelissen et al., 1999; Cornwell et al., 2008), (iv) and litter cellulose (Britson, Wardrop & Drohan, 2016), among others. Although economic spectrum traits correlate with decomposition (Cornwell et al., 2008), they are not direct measures of litter recalcitrance (Britson, Wardrop & Drohan, 2016).

1.3.2 Cell wall carbon components

Intrinsically complex carbons are the most likely to become recalcitrant (Lang et al., 2009). Particularly recalcitrant forms include lignin, tannins, and polyphenols, which have a longer residence time in soil. Specific enzymes or rarely-occurring fungi may be required to decompose them (Lawrence, Resh & Cover, 2013; Guenet et al., 2010). Lignin is thermally stable and decomposes slowest in soils because it is composed of heavily-linked benzene-propane monomers (Müller-Hagedorn & Bockhorn, 2007). In

contrast, cellulose forms long, linear polymers of glucose units that are more easily decomposed than lignin, but more stable than simple sugars such as hemicelluloses, which decompose the fastest (Müller-Hagedorn & Bockhorn, 2007).

Figure 1.2: Sample of representative wetland plant species: (a) *Myriophyllum crispatum*, (b) *Eucalyptus camaldulensis*, (c) *Juncus* species.

Estimating carbon components

Traits related to the plant economic spectrum can be measured using standardised, widely reproducible methods (Pérez-Harguindeguy et al., 2013). In contrast, estimation of carbon components is typically done with wet chemistry assays, a time-consuming process that also adversely impacts the environment because it requires the use of sulfuric acid and acetic anhydride, among other chemicals. Thermogravimetric analysis (TGA), widely used by biofuels researchers, can also be used to estimate biomass carbon (Hu et al., 2016; Cheng et al., 2015; Perejón et al., 2011). Litter mass loss during pyrolysis can be regarded as the sum of the degradation of the main plant tissue carbon components: hemicelluloses, cellulose, and lignin (Hu et al., 2016; Cheng et al., 2015; Perejón et al., 2011; Órfão & Figueiredo, 2001; Müller-Hagedorn & Bockhorn, 2007). The rate of mass loss curve must then be mathematically separated into individual peaks corresponding to the weight of each primary component. This method has been validated by studies comparing estimates to experimental measurements (Yang et al., 2006) and has been tested in multi-species comparisons of marine and coastal macrophyte species (Trevathan-Tackett et al., 2015) as well as in eucaplyt species (Órfão & Figueiredo, 2001).

In practice, this peak separation is typically conducted with commercial software (for example OriginPro as in Chen et al., 2017, PeakFit as in Perejón et al., 2011, Fityk as in Perejón et al., 2011, or Datafit as in Cheng et al., 2015). These softwares are not accessible to everyone and can obscure computational and statistical choices that impact estimation results. Given the clear connection between litter carbon complexity and rate of decomposition (Britson, Wardrop & Drohan, 2016; Lang et al., 2009), it is important to standardise the thermogravimetric analysis technique for carbon component estimation with computationally reproducible methods.

1.4 How does plant litter decompose?

Appropriate models are required to quantify decomposition rates and test the relative predictive abilities of traits on rates of decomposition (De Deyn, Cornelissen & Bardgett, 2008). During decomposition, mass is lost quickly initially and then slows (Olson, 1963), and is most commonly approximated using the negative exponential model. This model has a constant rate of decay over time. Despite its widespread use, it has been criticised for its relevance in modelling the decomposition of heterogeneous litter (Wieder & Lang, 1982; Cheshire et al., 1988; Prescott, 2010; Adair, Hobbie & Hobbie, 2010). Litter consists of a variety of structures (roots, stems, leaves), which contain varying amounts of carbon components that decompose at different rates at different phases of decay (Freschet, Aerts & Cornelissen, 2012a). A range of more flexible, multiple parameter decomposition models exist that are therefore more appropriate (Bruun, Six & Jensen, 2004; Feng, 2009; Manzoni et al., 2012).

1.5 Statement of problem

We have an imperfect understanding of the carbon dynamics of different vegetation communities whose varied litter decomposes to produce the organic carbon that is stored in the soil. Although the productivity of vegetation communities alone may be not be sufficient to predict soil carbon storage in wetlands, the relative abundance of complex carbons deposited by species may be an important indirect driver of carbon storage. The diversity of the carbon components in structural tissue raises difficult questions about how to develop standardised and reproducible ways to measure them, how they relate to proposed unified plant strategies, and which kind of decomposition models we should use to appropriately account for them.

1.6 Thesis aims

My research aims to improve our understanding of plant contribution to soil carbon, from the scale of a leaf to the wider landscape, and aid in clarifying processes of plant decay in wetlands and carbon storage in general. Specifically, I aim to: (1) examine the relative contribution of productivity of the local plant community to carbon stock in wetlands compared to other drivers, and therefore improve our predictive ability to the global scale; (2) explore ways to measure these traits and quantify covariation between them; and (3) empirically test the contribution of these traits to litter decomposition. Throughout this work I use Bayesian, hierarchical modelling approaches that improve our ability to distinguish between sources of variation. I outline the aims of each chapter in the next section and present in Fig. 1.3 the broader aim and questions associated with each chapter.

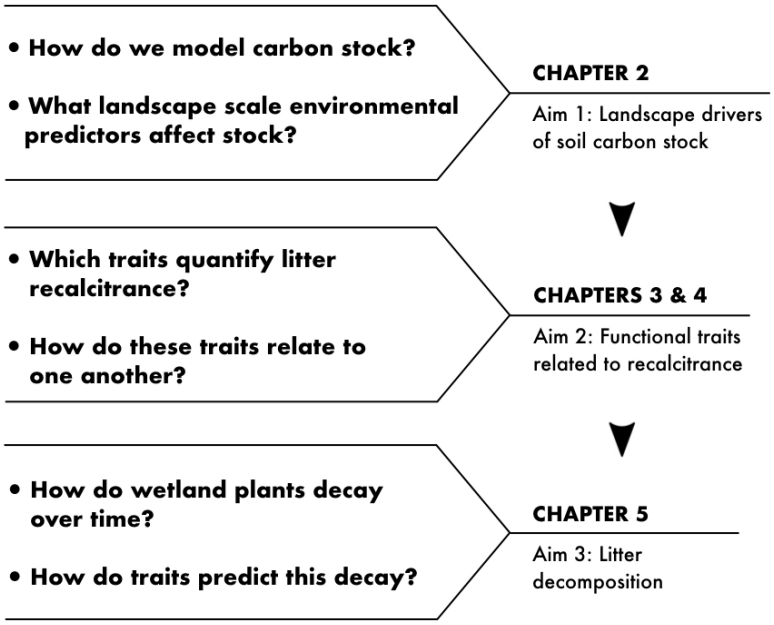

Figure 1.3: Questions addressed by each chapter contributing to the three overall aims.

1.7 Thesis outline

Chapter 2: Drivers of soil carbon storage in freshwater wetlands of south eastern Australia

This chapter quantifies the impact of landscape-scale environmental drivers on organic carbon storage in soil. I test prediction of soil carbon from 100 wetlands located in the state of Victoria, Australia with a model using spatially-explicit environmental data. This study is the first attempt to model unbiased regional sampling of freshwater wetlands with continuous environmental data.

Chapter 3: Decoupling plant economics traits and biomass carbon composition in wetland litter

This chapter explores innovative analytic techniques for estimating carbon complexity in litter (thermogravimetric analysis) and seeks to understand the relationship of carbon complexity to traditional functional traits and to litter recalcitrance in general. I measure traits in 29 wetland plant species and address these aims with phylogenetic analysis and principal component analysis.

Chapter 4: mixchar: An R package for the deconvolution of thermal decay curves

Thermogravimetric analysis of litter biomass requires application of a statistical mixture model to estimate the relative contribution of different carbon components. This chapter introduces an open-source implementation of this mixture model in the statistical programming language, R.

Chapter 5: Understanding variation in litter decomposition in a multi-species mesocosm

This chapter seeks to understand how well functional traits and carbon components estimated in the previous chapters predict rates of litter decomposition. I conduct a mesocosm decomposition experiment of the same 29 wetland plant species introduced in Chapter 3 and evaluate a series of increasingly complex non-linear models of decomposition with a hierarchical, Bayesian implementation.

Chapter 6: General Discussion

This chapter synthesizes my findings and discusses their significance and implications for understanding how plants contribute to wetland soil carbon stock. I also place the statistical approaches used in this thesis into a broader context and provide details about future work.

Appendices

Appendices contain supplementary material associated with each chapter (Appendices A– D) as well as two publications that I co-authored and that relate to this thesis (Appendix E). The first publication relates to work described in Chapter 2, and the second is a chapter of a book about wetland plant vegetation.

2

Drivers of soil carbon storage in freshwater wetlands of south eastern Australia

Abstract

Freshwater wetlands are globally significant reservoirs of soil carbon. Diverse vegetation, inundation regimes, geomorphology, and climate affect the amount and persistence of carbon in the soil in these ecosystems. Attempts to quantify the relative impact of these environmental drivers have relied upon datasets with only a few sites and a limited number of site-specific samples. Such data limitations led to an inability to model carbon density profile with depth, or include spatially variable predictors. In this study, we collected soil carbon data from 100 wetlands in Victoria, southeastern Australia, constituting one of the largest datasets of wetland soil carbon measurements from a single empirical study. These data allowed us to estimate the soil carbon density profile through depth using a curvilinear density depth response, and to integrate across that profile to generate a model of landscape-level drivers of carbon stock. We used this model to evaluate the importance of hydrology, geomorphology, climate, and vegetation structure using continuous spatial data. Our model of the soil carbon density profile demonstrates that, in general, organic carbon density decreases with depth, but that the shape of that decline varied considerably among wetlands. We found that carbon was highest among wetlands with intermediate levels of precipitation but with infrequent permanent water cover. The hierarchical model and out-of-sample prediction methods described here provide an analytical framework for future analyses of soil carbon stock in wetlands that guard against overfitting and enable appropriate extrapolation. These advances could be important for extrapolation used in global carbon cycle modelling, spatial conservation prioritisation of inland wetlands, and carbon offset and mitigation efforts.

2.1 Introduction

Carbon stored in wetland soil contributes substantially to the amount of carbon stored globally. Wetland systems hold 20—30 % of all terrestrial carbon (Lal, 2007; Mitra, Wassmann & Vlek, 2005). Density of soil organic carbon depends on relative rates of carbon import via litter deposition from primary production and carbon export via soil microbial and microfaunal respiration from decomposition. Tidal ecosystems store more carbon per unit area than freshwater wetlands because saline conditions and high exogenous flows quickly and densely accumulate carbon in soil (Chmura et al., 2003; Ewers Lewis et al., 2018; Macreadie et al., 2017), but despite their slower rates of soil carbon accumulation, freshwater wetlands cannot be ignored. Occupying globally only 5—8 % of land area (Mitsch & Gosselink, 2007), they are estimated to hold up to ten times more carbon globally than tidal wetlands (Nahlik & Fennessy, 2016) due to their wider extent.

Carbon storage rates in freshwater wetlands vary dramatically both among and within wetlands (Pearse et al., 2018) due to the diverse biota and inundation conditions found across sites (Mitra, Wassmann & Vlek, 2005; Mcleod et al., 2011). There is a critical need to understand how environmental factors drive the accumulation of carbon in freshwater wetlands in order to predict carbon storage on a global scale. However, existing studies of carbon storage in freshwater wetlands are mostly limited to small-scale or site-specific comparisons (Bernal & Mitsch, 2012; Villa & Mitsch, 2015). Further, many studies contradict one another with respect to exactly how hydro-geomorphology and vegetation affect carbon storage. Bernal & Mitsch (2012) found that carbon stocks were higher in depressional wetlands than riverine ones in a temperate climate, but found the reverse to be true in a follow-up study in the tropics (Bernal & Mitsch, 2013). Others have noted no difference between estuarine, depressional, and perilacustrine wetlands (Marín-Muñiz, Hernández & Moreno-Casasola, 2014). We may expect hydrogeomorphic attributes such as duration of flooding to affect soil carbon via inhibition of decomposition, but inundation alone is an insufficient predictor (Villa & Mitsch, 2015). State- and region-wide wetland inventories are necessary for us to understand how carbon is distributed and accumulated.

Some recent large-scale studies have begun to address this gap in our understanding of underlying mechanisms of carbon storage in wetlands (Nahlik & Fennessy, 2016; Carnell et al., 2018). However, these studies tend to rely upon broad classification of sites by region and/or wetland type. Although wetland classifications often incorporate aspects of both hydro-geomorphology and relevant plant community, they are far from uniform across the globe (Brinson, 1993; Cowardin et al., 1979). Any broad-scale prediction therefore must rely on the assumption that wetlands of the same type exhibit the same carbon storage potential, but under vastly different conditions. The U.S. Army Corps of Engineers uses the Brinson classification system (Brinson, 1993), which separates wetlands by geomorphology (depressional, riverine, fringe, or peat), water supply (precipitation, groundwater-fed, or surface-fed), and water flow (vertical, unidirectional, or bidirectional). This multifaceted approach contrasts with the U.S Fish and Wildlife Service, which use the Cowardin classification system. This system

distinguishes broadly between marine, estuarine, riverine, palustrine, and lacustrine systems (Cowardin et al., 1979). In the state of Victoria, Australia, research agencies tend to use the Corrick and Norman scheme, which combines inundation and vegetation categories into classes such as 'deep freshwater marsh' and 'shallow herbland' (Corrick & Norman, 1980). Given the diversity of classification systems, both between and within countries, categorising carbon storage by these broad criteria might mask finer scale variability in actual drivers of carbon storage. Models of carbon stocks using global spatial data, instead of classification categories, would greatly improve upon existing models. These could enable more confident prediction to areas which have similar soil carbon dynamics but where no sampling has taken place (Sanderman et al., 2018).

In this study, we model the influence of landscape-scale environmental factors that drive soil carbon stock among a network of inland wetlands in the state of Victoria, Australia (covering more than 200,000 km^2). We aimed to: (i) determine how sites differ in their vertical profiles with depth, (ii) generate an integrated stock assessment using site-specific profiles, and (ii) evaluate the ability of continuous environmental variables to predict carbon stock.

2.2 Materials and Methods

Sample collection

This study was conducted in inland wetlands across the state of Victoria in south-eastern Australia (n = 100; Fig. 2.1). These wetlands experienced ephemeral to permanent inundation, and are fed by varying sources ranging from surface water runoff, groundwater, and river flooding. These sites support diverse plant communities that are adapted to the local inundation conditions and vary not only seasonally but on longer flooding timescales. The study was conducted in collaboration with the Victorian Catchment Management Authorities (CMAs) and the Victorian State Government Department of Environment, Land, Water and Planning (DELWP), and in part because of this, we spread our sampling effort evenly across the 10 CMA regions of Victoria. We also chose wetlands across six key wetland categories defined by Corrick & Norman (1980) and used in other work supported by DELWP: freshwater meadow, shallow freshwater marsh, deep freshwater marsh, permanent open freshwater, saline wetlands, and alpine wetlands (for further discussion of stock variation by wetland type for this data, see previous work Carnell et al., 2018).

Sampling was conducted in Austral spring/summer between August 2015 and February 2016. We collected five soil cores at each wetland and randomly selected a subset for analysis (typically three cores, but in some cases up to five; Fig. 2.2a). At each site, we placed replicate cores 50 m apart within a predominant vegetation zone (zones could typically delineated by consistent single or set of species). At each sampling point we hammered a 5 cm diameter PVC pipe (hereafter referred to as 'the core') into the soil until 1 m, or until refusal. The depth at refusal varied considerably among cores and sites, and most indicated the start of a thick clay layer. For some

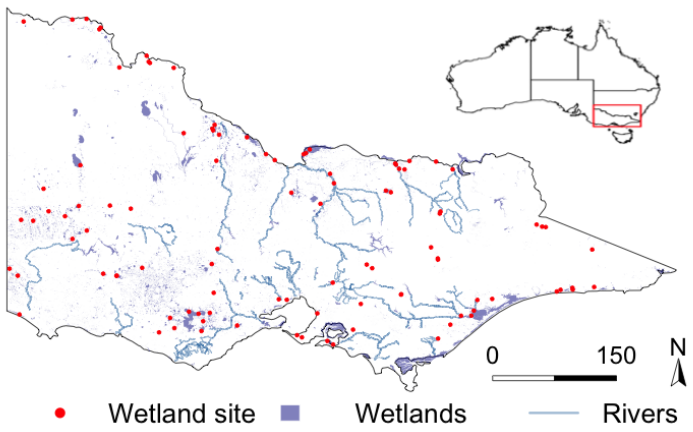

Figure 2.1: Wetlands and waterbodies in Victoria and location of 100 study sites.

areas this was as shallow as 0.16 m (typically temporary open water bodies), while other wetlands contained organic peat material well past 1 m. Core collection using this approach resulted in some compaction, which we accounted for by measuring the difference between the amount of soil sampled and the depth the core was hammered into the ground. We assumed constant compaction along the core. After the core was in place we sealed it by inserting a rubber plug. After removing the core we stabilised the top layer of sediment with a foam plug and capped the ends with a plastic cover and masking tape to prevent moisture loss.

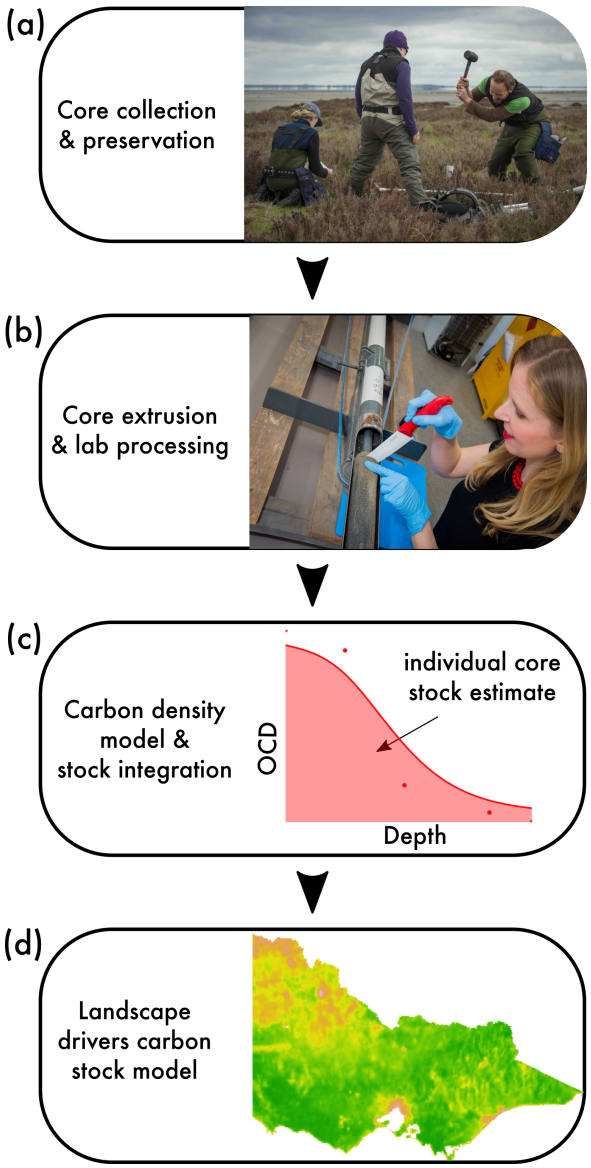

FIGURE 2.2: Methodology for core collection and analysis. (a) PVC pipes were hammered into the soil until 1 m, or until depth of refusal. We sealed cores with plastic lids and duct tape. (b) Cores were extruded in the lab and sliced into 2 cm sections at regular intervals before being sent for lab analysis. (c) Organic carbon densitywas extrapolated across depth using a hierarchical generalised additive model, before integration for stock estimation. (d) Spatially-explicit landscape environmental data were used to predict carbon stock across the state. Photo credit: Deakin University, Burwood VIC.

Carbon analysis

In the laboratory we extruded the soil from the replicate cores. We sliced each core into 2 cm samples at 0—2 cm, 12—14 cm, 28—30 cm, 48—50 cm, 74—76 cm, and 98—100 cm to send to the laboratory (Fig. 2.2b). When depth at refusal was shallower than 1 m, we sliced an additional sample at the deepest depth. The number of samples

per core varied due to variation in core depth.

We dried each 2 cm sample at 50 °C for 48—72 hours and homogenised them with a stainless steel mortar and pestle (Retch RM200) before exposing them to gamma irradiation at 50 kGray for 60 hours (by Steritech, Dandenong, Victoria). This irradiation removes potential infection of *Daktulosphaira vitifoliae*, since some of our samples came from known Phylloxera Infested Zones This irradiation process has been demonstrated to have no major influence on carbon measurements in soil samples (Baldock et al., unpublished data).

We sent the samples to the Commonwealth Scientific and Industrial Research Organisation (CSIRO) in South Australia for carbon analysis (a detailed summary of their protocol can be found in Appendix D). CSIRO provided us with an organic carbon estimate of each sample. We estimated organic carbon density ($mg\ cm^{-3}$) by multiplying the estimate by dry bulk density: the dry weight of sample divided by volume, in this case $\pi * 2.5^2 * 2$ because each slice sample had a radius of 2.5 cm and a thickness of 2 cm.

Carbon stock estimation

We modelled organic carbon density for sample k in core j and site i (C_{ijk}) as lognormally distributed (Eq. 2.1), where μ_{ijk} can be described by a hierarchical generalised additive model (Fig. 2.2c). This model consists of: a random intercept for site i = 1, ..., 100 (α_i), a random intercept for core j = 1, ..., 305 (γ_j), a regression spline of depth ($f(z_{ijk})$), and a regression spline incorporating the effect of site-level smoothers on depth ($g_i(z_{ijk})$) (Eq. 2.2).

$$ln(C_{ijk}) \sim N(\mu_{ijk}, \sigma^2) \tag{2.1}$$

$$\mu_{ijk} = \alpha_i + \gamma_j + f(z_{ijk}) + g_i(z_{ijk}) + \epsilon_{ijk} \tag{2.2}$$

where ϵ_{ijk} is the Gaussian error term. A hierarchical GAM is appropriate in this context because not only do we expect samples to vary the intercept of their relationship with depth by core and site, but we also expect site to affect the *shape* of the relationship with depth. We can also share information from the wider dataset via the mean regression spline of depth, giving us more information for cores that had fewer samples and therefore less well-resolved curves with depth.

To use this model to estimate stock ($Mg\ h^{-1}$) for each core (S_{ij}), we generalise the function for organic carbon at depth by removing the sample-level error term ($h_{ij}(x)$; Eq. 2.3) and integrate under this function across the maximum depth achieved at a site (Eq. 2.4):

$$h_{ij}(x) = \alpha_i + \gamma_j + f(x) + g_i(x) \tag{2.3}$$

$$S_{ij} = \int_0^{m_i} e^{h_{ij}(x)} dx \tag{2.4}$$

$$m_i = \max_k(z_{ijk}) \tag{2.5}$$

Landscape scale drivers of carbon stock

We used a separate model to next estimate the landscape environmental variables that predict stock (Fig. 2.2d). We collected spatial data layers related to climate, hydrology, geomorphology, and vegetation (Table 2.1). Primary production is typically high in wetlands (Peregon et al., 2008), meaning large volumes of both locally-produced and exogenous litter are brought in and deposited into the wetland. The degree to which a wetland is an effective sink for exogenous carbon depends on the size and condition of its catchment and the flow and consistency of its hydrologic connectivity (Moreno-Casasola, Hernández & C, 2017; Gallant & Dowling, 2003). Inundation can also promote anoxic conditions ideal for limited litter decomposition (Herndon et al., 2015).

Spatial layers collected from a range of Victorian government data sources were collated as candidates to explain spatial variation. Mean annual temperature, annual precipitation, and aridity were highly correlated with each other and therefore only one is used in the model (Fig. A.1). We selected annual precipitation because of its direct impact on the rate of water delivery to a site. Although we expect soil texture and clay content to affect carbon storage in soil, on a regional scale clay they are not expected to be important predictors (Vaughan et al., 2019; Zhong et al., 2018).

We model stock for core j and site i (S_{ij}) with a a lognormal distribution (Eq. 2.6), where η_{ij} can be described by a generalised additive model. This model consists of a separate regression spline for each layer of 1, ... n = 7 layers ($f_n(x_{ijn})$; Eq. 2.7).

$$ln(S_{ij}) \sim N(\eta_{ij}, \rho^2) \tag{2.6}$$

$$\eta_{ij} = f_1(x_{ij1}) + ... + f_n(x_{ijn}) + \epsilon_{ij} \tag{2.7}$$

We implemented an additional penalty for each smooth term. If all the smoothing parameters for the term tend to infinity, the term is selected out of the model (Marra & Wood, 2011). We prepared spatial layers with the *raster* package (Hijmans, 2019), and fit both GAMs with the *mgcv* package (Wood, 2017) in the statistical computing environment R (R Core Team, 2013).

We evaluated the predictive performance of the carbon stock model by cross-validating its predictive performance on data for a site held out when training the model initially (Hooten & Hobbs, 2015). For each run of the model, we split the dataset into training data (including all but one site) and test data (the held-out site). The model was then run 100 times, giving each site the opportunity to be the

Table 2.1: Wetland characteristics tested as potential predictors of soil carbon density. ANUCLIM version 6.1 estimated to 9 arc-second based on GeoScience Australia's 9 second Digital Elevation Model (Xu, Kesteven & Hutchinson, 2018). *spatial layers indicate layers excluded due to high correlation (>0.7) with other layers.

Variable category	Spatial data	Unit	Source	Description
Climate	Temperature*	°C	ANUCLIM	Mean annual temperature 250 m resolution
	Precipitation	mm	ANUCLIM	The sum of monthly precipitation 250 m resolution
	Aridity*	index	Atlas of Living Australia	Ratio of mean annual monthly precipitation to potential evaporation
Hydrology	Topographic Wetness Index	index	ANUCLIM	$TWI = \ln \frac{\alpha}{\tan B}$, where α is upstream contributing area and B is slope in radians at 250 m resolution
	Water Observations from Space	%	Geoscience Australia	Percent of cloud-free Landsat observations with surface water visible at 25 m resolution
Geomorphology	Multiresolution Valley Bottom Flatness	index	ANUCLIM	Integrated estimate of valley bottom flatness at 250 m resolution
	Catchment size	m^2	Bureau of Meteorology, Australian Government	Area of AHGF Catchment from The Australian Hydrological Geospatial Fabric
Vegetation	Normalized Difference Vegetation Index	index	Bureau of Meteorology, Australian Government	Spectral reflectance measurements ratio $NDVI = \frac{NIR-Red}{NIR+Red}$ at 250 m resolution
	Native vegetation in catchment	ratio	Bureau of Rural Sciences, Australian Government	Percent of native vegetation cover: native vegetation cover consists of classes 0, 1, 2, and 3 of Vegetation Assets, States and Transitions (VAST) dataset

'test' data. Sites were used as the cross-validation grouping because we were interested in the ability of environmental attributes to predict to an entirely new site rather than to individual core estimates. Model evaluation was conducted by calculating the R^2 of each model (across all folds).

2.3 Results

Organic carbon density

The hierarchical organic carbon density model fit the data well ($R^2 = 0.63$; Fig. A.2) and we can take away three main conclusions. First, on average organic carbon density decreases with depth (Fig. 2.3a), and second, this smooth curve varies in its intercept, or average density, both within wetlands (variance of core-level intercept = 0.22; Fig. 2.3b) and between wetlands (variance in site-level intercept = 0.48). Last, sites differ not only in their average log-carbon density but also in the shape of their functional responses to depth (Fig. 2.3c). When the depth by site spline is removed, the resulting model explains just 0.58 of deviance compared to 0.8 for the full model.

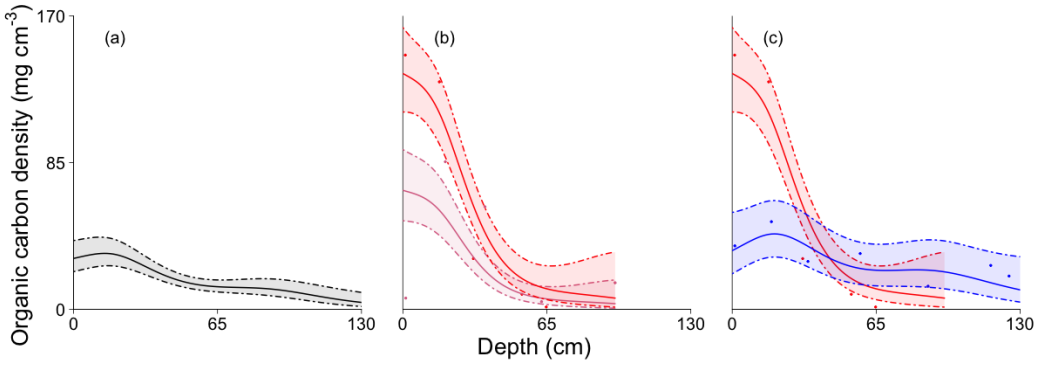

FIGURE 2.3: Predictions from organic carbon density model. (a) Depth spline with 2 standard error. (b) Variation in intercept by core for two example cores from Dereel Lagoon Wildlife Reserve. (c) Variation in shape of functional relationship with depth by site with two example sites (Dereel Lagoon WR and Ewing Morass State Wildlife Reserve).

Stock estimates for each core ranged from 23.78 to 1126.2 Mgh^{-1} (to maximum depth at each site).

Landscape predictors of carbon stock

Cross-validated predictive performance suggests the landscape-scale model was reasonably successful at predicting carbon stock at new sites ($R^2 = 0.34$). The model, when run on all the data, explained 66% of the deviance, which indicates considerable support. Model evaluation suggests all the smooth terms significantly improved model fit (Table A.1). As smooth terms, there is no coefficient for their impact on carbon stock, but prediction plots for each model term (holding all other variable values to their mean) give us some indication of the effect of each variable on carbon stock prediction (Fig. 2.4).

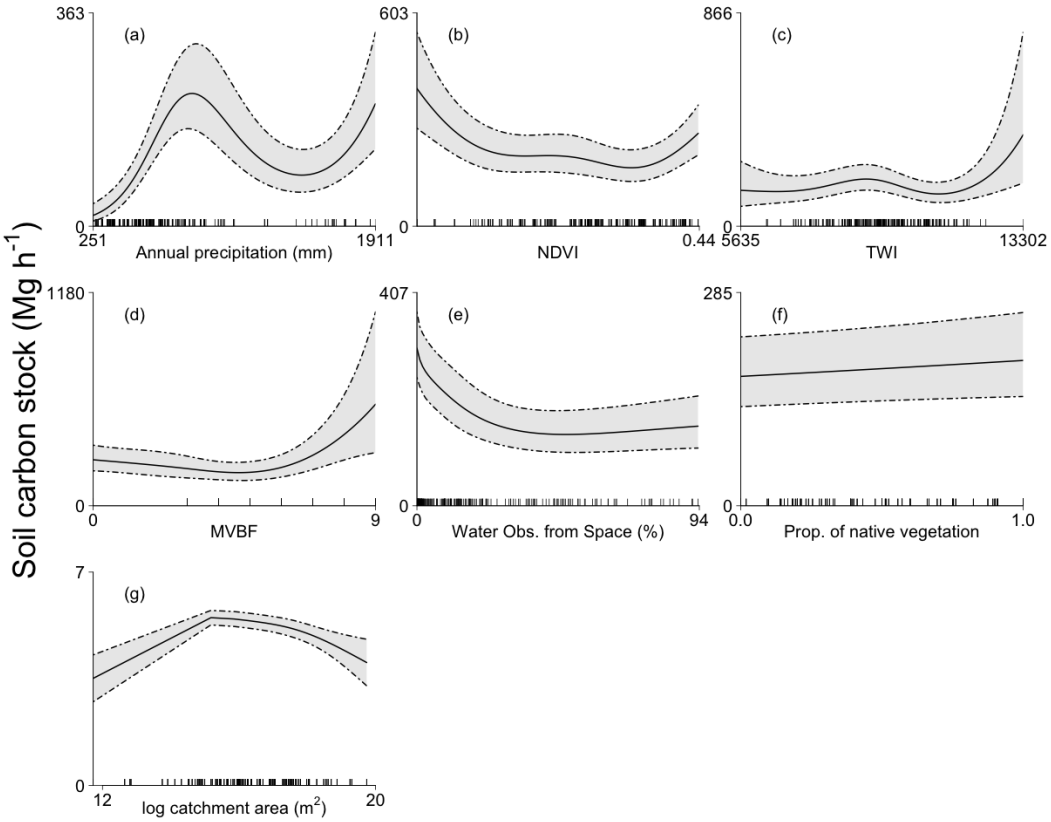

Figure 2.4: Predictions from soil carbon stock model for each variable included, holding the other variables at their mean value. Ticks along x-axis indicate number of datapoints. (a) Annual precipitation (mm), (b) Normalised Difference Vegetation Index, (c) Topographic Wetness Index, (d) Valley bottom flatness, (e) Water observation from space (%), (f) Proportion of native vegetation, and (g) log catchment area (m^2).

2.4 Discussion

Our study makes two main contributions to understanding soil carbon in wetlands on a landscape scale. First, using a hierarchical modelling approach for variation in soil carbon density, we determined that the nonlinear relationship of carbon against soil depth varies between wetlands. Second, we found that continuous environmental data could predict soil carbon stock in inland wetlands on a landscape scale.

Carbon density with depth

We found that SOC was densest in shallower sediment and declined with depth. This declining trend is indicative of accumulation of SOC and has been reported in a range of systems (Nahlik & Fennessy, 2016; Chanlabut, Gomontean & Srifa, 2019; Scharpenseel & Becker-Heidmann, 1992/ed; Ricker & Lockaby, 2015). The decrease in carbon with depth suggests we must be careful when extrapolating carbon density

at unmeasured depths: it is insufficient to assume the deepest measured carbon density is representative of deeper samples (as in Ma et al., 2015), or to use a simple linear decay model.

The shape and characteristics of the decline in SOC with depth varied between sites. This result has also been reported in an estuary system (Adame et al., 2015) and in Cypress swamps (Villa & Mitsch, 2015). This variation is unsurprising given the effect of land use and historical environmental conditions on the accumulation rate of sediment and persistence of SOC (Nahlik & Fennessy, 2016). Smoothing functions can help more accurately extrapolate SOC with depth given this variation (such as for organic carbon density in Carnell et al., 2018 and for bulk density in Nahlik & Fennessy, 2016). However, most of these attempts have relied upon models that assign a separate smoothing function to each core. A hierarchical modelling approach, such as the one presented in this study, is useful because it allows individual sampling points to learn from both the global mean relationship with depth as well as site-level relationships (as demonstrated in relation to diversity metrics Marion, Fordyce & Fitzpatrick, 2018). This is particularly useful where there are few depth samples per core, which can lead to biased estimates if a separate spline is fit to each core. Future work to improve interpolation across the depth profile and extrapolation to unmeasured depths could build on this hierarchical model by using environmental variables themselves to predict the depth function.

Reliable extrapolation of carbon density at depth is important because carbon stock is an integrated measure of carbon density at depth, and relies on reporting to a common depth. The Intergovernmental Panel on Climate Change (IPCC) guidelines suggest that soil carbon stock for mineral soil wetlands be reported to a depth of 30 cm (as in Conti & Díaz, 2013) or 1 m for coastal wetlands (Hiraishi et al., 2014). More reliable estimation of SOC with depth will not only improve estimates that meet these guidelines, but perhaps enable us to more confidently extrapolate deeper than 30 cm, because restricting stock measurement to 30 cm can mask significant carbon stored in freshwater wetlands up to 1 m and beyond (Grover, Baldock & Jacobsen, 2012). In this study we were able to sample 16.4 —136 cm deep, illustrating a common, but wide range for penetration of inland wetland soils with traditional coring techniques.

Landscape drivers of soil carbon stock

The prediction plots for landscape drivers of carbon stock indicate that intermediate levels of inundation produced some of the highest carbon stock. Carbon was highest among wetlands with intermediate levels of precipitation and in areas with infrequent permanent water cover. Higher precipitation may be a good predictor of carbon stock because it supports higher productivity, carries more external litter material to a site, or reduces decomposition rate (Mitsch & Gosselink, 2007). We found that wetlands that are flooded more regularly had low carbon stock, which may be related to little carbon from primary productivity in the submerged zone (Keddy, 2010). However, we must be wary about generalising this pattern because Water Observation from Space data does not tell us about the timing or permanence of inundation and is subject to

higher error in regions with frequent cloud-cover regions. Despite these limitations, this result matches other work that indicates inundation-induced anaerobic conditions resulting in reduced decomposition is not the only predictor for carbon stock (Villa & Mitsch, 2015).

Normalised Difference Vegetation Index (NDVI), a proxy for productivity, appeared high in both low- and high-carbon areas, so although we expect productivity to be associated with high soil carbon stock (Whitaker et al., 2015; Wang, Xu & Wan, 2016; Marín-Muñiz, Hernández & Moreno-Casasola, 2014; Ceballos, Frangi & Jobbágy, 2013), it is perhaps productivity of certain kinds of vegetation that accounts for the effect. It is also possible that vegetation communities at the site have changed significantly over time, affecting historical SOC in the core (Lal, 2004).

Global prediction implications

We found that spatial environmental data at a maximum resolution of 250 m was reasonably successful at predicting out-of-sample carbon stock. The Victorian wetland landscape was a good test case because of its diversity of arid zone wetlands that flood at a wide range of intervals, from seasonally to once every 50 years. Inundation and precipitation layers were particularly useful in this context and will likely be important on a global scale. However, we must be cautious in using remote sensing data for global prediction because it is susceptible to error associated with variation in local climatic conditions such as cloud cover (Weng & Fu, 2014). In addition, remote sensing data may be less reliable for picking up environmental characteristics of small wetlands because the resolution may be too low (Tootchi, Jost & Ducharne, 2019).

Given these precautions, prediction using globally available data is a vital step to targeting wetlands for conservation and carbon offsetting, particularly for data-poor wetlands. This type of prediction methodology is already being developed for mapping forest aboveground carbon stock (Cartus et al., 2014) and mangrove soil carbon (Sanderman et al., 2018), but not yet for freshwater carbon. On a global scale, continuous environmental data with out-of-sample validation is an important way forward to improving prediction across the diversity of freshwater and inland wetlands.

2.5 Acknowledgements

We thank Steve Krueger, Booyanuj Yukate, and Kelsey Johnson for their considerable help in both the field and laboratory. We also thank Jan Barton, Alex Pearse, Tessa Evans, and Quinn Olivier for assistance in the field. We sincerely thank Bruce Hawke for running all our soil samples. We thank Janet Holmes, Tamara van Polanen Petel (DELWP), Paul Reich (ARI), Rohan Hogan (NCCMA), Natalie Dando (NECMA), Adam Bester (GHCMA), and Simon Casanelia (GBCMA) for their support in the development and execution of this project. Funding was provided by Department of Environment, Land, Water & Planning grant to PEC and PIM. An Australian Research Council DECRA Fellowship (DE130101084) and an Australian

Research Council Linkage Project (LP160100242) to PIM. Funding was provided to PM by the Generalitat de Catalunya (Grant 2014 SGR-1356) and an Australian Research Council LIEF Project (LE170100219). Funding was provided to SMW by the Australian Research Council Centre of Excellence for Environmental Decisions, the Holsworth Wildlife Research Endowment & the Ecological Society of Australia, and the Melbourne International Research Scholarship and Melbourne International Fee Remission Scholarship. This work is contributing to the ICTA "Unit of Excellence" (MinECo, MDM2015-0552). Permit number 10007689 was obtained for sampling in National Parks.

3

Decoupling plant economics traits and biomass carbon composition in wetland litter

Abstract

Leaf economics spectrum theory suggests that a range of functional traits correlate along a spectrum of nutrient level that can be used to generalise litter quality. Excluded among this suite of traits are direct measures of carbon composition of litter, despite their relevance to a range of ecosystem processes including decomposition. In this study, we measure morphologicl and chemical traits across the economics spectrum as well as relative carbon composition and ask how these traits covary. In total, we measure seven traits for 29 wetland plant species: litter area per mass, dry matter content, nitrogen content, total carbon, hemicellulose, cellulose, and lignin content. We use thermogravimetric analysis to estimate the relative composition of the carbon compounds. To replace proprietary software currently used in the modelling step of this estimation technique, we demonstrate use of an open-source statistical R package called 'mixchar' that we developed for this purpose. Litter chemistry varied by functional group: terrestrial dry species had the highest lignin concentration and emergent amphibious and terrestrial damp species had the highest cellulose concentration. Litter area per mass, dry matter content, and nitrogen content were correlated along a single plane, as predicted according to leaf economics spectrum theory. In general, species invested in predominantly lignin- or cellulose- based tissue, and variation along this spectrum of carbon complexity was orthogonal in multivariate trait space to the economics spectrum traits. This decoupling supports using multiple traits when using traits to predict ecosystem processes such as decomposition.

3.1 Introduction

Functional traits can be used to quantify litter quality, and have been tied to plant effects on a range of ecosystem functions (Díaz et al., 2007; Lavorel & Garnier, 2002; Violle et al., 2007). The nutrient and carbon make-up of plant litter itself is strongly related to decay rates (Cornwell et al., 2008), because litter of different quality will decompose to varying degrees and at different rates (Liao et al., 2008; Valéry, Bouchard & Lefeuvre, 2004). Although plant litter can become more recalcitrant, or resistant to decay, due to a variety of abiotic and biotic conditions, such as oxygen availability, water levels, pH, ambient nutrients, and the presence of microbial and macroinvertebrate decomposer communities, functional traits predict decomposition of both leaf litter (specific leaf area/leaf mass area and leaf nitrogen; de Vries et al., 2012; Cornwell et al., 2008, and leaf carbon; Britson, Wardrop & Drohan, 2016) and plant litter more generally (litter carbon and dry matter content of all litter, including stems, leaves, roots etc; Freschet, Aerts & Cornelissen, 2012a).

Covariation among leaf traits defines a 'leaf economics spectrum' of trait variation, in which nearly 3/4 of the total variation of key leaf traits is described by a single axis in multidimensional trait space (Wright et al., 2004). Fast-growing, 'nutrient acquisitive', species produce large quantities of high-quality litter, characterised by a high nitrogen content and high specific leaf area. Slow-growing, 'nutrient conservative', species grow dense structural tissue that is high in dry matter content (Aerts & Chapin, 2000). In aquatic environments this spectrum can also divide between submerged species with nitrogen-rich tissue and emergent species that have denser tissue (Godshalk & Wetzel, 1978). A similar coordinated spectrum has since been described in wood (Chave et al., 2009), roots (Roumet et al., 2016), and across multiple plant organs (Freschet, Aerts & Cornelissen, 2012a; Reich, 2014) using different traits.

The plant economics spectrum generalises traits along a 'fast—slow spectrum' that coordinates nutrient, water, and carbon cycling, including rates of decomposition (Reich, 2014). Litter nitrogen increases decomposition rate because it increases loss of lignin, nitrogen, and soluble carbon (Talbot & Treseder, 2012). But mass loss can be initially fast and subsequently quite resistant to decay (López-Mondéjar et al., 2016), and it is well established that the amount of lignin, in particular, strongly predicts this resistance to decay (Britson, Wardrop & Drohan, 2016; Cornwell et al., 2008; Makkonen et al., 2012; Freschet, Aerts & Cornelissen, 2012a). Composed of heavily-linked benzene-propane monomers, lignin is thermally stable and slow to decompose in soils (Müller-Hagedorn & Bockhorn, 2007). Abiotic and biotic conditions can slow decomposition of even labile litter, but litter high in intrinsically complex carbon such as lignin, polyphenols, and tannins, is more likely to become recalcitrant (Fig. 3.1).

Besides recalcitrant carbons, other carbon forms such as hemicelluloses and cellulose also impact the rate of plant litter decomposition (Moorhead et al., 2014; Britson, Wardrop & Drohan, 2016). Cellulose forms long, linear polymers of glucose units that are more easily decomposed, but more stable than simple sugars such as hemicelluloses that are most easily decomposed (Müller-Hagedorn & Bockhorn, 2007). If the economics spectrum traits should be able to divide species by decomposition rate, we

would expect covariation between those traits and levels of carbon compounds that also impact rate of decay.

Methods for carbon component analysis can be categorised broadly as either acid detergent or gravimetric approaches, and are all estimations due to the complex nature of isolating the compounds (Hatfield & Fukushima, 2005). There is not one standard unambiguous method that will work for all samples, because even among acid detergent methods, estimates will vary depending on which detergent is used (Hatfield & Fukushima, 2005). Thermogravimetric analysis (TGA) is a gravimetric approach for carbon component estimation that assesses the degradation of plant material under increasing temperature. Mass loss under N_2 (i.e. pyrolysis) provides quantitative information about the biochemical components of a sample (Hu et al., 2016; Cheng et al., 2015; Perejón et al., 2011; Órfão & Figueiredo, 2001; Müller-Hagedorn & Bockhorn, 2007). This method has been validated by studies comparing estimates to experimental measurements (Yang et al., 2006). It has also been previously used to identify plant species' recalcitrance (for example in marine and coastal macrophytes Trevathan-Tackett et al., 2015, and eucaplyts Órfão & Figueiredo, 2001).

In this study we measured a range of morphological and chemical traits in 29 wetland plant species, including using TGA to estimate the partitioning of carbon components. The objective was to assess the structural complexity of common wetland plants and to evaluate how variation aligned with the leaf economics spectrum. We expected variation between chemically complex and simple carbons in species to covary with the division between nutrient conservative and nutrient acquisitive species suggested by the leaf economics spectrum. We explain how TGA works in greater detail for the audience of comparative ecologists.

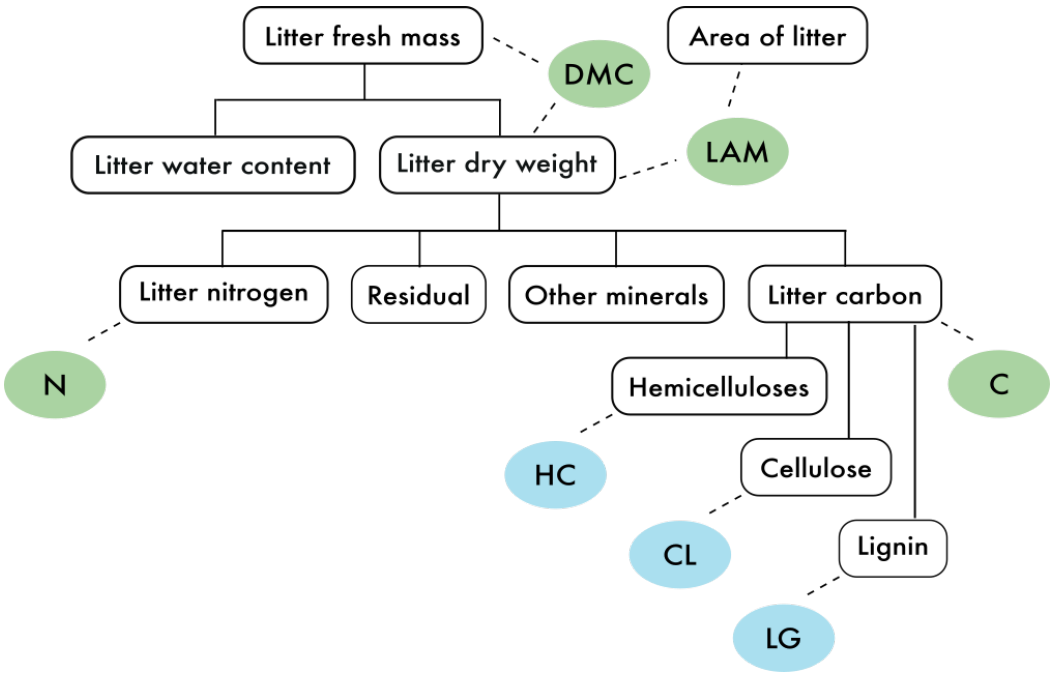

Figure 3.1: Breakdown of the relationships between functional traits (in ellipses) related to concepts of litter recalcitrance examined in this study: dry matter content (DMC), litter area per mass (LAM), litter nitrogen (N), litter carbon (C), litter hemicelluloses (HC), litter cellulose (CL), and litter lignin (LG).

3.2 Materials and Methods

Litter collection

In late austral summer 2016 we collected plant litter derived from photosynthetic tissue of 29 wetland plant species from three wetlands in Victoria, Australia (wetlands within 60 km of -37.455, 144.985). We collected litter from one riverbank, one floodplain wetland, and one shallow groundwater- and surfacewater- fed forbland. This region has a broadly Mediterranean climate, and so this is the peak of the dry season, when plants are fully mature and senescence is about to occur. Since the aim of our study was to examine traits related to litter recalcitrance, we measured aboveground plant biomass that would contribute to litter. For graminoids, litter included the culm and leaves, but not the inflorescence. For forbs and ferns, litter included the entire body of the plant excluding the flower. For tree species, leaves and petioles, leaflets and rachis, but not seeds, flowers, or stems were included. For the purposes of examining litter quality, empirical work has found that traits are reasonably coordinated among different plant parts (for example, leaves and stem, Reich, 2014; Jackson, Peltzer & Wardle, 2013).

For each species, we collected ten robust individuals located at least 5 m apart along a linear transect at a single site (Pérez-Harguindeguy et al., 2013). Plant litter was mostly collected from fallen material on the ground, but for some of the litter this was impossible (ie. *Sphagnum*). Litter was placed in moist plastic bags and stored

in dark coolers until transported to the lab, and then moved to a dark, refrigerated room.

The target species represented a range of functional groups classified according to the Brock & Casanova (1997) scheme (Table 3.1). Functional groups included: terrestrial dry species ('Tdr'; n = 5), terrestrial damp species ('Tda'; n = 9), amphibious fluctuation-tolerators ('AT'; n = 10), and amphibious fluctuation-responders ('AR': n = 5). These groups classify species according to the water levels in which they germinate, grow, and reproduce, and were chosen because tolerance to flooding is an important characteristic for wetland and riparian species (Catford et al., 2011).

Table 3.1: Hierarchical classification scheme of wetland plant species by habit and response to water. Devised by Brock and Casanova (1997).

Abbreviation	Primary category	Secondary category	Description
AR	Amphibious	Fluctuation-responders	Species that germinate in flooded conditions, grow in both flooded and damp conditions, and reproduce above the surface of the water.
AT	Amphibious	Fluctuation-tolerators	Species that germinate in damp or flooded conditions and tolerate variation in water level.
Tda	Terrestrial	Damp species	Species that germinate, grow, and reproduce on saturated soil.
Tdr	Terrestrial	Dry species	Species that germinate, grow, and reproduce where there is no surface water and water table is below the soil surface.

Fast–slow economics spectrum traits

We measured litter area per mass and litter dry matter content per published recommendations (Pérez-Harguindeguy et al., 2013), presenting the average of ten replicates per species. We measured the fresh weight of each sample within 24 hours of collection and then dried the fresh litter at 60 °C for 72 hours. Dried litter from all ten samples were combined and ground to $<40\mu m$ using a Retsch Centrifugal Mill ZM200. A subsample of approximately 150 mg was analysed for litter nitrogen and carbon content in a LECO Elemental Analyser (Department of Biomedical Engineering, University of Melbourne), using an EDTA standard (Table 3.2).

Table 3.2: Selected traits and measurement methods.

Abbreviation	Trait	Units	Method
LAM	Litter area per mass	m^2/g	One-sided area of fresh litter (m^2) divided by its oven-dry mass (g)
DMC	Litter dry matter content	mg/g	Oven-dry litter mass (mg) divided by water-saturated fresh litter mass (g)
N	Litter nitrogen content	wt%	Weight % elemental N in dry litter mass measured with LECO Elemental Analyser
C	Litter carbon content	wt%	Weight % elemental C in dry litter mass measured with LECO Elemental Analyser
HC	Litter hemicelluloses	wt%	Weight % hemicelluloses in dry litter mass from thermogravimetric analysis
CL	Litter cellulose	wt%	Weight % cellulose in dry litter mass from thermogravimetric analysis
LG	Litter lignin	wt%	Weight % lignin in dry litter mass from thermogravimetric analysis

Lignocellulosic biomass method

We used 10–20 mg subsamles of dry, ground litter of each species for thermogravimetric analysis (TGA). During TGA, biomass samples are pyrolysed, resulting in a graph of remaining weight in grams plotted against temperature (Fig. 3.2a). Each sample was pyrolysed in an N_2 environment from 30–800 °C at a temperature ramp of 10 °C/min using a Netzsch TGA-FTIR thermogravimetric analyser (Department of Biomedical Engineering, University of Melbourne). We ran identical analyses on cellulose (carboxy-methyl cellulose) and lignin samples (alkali lignin from Sigma Aldrich).

The negative first derivative of the thermogravimetric curve ('DTG curve'; Fig. 3.2b) describes the rate of mass loss. This multi-peaked plot has three main phases (Órfão & Figueiredo, 2001):

(i) Phase 1: A short period with a pronounced peak of moisture evolution, up until approximately 120 °C.

(ii) Phase 2: A wide mid-range of high mass loss, caused by devolatilisation of primary biomass carbon components, between approximately 120–650 °C.

(iii) Phase 3: A final period of little mass loss when carbonaceous material associated with the inorganic fraction decomposes, after approximately 650 °C.

Since the overall rate of mass loss (DTG) curve also represents the loss of extractives, water, inorganic matter, and volatiles (Hu et al., 2016), we isolate mass loss from biomass components by cropping the DTG data to Phase 2 (120–650 °C). The cropped DTG curve can then be used to estimate mass fractions of the main biomass carbon components by mathematically deconvolving the multi-peaked curve (Fig. 3.2c).

Although the biomass deconvolution curves for the three primary components overlap in the DTG curve, research has found the biomass fractions do not interact much during thermal volatilisation, but decompose reasonably independently (Yang et al., 2006). Because they decompose independently, the derivative mass loss equation ($\frac{dm}{dT}$) can be expressed as the sum of n independent reactions (Eq. 3.1), as follows (Órfão & Figueiredo, 2001):

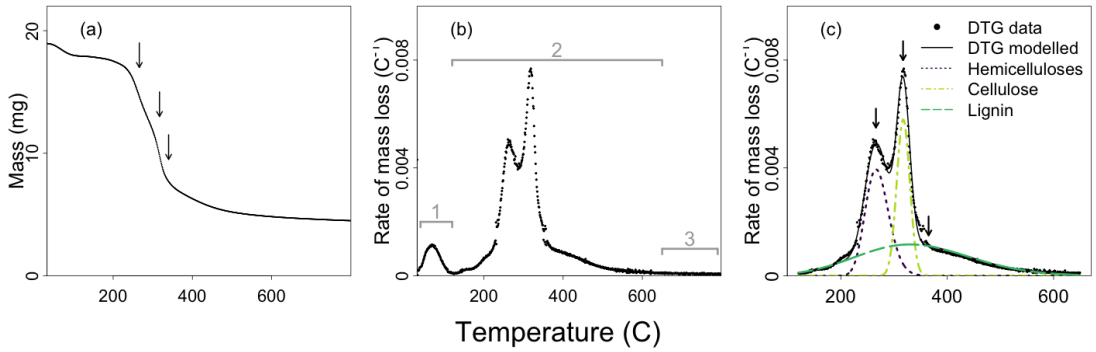

FIGURE 3.2: Detailed exploration of thermogravimetric analysis and mixture modelling (using data from *Juncus amabilis*): (a) Mass loss curve, heating rate = 10°C/min; (b) Negative first derivative thermogravimetric (DTG) curve displaying mass loss rate across temperature; (c) DTG curve overlaid with output of deconvolution. Rate of mass loss values (in b and c) scaled by initial mass of sample. Arrows on (a) and (c) indicate the locations of the peaks of the three deconolved curves. Line segments 1, 2, and 3 on (b) represent mass loss phases.

$$-\frac{dm}{dT} = \sum_{i=1}^{n} c_i \frac{d\alpha_i}{dT} \tag{3.1}$$

$$m = \frac{M_T}{M_0} \tag{3.2}$$

$$c_i = M_{0i} - M_{\infty i} \tag{3.3}$$

$$\alpha_i = \frac{M_{0i} - M_{Ti}}{M_{0i} - M_{\infty i}} \tag{3.4}$$

where mass (m) is expressed as a fraction of mass at temperature T (M_T) of the initial sample mass (M_0) (Eq. 3.2), c_i is the mass of component i that is decayed (Eq. 3.3), and the mass loss curve of each individual component ($\frac{d\alpha_i}{dT}$) is the derivative of α_i, the conversion of mass at a given temperature (M_{Ti}), from the initial (M_{0i}), given total mass lost between the initial and final ($M_{\infty i}$) temperature for each curve (Eq. 3.4).

Although most of our results can be described with only $n = 3$ peaks, corresponding to a single peak each of hemicelluose, cellulose, and recalcitrant carbon forms, primarily lignin (Park, Kwon & Ryu, 2015), some species yield a second hemicellulose peak at a lower temperature, resulting in $n = 4$ independent peaks. This is because the soluble carbohydrates in plant tissue can take many forms, including xylan, amylose, etc., which apparently degrade at different temperatures (see also Chen et al., 2017; Müller-Hagedorn & Bockhorn, 2007).

In order to use DTG data to estimate the mass fractions of carbon forms, we must determine the shape of $\frac{d\alpha_i}{dT}$. Many different functions have been proposed: the asymmetric bi-Gaussian (Sun et al., 2015), logistic (Barbadillo et al., 2007), Weibull (Cai

& Liu, 2007), asymmetric double sigmoidal (Chen et al., 2017), and the Fraser-Suzuki function (Perejón et al., 2011; Hu et al., 2016). Comparisons of several techniques (Svoboda & Málek, 2013; Perejón et al., 2011; Cheng et al., 2015) found that the Fraser-Suzuki function best fit these kinetic curves, since it allows for asymmetry (a parametric examination of the Fraser-Suzuki function can be found in Fig. B.1). We therefore use the Fraser-Suzuki function to describe the rate expression ($\frac{d\alpha_i}{dT}$; Eq. 3.5) as follows:

$$\frac{d\alpha_i}{dT} = h_i \; exp\Bigg\{ - \frac{ln2}{s_i^2}\Big[ln\Big(1 + 2s_i\frac{T - p_i}{w_i}\Big)\Big]^2\Bigg\} \tag{3.5}$$

where T is temperature (°C), and the parameters h_i, s_i, p_i, and w_i are height, skew, position, and width of the curve, respectively. In total, our model estimates 12 or 16 parameters, one for each parameter of Eq. 3.5 for either 3 or 4 primary components.

We used non-linear optimisation using residual sum of squares to fit the rate expression (as in Cheng et al., 2015). Starting values were selected based on curves depicted in the literature (Müller-Hagedorn & Bockhorn, 2007) and from the results of running an identical deconvolution on pure cellulose and lignin samples. Hemicelluloses decay in a reasonably narrow band beginning at a lower temperature (Müller-Hagedorn & Bockhorn, 2007), so we used 270 for position and 50 for width. Linear cellulose crystals decay at a higher temperature, but decay more rapidly after peak temperatures are reached, so starting position was set to 310 and width to 30. Lignin typically decays beginning at a high temperature and over a wide interval (Chen et al., 2015), so position and width began at 410 and 200, respectively.

Once each biomass carbon component's curve parameters have been fit, we can calculate the weight in the overall sample by integrating under the curve (expressed as weight %; Eq. 3.6). To estimate the uncertainty of the weight predictions of the litter samples we calculated the 95% interval of the weight estimates across a random sample of parameter estimates, drawn in proportion to their likelihood. We assumed a truncated multivariate normal distribution, since the parameters are constrained to positive values, using the modelling package *tmvtnorm* (Wilhelm & G, 2015).

$$\alpha_i = \int_{120}^{650} h_i \; exp\Bigg\{ - \frac{ln2}{s_i^2}\Big[ln\Big(1 + 2s_i\frac{T - p_i}{w_i}\Big)\Big]^2\Bigg\} dT \tag{3.6}$$

We interpret that the curve located around 250–270 °C corresponds to primary hemicelluloses (HC-2), around 310–330 °C to cellulose (CL), and around 330–350 °C to lignin (LG). If present, the fourth curve located below 200 °C corresponds to the most simple hemicelluloses (HC-1). In our later analyses the hemicelluloses trait (HC) refers to the sum of HC-2 and, if present, HC-1.

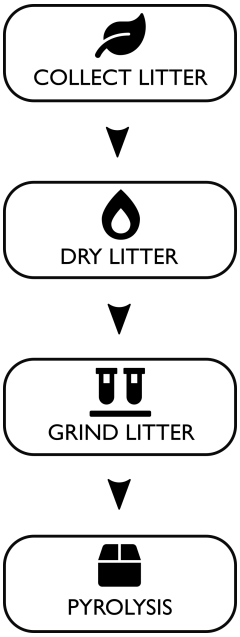

Figure 3.3: Data preparation and thermogravimetric analysis. We collected the litter from three freshwater wetlands surrounding Melbourne, Victoria (sites within 60 km of -37.455, 144.985). In the field, we placed the plant litter in moist plastic bags and stored them in dark coolers until we could transport them to the lab, where they were promptly dried at 60 °C for 72 hours. We ground our dry litter to <40 μm using a Retsch Centrifugal Mill ZM200. We pyrolysed 10–20 mg subsamples of dry, ground litter in an N_2 environment from 30–800 °C at a temperature ramp of 10 °C/min using a Netzsch TGA-FTIR thermogravimetric analyser (Department of Biomedical Engineering, University of Melbourne).

Data analysis

We fit the mixture model and associated analyses using functions available in our R package *mixchar* (Windecker & Golding, 2018). We optimised our starting values using the package *minpack.lm* (Elzhov et al., 2016). We used a correlation-based Principal Components Analysis (PCA) and pair-wise linear regressions to compare carbon components (HC, CL, and LG) with the plant economics traits (LAM, DMC, N, and C).

To examine evolutionary patterns in trait values among these species, we created a phylogeny, and compared branch length, 'patristic', distance to trait distance using the Mantel Test (Mantel, 1967). Genetic sequences for the rbcL and matK gene were accessed from GenBank (Table B.1). In those cases where both gene regions are not available for a species, a sequence of a species from the same genus was used. Sequences for each gene were aligned in Geneious 10.2.3 (Kearse et al., 2012) using the MAFFT (Katoh & Standley, 2013) plugin, the alignments were trimmed to reduce missing data, and subsequently concatenated. We constructed the phylogeny with the MrBayes (Ronquist et al., 2012) plugin in Geneious using the following parameters: GTR+I+G model; genes partitions unlinked; and chain run for 1 million generations

with a 100,000 generation burn-in. We obtained a 50% majority rule consensus tree, which we used for subsequent analyses.

Our analyses were conducted within the statistical computing environment, R (R Core Team, 2013).

3.3 Results

Partitioning of litter organic matter

Across all 29 species, the negative first derivative thermogravimetric deconvolution resulted in three or four consistent peaks (Fig. 3.4; all species in Fig. B.2–B.5). Four species had a fourth peak, which represents an additional hemicellulose type that decayed below 220 °C (*Cycnogeton procerum*, *Cyperus eragrostis*, *Marsilea drumondii*, and *Meuhlenbeckia florulenta*). The hemicellulose peak common to all samples occurred at a mean temperature of 264 °C with a standard deviation of 12 °C (Table B.2). Cellulose curves across all species peaked at a mean of 318 °C (SD 9 °C) and had the narrowest width (34 °C), when we compare to the two hemicelluloses (62 and 63 °C, respectively) and to lignin (242 °C; Table B.2). Lignin curves, in addition to being the widest, also occurred at the highest temperature (mean 336 °C and SD 12 °C; Table B.2).

The data obtained from decomposing the raw cellulose were best predicted by a single Fraser-Suzuki curve with a mean position of 276 °C, 33 °C width, and 0.0108 $°C^{-1}$ height (Fig. B.6). The lignin data were best predicted by a single curve with a mean position of 368 °C, 153 °C width, and 0.0027 $°C^{-1}$ height.

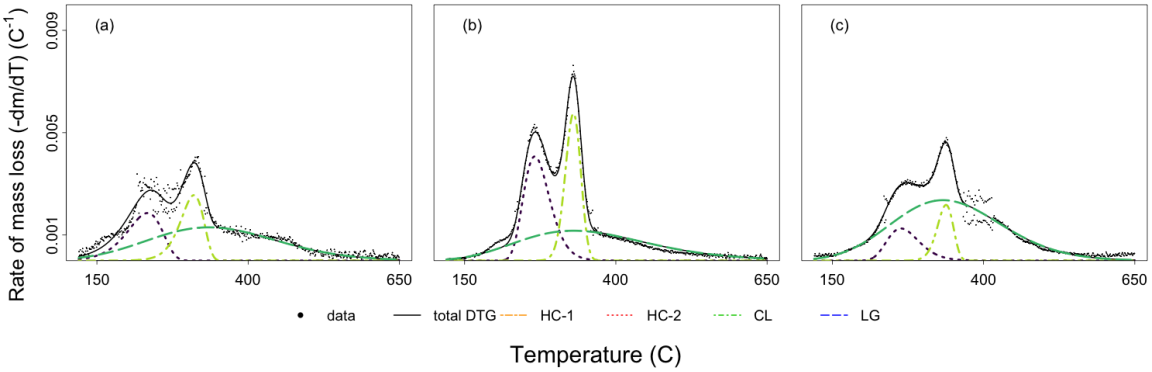

Figure 3.4: Output of deconvolution of thermogravimetric analysis curves for three example species (heating rate = 10°C/min). Rate of mass loss (DTG) values scaled by initial mass of sample. (a) *Nymphaea alba*, an amphibious fluctuation-responder forb; (b) *Restio tetraphyllus*, an amphibious fluctuation-tolerator graminoid; and (c) *Melaleuca squarrosa*, a terrestrial dry tree.

Although the width and position parameters for individual biomass carbon curves

were consistent among plant species, the height of the curves varied, changing the estimated weight of biomass components. Litter hemicelluloses and cellulose displayed a similar pattern by functional group. Amphibious fluctuation-tolerators and terrestrial damp species, the two intermediate functional groups along a spectrum of inundation tolerance, both had higher hemicelluloses and cellulose proportions than either amphibious fluctuation-responders or terrestrial dry species (Fig. 3.5e–f). Lignin was highest in terrestrial dry species, which is predominantly composed of tree species.

Overall, we found the lowest weight of lignin in the diminutive aquatic grass, *Paspalum distichum* (22.2 wt%; Table 3.3), and the highest in the woody acacia, *Acacia dealbata* (55.7 wt%; Table 3.3). Lignin was also quite high in the *Sphagnum*, which may be attributed to lignin-like phenolics (Bengtsson, Rydin & Hájek, 2018; Kremer et al., 2004). Hemicelluloses followed a reverse pattern, in which *A. dealbata* had the lowest total weight and the exotic sedge *C. eragrostis* the highest (7.8 and 31.1 wt%; Table 3.3). Cellulose was lowest in the Australian river red gum, *Eucalyptus camaldulensis* (7.2 wt%; Table 3.3), and highest again in *P. distichum* (31.1 wt%; Table 3.3).

Traits related to plant economics spectrum

Morphological and chemical traits related to the plant economics spectrum varied considerably among the 29 species studied. Despite the variation among amphibious fluctuation-responders, nearly all had higher LAM and N than other functional groups (Fig. 3.5a,c). Litter dry matter content (DMC) was lowest for the amphibious fluctuation-responders, and increased across functional groups as tolerance to inundation decreased (Fig. 3.5b). Litter C followed a fairly similar pattern to DMC (Fig. 3.5d).

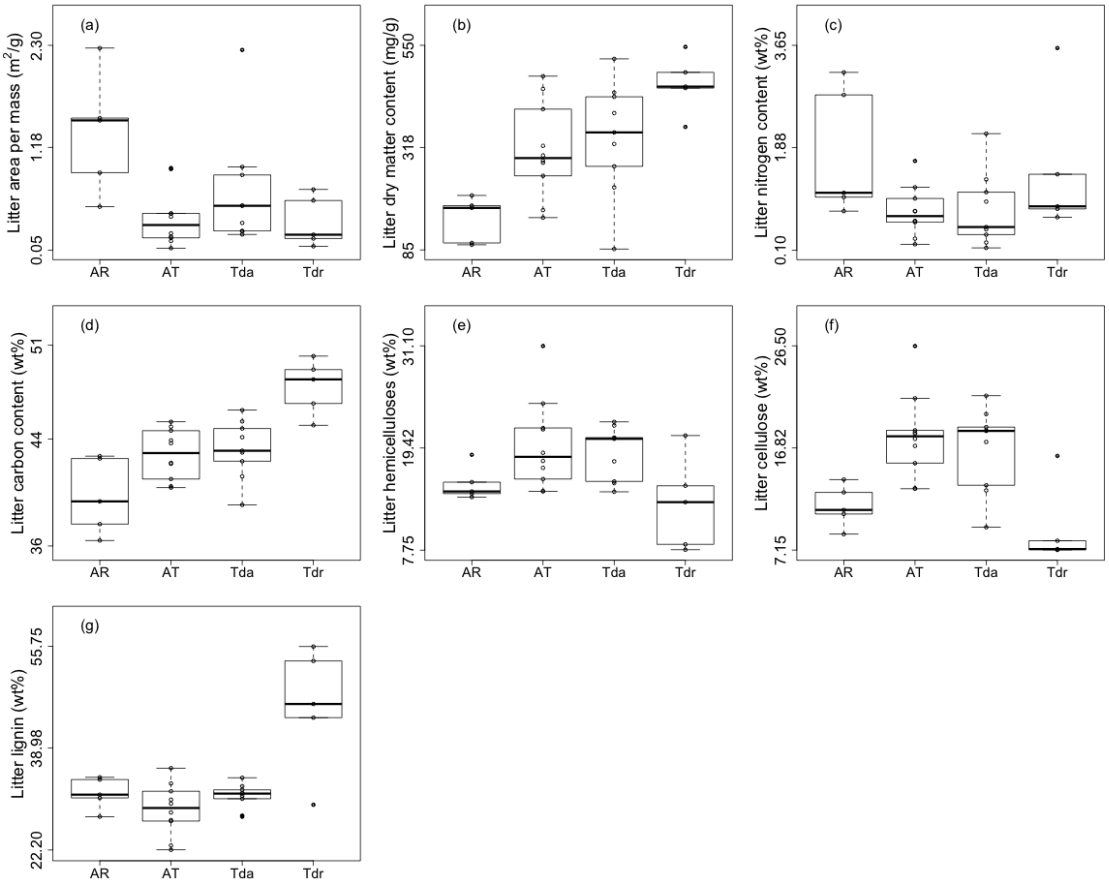

Figure 3.5: Boxplots of traits by functional group: (a) litter area per mass (m^2/g); (b) dry matter content (mg/g); (c) nitrogen content (wt%); (d) carbon content (wt%); (e) hemicelluloses (wt%); (f) cellulose (wt%); and (g) lignin (wt%) for amphibious fluctuation-responders (AR; n = 5), amphibious fluctuation-tolerators (AT; n = 11), terrestrial damp species (Tda; n = 8), and terrestrial dry species (Tdr; n = 5). Bold lines represent median values, boxes represent the interquartile range, and whiskers represent minimum and maximum values within 1.5 times the interquartile range.

TABLE 3.3: Trait values for all species. LAM and DMC values represent the average of 10 separate samples. Biomass carbon traits, N, and C values represent the estimates from a single subsample of the pooled biomass of all 10 litter samples. Biomass carbon traits are presented with lower and upper 95% confidence intervals of model estimates in brackets. Not all species had a second hemicellulose peak (HC-1).

				economics spectrum traits				Biomass carbon traits			
Family	Species	Functional group	Growth form	LAM (m^2/g)	DMC (mg/g)	N (wt%)	C (wt%)	HC-1 (wt%)	HC-2 (wt%)	CL (wt%)	LG (wt%)
Amaranthaceae	*Alternanthera denticulata*	Tda	Forb	0.54	275	1.3	41.2		15.6 [8.7, 26]	17.4 [13.1, 22]	32.7 [26.3, 39.4]
Crassulaceae	*Crassula helmsii*	AR	Forb	1.48	97	0.8	36.4		14.2 [0.7, 29.9]	8.7 [0, 29.9]	31.3 [29.4, 33.1]
Cyperaceae	*Baumea articulata*	AT	Graminoid	0.20	322	0.6	44.9		21.7 [20, 23.6]	21.5 [19.9, 23.1]	28.4 [26.8, 30]
Cyperaceae	*Baumea rubiginosa*	AT	Graminoid	0.24	405	0.2	42.1		24.5 [22.9, 26.2]	17 [16.2, 17.8]	27 [25.6, 28.3]
Cyperaceae	*Carex appressa*	Tda	Graminoid	0.26	396	0.5	42.3		20.6 [18.9, 22.4]	20 [18.4, 21.6]	27.7 [25.8, 29.6]
Cyperaceae	*Carex fascicularis*	AT	Graminoid	0.45	300	0.8	42.2		15.9 [13.8, 18.4]	18.5 [16.5, 20.7]	27.1 [24.9, 29.5]
Cyperaceae	*Cyperus eragrostis*	AT	Graminoid	0.42	253	0.6	40.5	5.7 [4.9, 6.6]	25.3 [21.4, 29.9]	13 [12.1, 14]	22.9 [18.4, 27.2]
Cyperaceae	*Eleocharis acuta*	AT	Graminoid	0.94	158	1.6	41.0		14.5 [12.7, 16.5]	18.2 [16.2, 20.1]	31.9 [30.3, 33.5]
Cyperaceae	*Gahnia filum*	Tda	Graminoid	0.22	433	0.2	44.1		22 [1.5, 58.8]	21.8 [2, 64.1]	27.9 [25.7, 30.1]
Fabaceae	*Acacia dealbata*	Tdr	Tree	0.60	365	3.6	50.2		7.8 [4.6, 12.4]	8 [4.8, 12.8]	55.7 [53.3, 58.3]
Haloragaceae	*Myriophyllum crispatum*	AR	Forb	0.53	180	1.1	39.3		14.5 [11.4, 18.4]	10.6 [7.4, 14.7]	27.7 [24.1, 30.8]
Juncaceae	*Juncus amabilis*	AT	Graminoid	0.15	451	0.8	45.3		21.6 [20.4, 22.8]	17.7 [16.6, 18.7]	30.5 [29.3, 31.7]
Juncaceae	*Juncus procerus*	Tda	Graminoid	0.26	352	0.5	43.1		20.5 [18.3, 22.8]	13.3 [12.3, 14.3]	32.1 [30.2, 34]
Juncaginaceae	*Cycnogeton procerum*	AR	Graminoid	0.90	101	3.2	37.6	6.2 [0.7, 19.8]	9.3 [7.3, 12]	11 [10, 11.9]	33.8 [22.3, 41.8]
Lamiaceae	*Lycopus australis*	Tda	Forb	0.88	326	0.9	45.3		14.4 [1.1, 61.2]	18.8 [0, 44.3]	34.1 [21.3, 45.6]
Marsileaceae	*Marsilea drummondii*	AR	Forb	2.27	209	1.0	42.5	4.8 [2.7, 7.4]	13.8 [6, 24.1]	13.8 [6.3, 25.5]	30.8 [25.4, 35.4]
Myrtaceae	*Eucalyptus camaldulensis*	Tdr	Tree	0.72	453	1.4	48.5		15.1 [9.8, 21.4]	7.2 [5.3, 9.4]	44 [37.8, 49.4]
Myrtaceae	*Melaleuca ericifolia*	Tdr	Tree	0.22	456	0.8	46.7		13.2 [10.4, 16.5]	7.2 [6.2, 8.2]	46.2 [43.6, 48.6]
Myrtaceae	*Melaleuca squarrosa*	Tdr	Tree	0.18	489	0.7	49.2		8.4 [6.3, 11]	7.2 [6.2, 8.3]	53.3 [50.8, 56]
Nymphaeaceae	*Nymphaea alba*	AR	Forb	1.50	186	2.8	42.7		13.8 [10.4, 18.1]	12.6 [10.6, 15.1]	34.2 [28.8, 39.4]
Poaceae	*Paspalum distichum*	AT	Graminoid	0.07	283	0.3	40.4		17.9 [7, 30.7]	26.5 [16, 39.6]	22.2 [20.2, 24.4]
Poaceae	*Phragmites australis*	AT	Graminoid	0.19	480	1.2	44.6		18.9 [17.1, 20.8]	18.3 [17.1, 19.5]	33.1 [31.7, 34.6]
Polygonaceae	*Meuhlenbeckia florulenta*	Tdr	Shrub	0.09	546	0.9	45.0	1.5 [0.1, 8.5]	19.3 [10.9, 31.2]	16.1 [13.6, 18.5]	29.6 [18.1, 39.2]
Polygonaceae	*Persicaria decipiens*	AT	Forb	0.95	176	0.6	43.7		17.2 [1.2, 36.4]	13 [0.8, 38.5]	29.8 [26.9, 32.8]
Polygonaceae	*Persicaria prostrata*	Tda	Forb	0.97	227	1.1	44.8		20.6 [6.4, 36]	12.8 [1, 34.7]	31.5 [27.1, 35.5]
Polygonaceae	*Rumex crispus*	Tda	Forb	2.25	87	2.1	39.1		15.4 [11.9, 19.7]	9.3 [6.9, 11.9]	31.6 [26, 36.3]
Restionaceae	*Restio tetraphyllus*	Tda	Graminoid	0.35	443	0.1	46.2		22.4 [21.4, 23.4]	18.5 [17.7, 19.2]	31.1 [30, 32.3]
Sphagnaceae	*Sphagnum sp*	Tda	Non-vascular	0.54	519	0.4	43.0		17.9 [13.7, 23.1]	18.4 [15.1, 22.3]	30.6 [28.7, 32.4]
Typhaceae	*Typha domingensis*	AT	Graminoid	0.45	288	1.0	43.9		14.5 [13, 16.2]	15.4 [14.5, 16.2]	35.7 [34.3, 37]

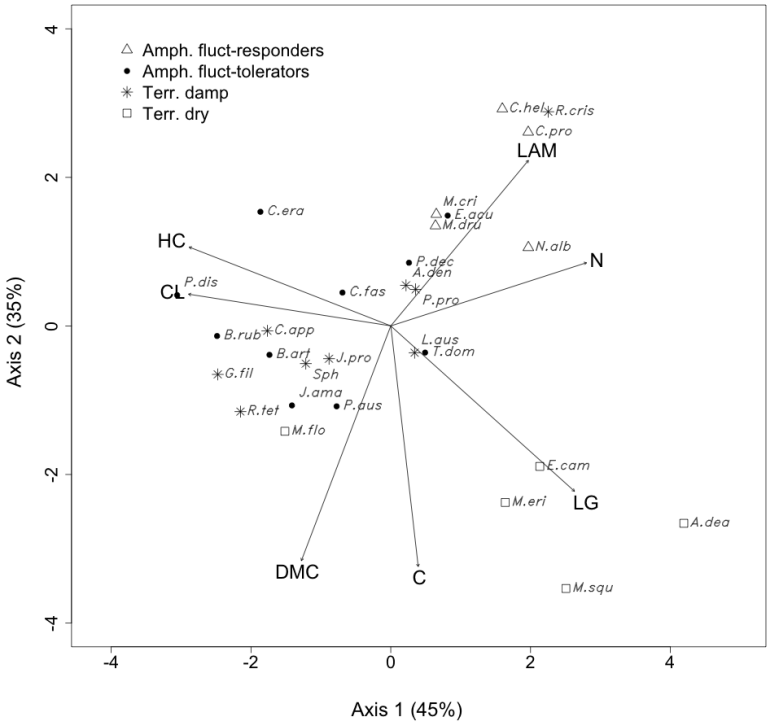

Figure 3.6: Principal Component Analysis of traits. Species' labels are the genus abbrevation and first three letters of species name.

Litter traits phylogeny

Only LAM was significantly (P = 0.01; Table B.3) correlated with branch length distance, indicating that those species with closer relatives have more similar LAM (Fig. B.7).

Multivariate patterns between fast–slow economics spectrum and biomass carbon traits

The first two axes of the PCA account for 80% of total variation among the species (45% for axis 1 and 35% for axis 2; Table B.4). Economics spectrum traits (LAM, DMC, and N) appear aligned, and correlate positively with one another. LAM and N (R^2 = 0.43) and DMC and C (R^2 = 0.7) are positively correlated with one another. As expected, LAM is negatively correlated with DMC (R^2 = -0.69) and with C (R^2 = -0.38), and N is negatively correlated with DMC (R^2 = -0.41; Fig. B.8). Biomass carbon components (HC, CL, and LG; Fig. 3.6) also appear aligned, and correlate accordingly. HC is positively correlated with CL (R^2 = 0.47), and both HC and CL correlated negatively with LG (R^2 = -0.73 and R^2 = -0.65, respectively; Fig. B.8).

Economics spectrum traits and biomass carbon components lie perpendicular to one another in multivariate trait space (Fig. 3.6). Although there is coordination

within each of these groupings, this orthogonality suggests that variation in one is not coupled to variation in the other. Functional groups are dispersed widely throughout trait space, but growth forms are clustered: tree species are aligned with the LG vector, graminoids are characterised by higher DMC and CL, and forbs are clustered around high LAM and N.

3.4 Discussion

Orthogonality of nutrient and biomass carbon trait axes

As expected according to LES theory (Wright et al., 2004; Diaz et al., 2004), and due to recognised coordination of traits between plant parts (Jackson, Peltzer & Wardle, 2013; Maire et al., 2013), we observed a coordinated axis of variation for litter traits between plant species with low LAM and high N and species with high DMC. We found that litter from our sample of wetland plant species were composed primarily of either more labile carbons, such as hemicelluloses and cellulose, or more complex lignin (Fig. 3.6). This division according to carbon complexity (Godshalk & Wetzel, 1978) lay orthogonal to coordination among morphological and chemical traits. Eviner (2004) similarly found labile carbon inputs and litter mass to be independent of each other, both of which relate to plant effects on soil carbon. Multidimensionality has also been observed in root traits: plants can construct roots with high or low specific root length of any tissue density (Kramer-Walter et al., 2016).

Growth forms cluster in multivariate trait space (Dorrepaal, 2007) and demonstrate different combinations of the extremes defined by our two observed axes of variation. Forb species tended to have nitrogen-rich tissue, reflecting a nutrient acquisitive strategy for investment in short-lived tissue primarily built for photosynthesis (Reich, 2014), and dominated by simple hemicellulose carbons (Chiariello, Mooney & Williams, 1989). Litter of graminoid species also invested in relatively labile carbon in the form of cellulose, but had high DMC, and low LAM and N, reflecting a nutrient conservative strategy associated with investment in structurally supportive tissue necessary for emergent vegetation (Rose & Crumpton, 1996). Tree species had higher amounts of complex lignin and also exhibited a more nutrient conservative strategy. These trait differences may reflect species' diverging strategies to respond to the same ecophysical structural requirements in wetland and riparian systems (Britson, Wardrop & Drohan, 2016) and match research suggesting growth forms do well at predicting decomposition rate across diverse species (Dorrepaal et al., 2005).

Phylogenetic conservatism does not appear to explain the trait correlations and ordinations we found, because only LAM was weakly correlated to phylogenetic tree distance (Table B.3). Although some previous research has found evidence of phylogenetic structuring, such as across fine root morphology traits (Valverde-Barrantes, Smemo & Blackwood, 2015), trait conservatism across clades is highly variable, so our result is not surprising and not definitive (Cornwell & Weedon, 2014). We must acknowledge the impact of measurement error in both the trait values as well as the phylogenetic branch lengths that could impact our ability to detect a relationship

(Ives, Midford & Garland, 2007). Future work would benefit from comparison between phylogram and chronogram techniques and from comparing across more species (Elliott, Knerr & Schmidt-Lebuhn, 2018).

Our study focused on wetland plant species because of relatively rapid sequestration of litter carbon in wetland systems and their relevance for global greenhouse gas emissions (Bridgham et al., 2006). Due to both acknowledged heterogeneity in plant economics spectrum trends across biomes (Wright et al., 2005), and to the specific set of constraints on a species' strategy in wetland systems (Moor et al., 2017), these results may be particular to freshwater and/or riparian systems (Catford & Jansson, 2014).

Implications for trait decomposition research

The orthogonal relationship between litter quality, defined by nitrogen levels and correlated with LAM and DMC, and litter carbon complexity define two independent aspects of litter recalcitrance. Empirical decay research supports this conclusion, as frequently it is a combination of leaf economics traits and immobile carbon chemistry that predict decay (Britson, Wardrop & Drohan, 2016; Cornelissen et al., 2001; Cornwell et al., 2008; Cornwell & Weedon, 2014; Freschet, Aerts & Cornelissen, 2012a; Jackson, Peltzer & Wardle, 2013). Nitrogen-rich litter decomposes more quickly because it supports faster microbial decomposition (Cornwell et al., 2008). But nitrogen-rich litter could be associated with tissue composed of either predominantly labile or recalcitrant carbon (Britson, Wardrop & Drohan, 2016). Multiple traits are required to understand a plant species' effect on decay, as one spectrum alone is not a substitute for the other.

TGA holds great promise for biomass carbon trait estimation

The mixture model applied in our study produces DTG curves that match those presented in the literature for similar biomass samples, (for example in eucalypts Órfão & Figueiredo, 2001). Weight estimates of biomass carbon traits derived from these predicted curves are also reasonable, but wide confidence intervals in some species suggest the DTG curve is not always confidently resolved (Fig. B.2–B.5). In particular, DTG curves with a less defined cellulose peak appear more sensitive to starting values or specification of parameter distribution, despite use of starting values that well predicted pure cellulose and lignin mass loss data (Fig. B.6). Considering the opportunities for rapid inter-species biomass carbon comparisons (Trevathan-Tackett et al., 2015), we recommend further investigation to test and standardise the TGA methodology.

3.5 Conclusion

We found that species vary in their investment in carbon components along a spectrum from complex lignin to simple cellulose and hemicellulose. This variation in carbon

investment is perpendicular to variation in LES traits that reflect fast–slow strategies for other ecosystem processes. This decoupling of attributes of litter recalcitrance suggests a multi-trait approach will therefore be essential for understanding species' litter recalcitrance and effects on ecosystem functions such as decomposition and soil carbon stock.

3.6 Acknowledgements

The authors would like to thank volunteers Paula Sanchez, Abbey Kinnish, Kelsey Johnson, Francesca Dina, Madeline Brenker, and Urtzi Enriquez Urzelai for assistance in the field, Dr James Camac for assisting with the reproducible workflow, Dr Todd McLay for constructing the species' phylogeny, and the University of Melbourne Department of Chemical and Biomolecular Engineering for training and access to the TGA-FTIR and LECO Elemental Analyser. Vegetation collection was conducted under Victorian Department of Environment, Land, Water and Planning Permit No 10007429. We thank the Australian Research Council Centre of Excellence for Environmental Decisions, the Holsworth Wildlife Research Endowment & the Ecological Society of Australia, and the Melbourne International Research Scholarship and Melbourne International Fee Remission Scholarship for support.

4

mixchar: An R package for the deconvolution of thermal decay curves

Abstract

Plant cell wall biomass is composed of a range of different types of carbon-based compounds. The proportions of the primary carbon types affect how cell walls decompose, an important ecosystem process because their decay contributes to soil carbon. Traditional methods of calculating these components involve wet chemistry methods that can be costly and degrade the environment. Thermogravimetric analysis is an alternative method, already used by biofuel researchers, that involves pyrolysing dry, ground plant litter and estimating contribution of carbon components from a resulting mass decay curve. Because carbon types break down relatively independently, we can apply a mixture model to the multi-peaked rate of mass loss curve to identify mass loss of each carbon component. The `mixchar` package conducts this peak separation analysis in an open-source and reproducible way using R. `mixchar` has been tested over a range of plant litter types, composed primarily of the fiber components: hemicellulose, cellulose, and lignin.

This manuscript is in review at the Journal of Open Research Software and is presented in that format here.

Software paper for submission to the Journal of Open Research Software

---

(1) Overview

Title
mixchar: An R package for the deconvolution of thermal decay curves

Paper Authors
1. Windecker, Saras M.
2. Vesk, Peter A.
3. Trevathan-Tackett, Stacey M.
4. Golding, Nick.

Paper Author Roles and Affiliations
1. Research Fellow, School of BioSciences, University of Melbourne, Parkville VIC 3010, Australia
2. Associate Professor, School of BioSciences, University of Melbourne, Parkville VIC 3010, Australia
3. Research Fellow, Deakin University, Geelong, Centre for Integrative Ecology, School of Life and Environmental Sciences, Burwood VIC 3125, Australia
4. Research Fellow, School of BioSciences, University of Melbourne, Parkville VIC 3010, Australia

Abstract
Plant cell wall biomass is composed of a range of different types of carbon-based compounds. The proportions of the primary carbon types affects how cell walls decompose, an important ecosystem process because their decay contributes to soil carbon. Traditional methods of calculating these components involve wet chemistry methods that can be costly and degrade the environment. Thermogravimetric analysis is an alternative method, already used by biofuel researchers, that involves pyrolysing dry, ground plant litter and estimating contribution of carbon components from a resulting mass decay curve. Because carbon types break down relatively independently, we can apply a mixture model to the multi-peaked rate of mass loss curve to identify mass loss of each carbon component. The `mixchar` package conducts this peak separation analysis in an open-source and reproducible way using R. `mixchar` has been tested over a range of plant litter types, composed primarily of the fiber components: hemicellulose, cellulose, and lignin.

Keywords
biofuel; carbon; decomposition; Fraser-Suzuki; kinetics; mixture model; plant traits; thermogravimetric analysis

Introduction

Plant cell wall biomass is composed of a range of different types of carbon-based compounds [3, 16, 11]. We can use the relative proportion of these carbon components to understand species characteristics, such as litter decomposition [6]. Traditional methods for calculating lignocellulosic biomass involve wet chemistry assays for carbon component analysis [8] through the use of sulfuric acid and acetic anhydride, among other chemicals. These chemicals, however, can adversely impact the environment and lead to loss of lignocellulose and other compounds [10]. Thermogravimetric analysis (TGA) is an alternative method, already in use among biofuel researchers, to approximate these plant fiber compounds [11, 5]. In this method, we use mass loss data obtained by heating a biomass sample in an N_2 environment, termed pyrolysis, to estimate the different carbon components.

Mass loss during complete pyrolysis is the sum of the degradation of the main components of the sample, often simplified to the three main components of lignocellulose: hemicelluloses, cellulose, and lignin [18, 16, 15]. The rate of mass loss is generally a multi-peaked curve, that can then be mathematically separated into its constituent parts with a mixture model, in a process termed 'deconvolution' [17, 13]. The component peaks identified by the mixture model represent the proportion of initial mass of each component lost during pyrolysis. The integral, or area under the peak, therefore gives us an estimate of the proportion of that component in the overall sample. A number of studies have validated this approach, using thermogravimetric analysis with deconvolution, with studies comparing its estimates of carbon components to those achieved with wet chemistry measurements [27]. Other researchers have also previously used this method to identify plant species' recalcitrance, such as in marine and coastal macrophytes [25], and in eucalyptus trees [16].

For the most part, researchers have used commercial software to deconvolve the rate of mass loss curve [for example OriginPro 3, PeakFit 18, Fityk 18, or Datafit 5]. The majority of proprietary software employ point-and-click interfaces that prevent independent replication of the deconvolution analysis. The inability of other researchers to reproduce readily another's experimental results using this software, a guiding principle of functional trait measurement [19], might in part explain why thermogravimetric analysis has not been widely adopted by functional ecologists.

The `mixchar` package in R is an open-source tool for the deconvolution of thermal decay curves from thermogravimetric analysis. Although the nonlinear mixture model used for peak separation at the core of this package could be used for many different purposes, our `mixchar` package provides specific guidelines for using thermal decay curve analysis to estimate carbon components. Detailed vignettes and several default plotting options are included in `mixchar` so that researchers interested in adopting this method can readily do so for the purpose of estimating carbon components in plant biomass samples.

Implementation and architecture

Litter collection and preparation

We collected the litter for development of this package from three freshwater wet-

lands surrounding Melbourne, Victoria (sites within 60 km of -37.455, 144.985). We then dried the samples as quickly as possible after collection to ensure our component estimates were an accurate representation of the original composition of the litter samples we collected. In the field, we placed the plant litter collected for this analysis in moist plastic bags and stored them in dark coolers until we could transport them to the lab where they were promptly dried at 60 °C for 72 hours. We ground our dry litter to <40 μm using a Retsch Centrifugal Mill ZM200.

We pyrolysed 10–20 mg subsamples of dry, ground litter in an N_2 environment from 30–800 °C at a temperature ramp of 10 °C/min using a Netzsch TGA-FTIR thermogravimetric analyser (Department of Biomedical Engineering, University of Melbourne).

We developed and tested the functions of our `mixchar` package using the thermogravimetric decay data of the litter of 29 different plant species. Two species from our data are available as datasets in the package —the freshwater reed *Juncus amabilis* (accessed as `juncus`) and the freshwater fern *Marsilea drumondii* (accessed as `marsilea`). The data resulting from the pyrolysis is mass loss (mg) against temperature (Fig. 1).

```
library(mixchar)
head(juncus)

##   temp_C mass_loss
## 1 31.453 -0.000931
## 2 31.452 -0.001340
## 3 31.450 -0.001350
## 4 31.450 -0.001660
## 5 31.450 -0.001680
## 6 31.450 -0.001800
```

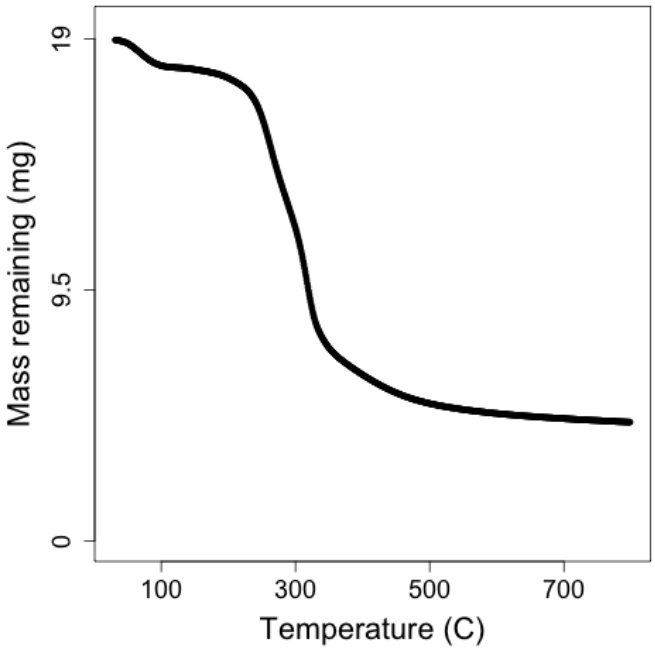

Figure 1 Mass across temperature for *Juncus amabilis*.

Deconvolution using mixchar

Rate of mass loss

After completing the thermogravimetric analysis, the resulting data can be loaded into R. Using `mixchar`, the `process` function calculates the rate of mass loss by taking the derivative of mass loss over temperature data. To do so, `process()` needs the following dataset features: the initial mass of the sample, the name of the temperature data column, and the name of the mass column (mg). Since TGA-FTIR instruments can export data in variable units, the mass column can be specified either as mass loss data with the `mass_loss` argument or as mass data with the `mass` argument.

```
deriv_juncus <- process(juncus,
                        init_mass = 18.96,         # initial mass of sample
                        temp = 'temp_C',           # temperature data column name
                        mass_loss = 'mass_loss',   # mass loss data column name
                        temp_units = 'C')          # 'C' is the default setting
deriv_juncus

## Derivative thermogravimetry data (DTG) calculated for
##  768 datapoints from 31.5 to 798.52 degrees C.
```

The `process` function produces the modified dataframe, which includes the derivative thermogravimetric rate of mass loss data (DTG), the initial mass value that was supplied, and the maximum and minimum temperature values in the data. Plotting the output of the `process` function yields the mass of sample across temperature curve (Fig. 1) and the rate of mass loss curve (Fig. 2). The rate of mass loss is a multi-peaked curve encompassing three main phases [16]:

1. A short period with a pronounced peak of moisture evolution, up until approximately 120 °C.

2. A wide mid-range of high mass loss, caused by devolatilisation of primary biomass carbon components, between approximately 120–650 °C.

3. A final period of little mass loss when carbonaceous material associated with the inorganic fraction combusts, after approximately 650 °C.

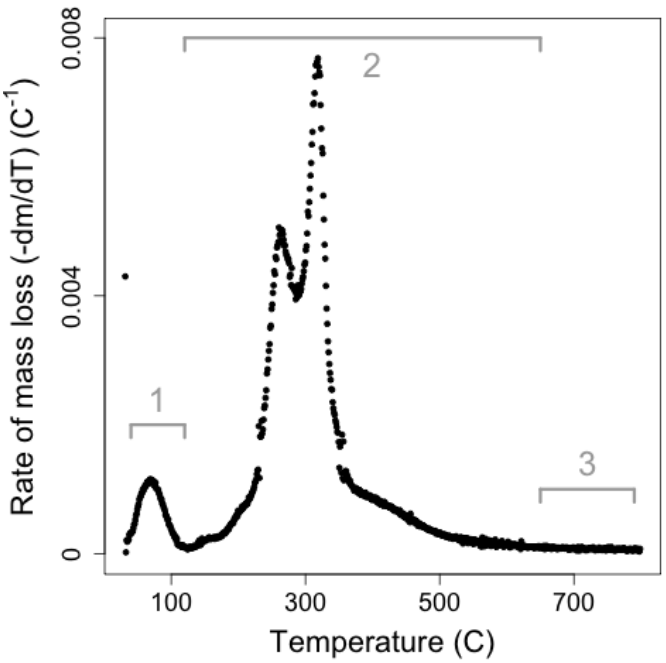

Figure 2 Derivative thermogravimetric rate of mass loss across temperature, scaled by initial mass of sample for *Juncus amabilis*. Line segments 1, 2, and 3 represent mass loss phases.

Subset DTG data

Since the overall DTG curve represents the loss of extractives, water, inorganic matter, and volatiles in addition to the components in which we are interested [11], we isolate mass loss from our primary biomass components by subsetting the DTG data to Phase 2. The `deconvolve` function defaults to temperature bounds at 120 °C and 700 °C, but these can be modified with the `lower_temp` and `upper_temp` arguments.

Non-linear mixture model

Biomass components combust relatively independently because they do not interact very much during thermal volatilisation [27]. Therefore, the subsetted DTG curve can be mathematically deconvolved into constituent parts using a mixture model. The derivative rate of mass loss equation ($\frac{dm}{dT}$) can be expressed as the sum of n independent reactions (Eq. 1), as follows [16]:

$$-\frac{dm}{dT} = \sum_{i=1}^{n} c_i \frac{d\alpha_i}{dT} \tag{1}$$

$$m = \frac{M_T}{M_0} \tag{2}$$

$$c_i = M_{0i} - M_{\infty i} \tag{3}$$

$$\alpha_i = \frac{M_{0i} - M_{Ti}}{M_{0i} - M_{\infty i}} \tag{4}$$

where mass (m) is expressed as a fraction of mass at temperature T (M_T) of the initial sample mass (M_0) (Eq. 2), c_i is the mass of component i that is decayed (Eq. 3), and the mass loss curve of each individual component ($\frac{d\alpha_i}{dT}$) is the derivative of α_i, the conversion of mass at a given temperature (M_{Ti}), from the initial (M_{0i}), as a proportion of total mass lost between the initial and final ($M_{\infty i}$) temperature for each peak (Eq. 4).

Although the carbon distribution of many species can be described with only $n = 3$ peaks, corresponding to a single peak for each of hemicelluose, cellulose, and lignin, some litter samples yield a second hemicellulose peak at a lower temperature, resulting in $n = 4$ independent peaks. This is because the soluble carbohydrates in plant tissue can take many forms, including xylan, amylose, etc., which apparently degrade at different temperatures [see also 3, 15]. `deconvolve()` will decide whether three or four peaks are best using an internal function that determines if there is a peak below 220 °C. Alternatively, upon inspection of the curve, users can specify the number of peaks with the `n_peaks` argument.

In order to fit the mixture model to the data, we must decide upon the shape of the individual peaks ($\frac{d\alpha_i}{dT}$) that are summed to produce it. Many different functions have been proposed: the asymmetric bi-Gaussian [23], logistic [1], Weibull [2], asymmetric double sigmoidal [3], and the Fraser-Suzuki function [18, 11]. Researchers have compared several techniques [24, 18, 5] and found that the Fraser-Suzuki function best fit these kinetic peaks. This is because the Fraser-Suzuki function allows for asymmetry (a parametric examination of the Fraser-Suzuki function can be found in Fig. 3). We therefore use the Fraser-Suzuki function to describe the rate expression of a single peak (Eq. 5) as follows:

$$\frac{d\alpha_i}{dT} = h_i \; exp\Bigg\{ -\frac{ln2}{s_i^2}\Big[ln\Big(1 + 2s_i\frac{T - p_i}{w_i}\Big)\Big]^2\Bigg\} \tag{5}$$

where T is temperature (°C), and the parameters h_i ($^\circ C^{-1}$), s_i, p_i (°C), and w_i (°C) are height, skew, position, and width of the peak, respectively. In total, our model estimates 12 or 16 parameters, one for each parameter of Eq. 5 for either three or four primary components.

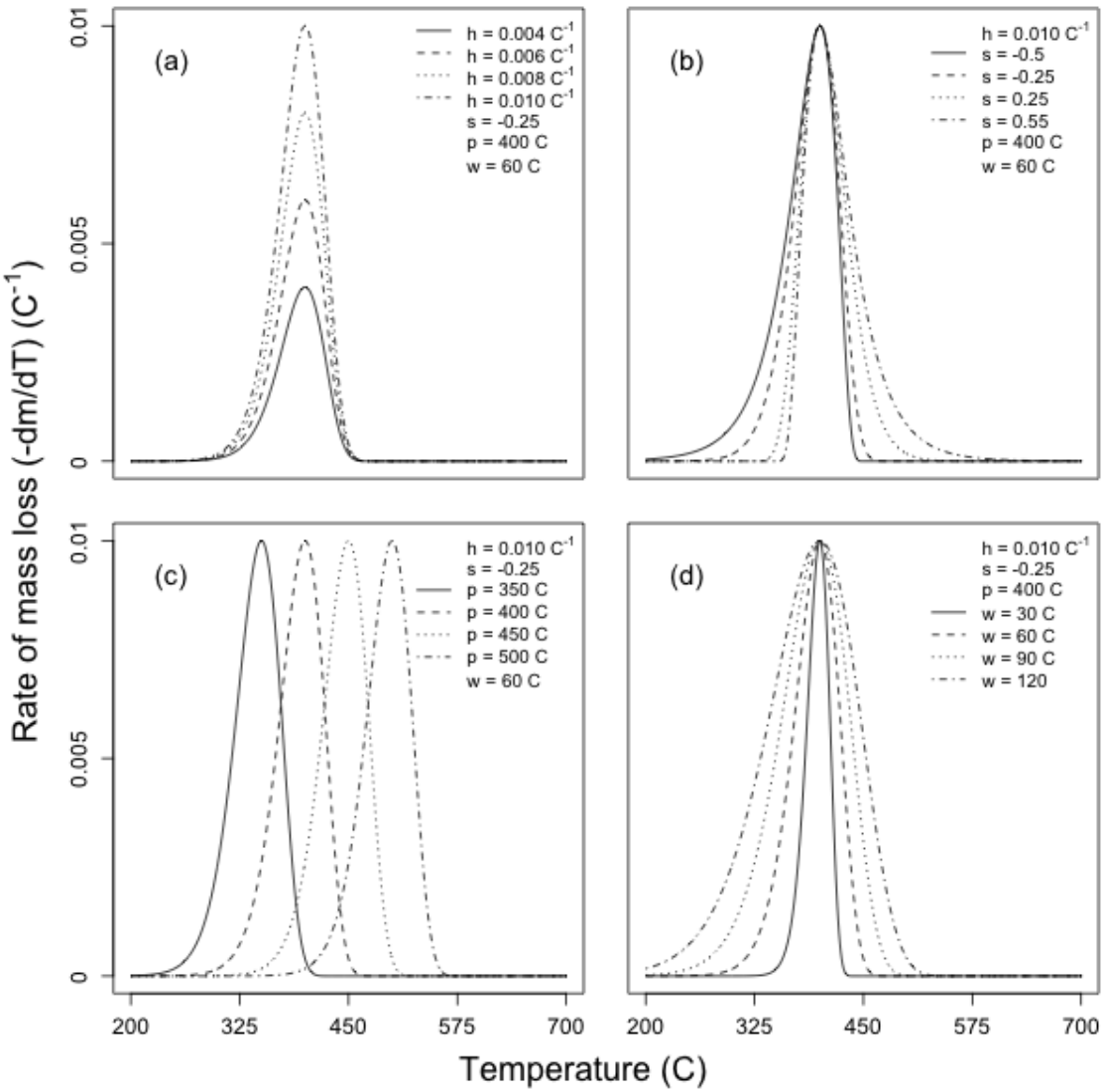

Figure 3 Parametric study of the Fraser-Suzuki function for deconvolution of derivative thermogravimetric biomass curves: Effect of modifying (a) height; (b) skew; (c) position; and (d) width.

Likelihood functions in mixture models have multiple maxima, and therefore expectation-maximisation algorithms are highly dependent on starting value selection [21, 22]. The vector of starting values for the 12 or 16 estimated parameters is based on curves depicted in the literature [15] and from the results of running an identical deconvolution on pure cellulose (carboxy-methyl cellulose) and lignin (alkali lignin from Sigma Aldrich). Hemicelluloses decay in a reasonably narrow band beginning at a lower temperature [15], so we use 270°C for position and 50°C for width. Linear cellulose crystals decay at a higher temperature, but decay more rapidly after peak temperatures are reached, so we set its starting position to 310°C and width to 30°C. Lignin typically decays beginning at a high temperature and over a wide interval [4], so we begin position and width at 410°C and 200°C, respectively.

In an effort to ensure the same starting vector would be useful across a wide variety of different samples, we employ an extra optimisation step before fitting the model. The `deconvolve` function first optimises the given starting value vector with 300 restarts of the `NLOPTR_LN_BOBYQA` algorithm [20] with the `nloptr` [12] package. In this way, we can set the given starting value vector so that it works properly on a wide range of samples, and at the same time the starting values we ultimately give to the model are as close as possible to the global maxima for a given dataset.

To fit the non-linear mixture model, we send the optimised starting value vector to the `nlsLM()` function in the `minpack.lm` [7] package, which uses the Levenberg-Marquardt algorithm to minimise residual sum of squares.

The default starting values and two-stage optimisation worked well for our thermogravimetric decay dataset for 29 plant species, encompassing herbaceous, graminoid, as well as woody species. Although this result is encouraging it is not altogether surprising because these data were pyrolysed using the same TGA-FTIR instrument. For this reason, the package was also tested on thermogravimetric data processed from a different instrument, as well as plants from marine ecosystems. Default settings produced well-fit curves for leaf samples from the seagrass species *Thalassia testudinum*, and rhizome and root samples from the seagrass species *Zostera marina* [Fig. 4; data for both from 25].

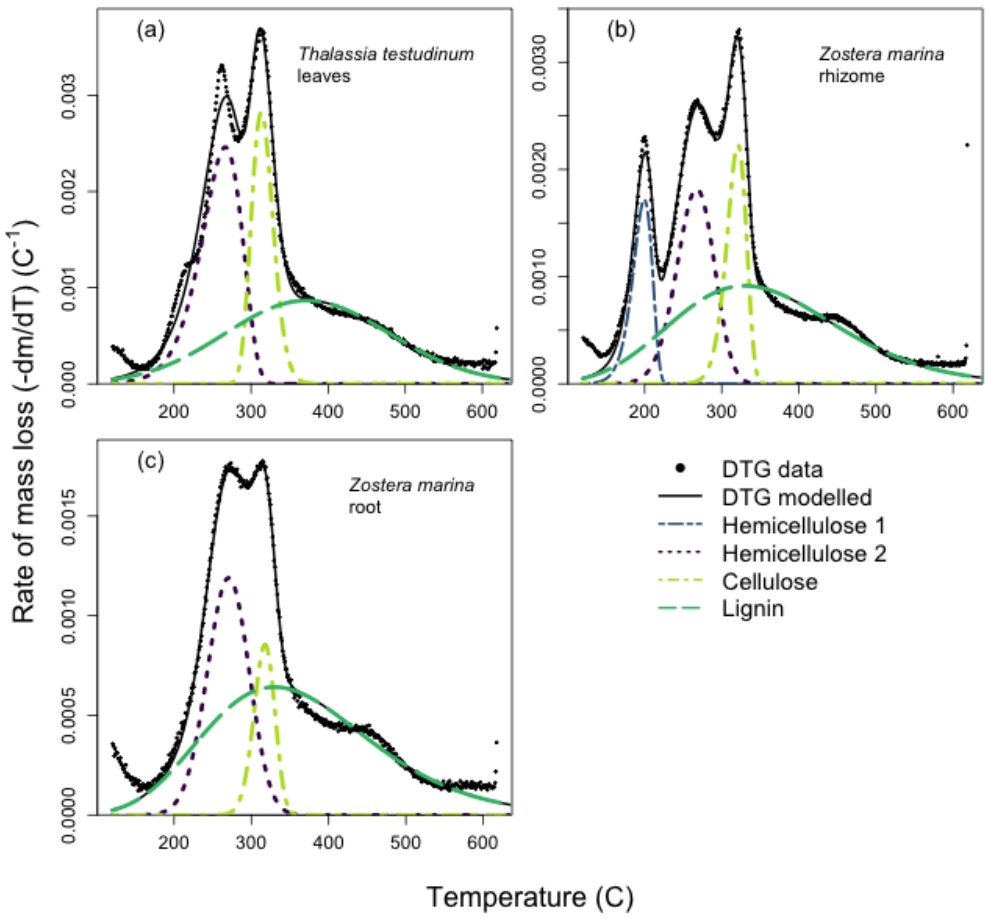

Figure 4 Mass loss and component estimation using default settings for test samples.

Default `mixchar` settings did not, however, perfectly identify the fourth peak in the deconvolution of macroalgae species *Ecklonia radiata* blades [Fig. 5a; 25]. In this case, we can use the option to specify our own starting values, with the `start_vec`, `lower_vec`, and `upper_vec` arguments, in order to better guide the model (Fig. 5b).

```
start_vec <- c(0.002, -0.15, 250, 50,          # for hemicellulose 1
               0.003, -0.15, 310, 50,          # for hemicellulose 2
               0.006, -0.15, 350, 30,          # for cellulose
               0.001, -0.15, 410, 200)         # for lignin

# change the upper bounds to ensure the starting vector values are within
# the allowed range
ub <- c(2, 0.2, 260, 80,
        2, 0.2, 330, 90,
        2, 0.2, 380, 50,
        2, 0.2, 430, 250)

e.radiata_decon <- deconvolve(e.radiata,
                              n_peaks = 4,
                              start_vec = start_vec,
                              upper_vec = ub,
```

```
                                lower_temp = 150,
                                upper_temp = 600)
```

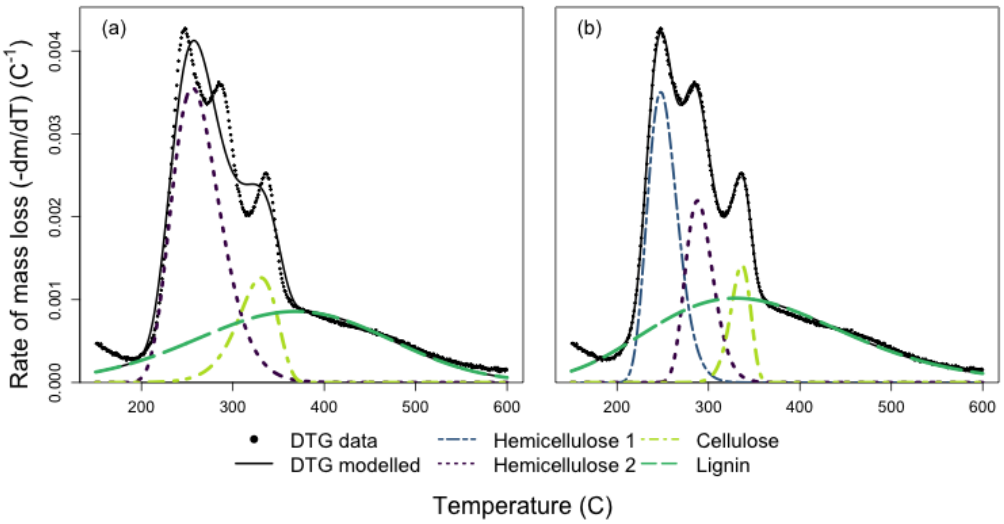

Figure 5 Component estimation for *Ecklonia radiata* blades with default (a) and specified starting values (b).

Component weights
After we fit our curve parameters, we can pass each component's parameter estimates to a single Fraser-Suzuki function and integrate under the peak to calculate the weight of the component in the overall sample (Eq. 6). To estimate the uncertainty of the weight predictions, `deconvolve` will calculate the 95% interval of the weight estimates across a random sample of parameter estimates, drawn in proportion to their likelihood. We assume a truncated multivariate normal distribution, since the parameters are constrained to positive values, using the modelling package `tmvtnorm` [26].

$$\alpha_i = \int_{120}^{650} h_i \; exp\Big\{ - \frac{ln2}{s_i^2}\Big[ln\Big(1 + 2s_i\frac{T - p_i}{w_i}\Big)\Big]^2\Big\}dT \tag{6}$$

We interpret that the peak located around 250–270 °C corresponds to primary hemicelluloses (HC), around 310–330 °C to cellulose (CL), and around 330–350 °C to lignin (LG). If present, the fourth peak located below 200 °C corresponds to the most simple hemicelluloses (HC-1). The second dataset included in the package, `marsilea`, provides an example of a four-peak deconvolution. A worked example can be found in the package vignettes.

Package outputs
The output of the `deconvolve` function is a list of five items:

1. the dataset that results from the `process` function, useful for testing other modelling approaches or plotting options, and accessed with `rate_data()`:

```
DTG_data <- rate_data(output_juncus)
head(DTG_data)

##       temp_C        deriv   mass_T
## 5325 120.514 9.570652e-05 17.91630
## 5384 121.501 9.885901e-05 17.91445
## 5445 122.515 1.003878e-04 17.91252
## 5505 123.514 9.133606e-05 17.91079
## 5565 124.513 6.493836e-05 17.90956
## 5625 125.509 8.578618e-05 17.90794
```

2. the temperature values at which the data were cropped for analysis, accessed with `temp_bounds()`:

```
temp_bounds(output_juncus)

## [1] 120 700
```

3. the output of the mixture model. Peak 1 is hemicellulose; peak 2 is cellulose; and peak 3 is lignin. If present, the optional fourth peak located at the lowest temperature interval will be listed as peak 0. Accessed with `model_fit()`:

```
model_fit(output_juncus)
```

```
## Nonlinear regression model
##   model: deriv ~ fs_mixture(temp_C, height_1, skew_1, position_1,
##     width_1, height_2, skew_2, position_2, width_2, height_3,
##     skew_3, position_3, width_3)
##   data: dataframe
##   height_1   skew_1     position_1 width_1    height_2   skew_2
##   3.944e-03  1.258e-01  2.662e+02  5.106e+01  5.793e-03  1.344e-02
##   position_2 width_2    height_3   skew_3     position_3 width_3
##   3.173e+02  2.866e+01  1.163e-03  1.085e-01  3.300e+02  2.500e+02
##   residual sum-of-squares: 9.299e-06
##
## Number of iterations to convergence: 23
## Achieved convergence tolerance: 1.49e-08
```

4. the number of peaks:

```
output_juncus$n_peaks

## [1] 3
```

5. and the mean, 2.5% and 97.5% estimates, median, and standard deviation of the weight of each component that can be accessed with `component_weights()`:

```
component_weights(output_juncus)

##           HC         CL         LG value_type
## 1 21.5600422 17.6748693 30.6629891       mean
## 2 20.4327310 16.6433643 29.5201899       2.5%
## 3 21.5980403 17.6367428 30.6535159        50%
## 4 22.7575067 18.6700545 31.8302178      97.5%
## 5  0.5978226  0.5128315  0.5914671         sd
```

Plotting

Plotting the output of the `deconvolve` function shows the underlying DTG data, the overall mixture model curve, as well as the component peaks of the deconvolution (Fig. 6). The default plot is in black and white, but a colour version that uses colour-blind friendly `viridis` colours [9] is available by specifying `bw = FALSE`.

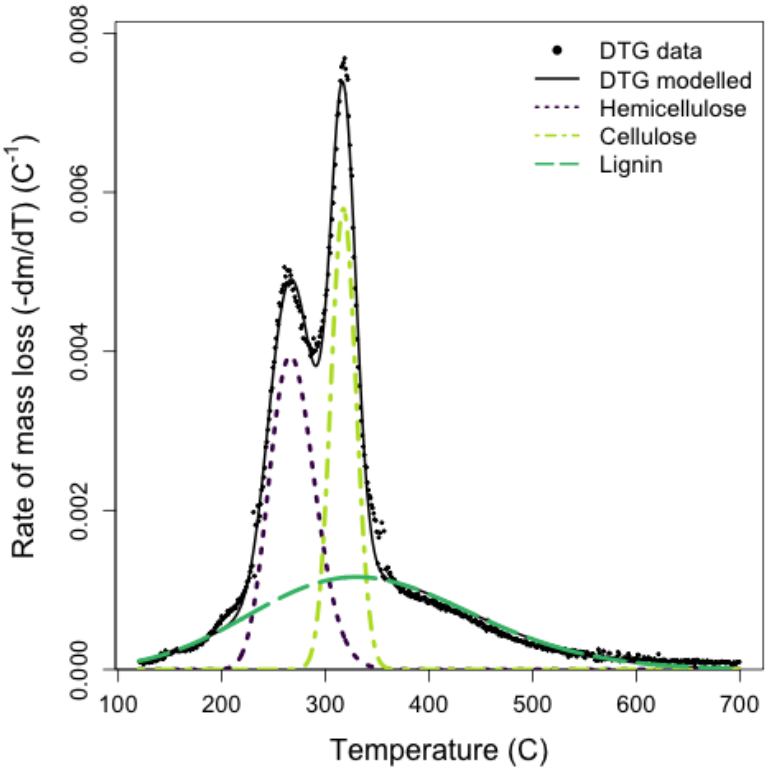

Figure 6 Deconvolution of *Juncus amabilis* example dataset. Mass loss data overlaid with output of deconvolution. Rate of mass loss scaled by initial mass of sample.

The Fraser-Suzuki family of functions are exported (Table 1) to allow users to create their own plots from the model outputs in conjunction with the parameter estimates, accessed as follows:

```
juncus_parameters <- model_parameters(output_juncus)
juncus_parameters

##    parameter_name parameter_value
```

```
## 1        height_1    3.944240e-03
## 2          skew_1    1.258171e-01
## 3      position_1    2.661764e+02
## 4         width_1    5.105925e+01
## 5        height_2    5.792848e-03
## 6          skew_2    1.344097e-02
## 7      position_2    3.172997e+02
## 8         width_2    2.866180e+01
## 9        height_3    1.162606e-03
## 10         skew_3    1.085210e-01
## 11     position_3    3.300000e+02
## 12        width_3    2.500000e+02
```

Table 1 Exported functions.

Function family	Function name	Description
Data	`juncus`	Example thermogravimetric data for *Juncus amabilis*
Data	`marsilea`	Example thermogravimetric data for *Marsilea drumondii*
Basic use	`process()`	Calculates the derivative rate of mass loss of thermogravimetric data
Basic use	`deconvolve()`	Deconvolves derivative rate of mass loss data
Accessor function	`temp_bounds()`	Access temperature bounds used to crop data for mixture model
Accessor function	`rate_data()`	Access processed dataframe including mass loss, rate of mass loss, and temperature
Accessor function	`model_fit()`	Access fit of nonlinear mixture model
Accessor function	`component_weights()`	Access mean, upper, and lower bounds for component weight estimates
Accessor function	`model_parameters()`	Access parameter estimates
Fraser-Suzuki function	`fs_function()`	Fraser-Suzuki equation for a single peak
Fraser-Suzuki function	`fs_mixture()`	Fraser-Suzuki mixture model equation
Fraser-Suzuki function	`fs_model()`	Non-linear model implementation of Fraser-Suzuki mixture model
S3 method	`print(<process>)`	Default print method for process object (derived from `process()`)
S3 method	`plot(<process>)`	Default plot method for process object (derived from `process()`)
S3 method	`print(<deconvolve>)`	Default print method for decon object (derived from `deconvolve()`)
S3 method	`plot(<deconvolve>)`	Default plot method for process object (derived from `deconvolve()`)

Quality control

All the functions of `mixchar` were tested to see if they produce the desired output. The workflow was tested on thermogravimetric data from two different TGA-FTIR instruments, and on samples outside those used to build the package.

The structure of the package successfully passed the CRAN R CMD check with no errors or warnings, or notes and the results from this check can be found on CRAN.

(2) Availability

Operating system
The package was tested on Windows, Mac OS X, and Linux.

Programming language
R version 3.2.0 or higher.

Additional system requirements
An internet connection is required to install the `mixchar` package.

Dependencies
R packages: `graphics`, `minpack.lm`, `nloptr`, `stats`, `tmvtnorm`, `zoo`.

List of contributors
This package was created by Saras Windecker and Dr. Nick Golding.

Software location:
Archive

Name: CRAN
Persistent identifier: `https://CRAN.R-project.org/package=mixchar`
Licence: MIT and open license as found on
`https://cran.r-project.org/web/packages/mixchar/LICENSE`
Publisher: Saras Windecker
Version published: 0.1.0
Date published: 16/08/2018

Code repository

Name: Github
`https://github.com/smwindecker/mixchar/`
Persistent identifier: DOI:10.5281/zenodo.1343849
https://doi.org/10.5281/zenodo.1343849
Licence: MIT and open license as found on
`https://github.com/smwindecker/mixchar/releases/tag/v0.1.0.`
Date published: 11/08/2018

Language
R

(3) Reuse potential

This package was designed with both the user and developer in mind. There are several vignettes available with the package and on the package website (`https://smwindecker.github.io/mixchar/`) facilitating exploration of package functionality. We expect that this package will be useful to researchers already using thermogravimetric analysis for biomass component estimation, as well as to functional ecologists seeking to test out this approach as an alternative to wet chemistry methods. For all users, this method improves on most current softwares available to them,

as it is fully open-source and transparent.

Finite mixture models are used to cluster continuous multivariate data. Statistical inference of mixture models is notoriously difficult because of their flexibility [14]. This is especially true for the Fraser-Suzuki function, which has an additional parameter compared to a Gaussian distribution. Many combinations of peaks can create the same overall derivative thermogravimetric curve, and so informed starting values are necessary as they can substantially affect fit. To use `mixchar` well, we need in some cases to modify the default starting values.

For those who wish to contribute to the package, it is hosted on Github. Contributors can log issues, for example concerning alternative data formats, via the issues tracker (`https://github.com/smwindecker/mixchar/issues`) or submit a pull request to add functionality to the package.

Acknowledgements
The authors would like to thank Dr. Nick Tierney and David Wilkinson for reviewing an early version of the package as well as CRAN reviewers for useful additions. We would like to thank volunteers Paula Sanchez, Abbey Kinnish, Kelsey Johnson, Madeline Brenker, and Urtzi Enriquez Urzelai for their assistance in the field collecting plant specimens. We would also like to thank the University of Melbourne Department of Chemical and Biomolecular Engineering for access to and training on the TGA-FTIR. Plant samples used to build and verify the model were conducted under Victorian Department of Environment, Land, Water and Planning Permit No 10007429.

Funding statement
The authors would like to acknowledge the generous support we received from the Australian Research Council Centre of Excellence for Environmental Decisions, the Holsworth Wildlife Reseach Endowment & The Ecological Society of Australia, and from University of Melbourne, which provided the primary author with a Melbourne International Research Scholarship and a Melbourne International Fee Remission Scholarship from University of Melbourne.

Competing interests
The authors declare that they have no competing interests.

References

[1] F. Barbadillo, A. Fuentes, S. Naya, R. Cao, J. Mier, and R. Artiaga. Evaluating the logistic mixture model on real and simulated TG curves. *Journal of thermal analysis and calorimetry*, 87(1):223–227, 2007.

[2] J. Cai and R. Liu. Parametric study of the nonisothermal n th-order distributed activation energy model involved the Weibull distribution for biomass pyrolysis. *Journal of Thermal Analysis and Calorimetry*, 89(3):971–975, 2007.

[3] C. Chen, W. Miao, C. Zhou, and H. Wu. Thermogravimetric pyrolysis kinetics of bamboo waste via Asymmetric Double Sigmoidal (Asym2sig) function deconvolution. *Bioresource Technology*, 225:48–57, Feb. 2017. ISSN 09608524. doi: 10.1016/j.biortech.2016.11.013.

[4] Z. Chen, M. Hu, X. Zhu, D. Guo, S. Liu, Z. Hu, B. Xiao, J. Wang, and M. Laghari. Characteristics and kinetic study on pyrolysis of five lignocellulosic biomass via thermogravimetric analysis. *Bioresource Technology*, 192:441–450, Sept. 2015. ISSN 09608524. doi: 10.1016/j.biortech.2015.05.062.

[5] Z. Cheng, W. Wu, P. Ji, X. Zhou, R. Liu, and J. Cai. Applicability of Fraser–Suzuki function in kinetic analysis of DAEM processes and lignocellulosic biomass pyrolysis processes. *Journal of Thermal Analysis and Calorimetry*, 119(2):1429–1438, Feb. 2015. ISSN 1388-6150, 1588-2926. doi: 10.1007/s10973-014-4215-3.

[6] W. K. Cornwell, J. H. C. Cornelissen, K. Amatangelo, E. Dorrepaal, V. T. Eviner, O. Godoy, S. E. Hobbie, B. Hoorens, H. Kurokawa, N. Pérez-Harguindeguy, H. M. Quested, L. S. Santiago, D. A. Wardle, I. J. Wright, R. Aerts, S. D. Allison, P. van Bodegom, V. Brovkin, A. Chatain, T. V. Callaghan, S. Díaz, E. Garnier, D. E. Gurvich, E. Kazakou, J. A. Klein, J. Read, P. B. Reich, N. A. Soudzilovskaia, M. V. Vaieretti, and M. Westoby. Plant species traits are the predominant control on litter decomposition rates within biomes worldwide. *Ecology Letters*, 11(10):1065–1071, Oct. 2008. ISSN 1461023X, 14610248. doi: 10.1111/j.1461-0248.2008.01219.x.

[7] T. V. Elzhov, K. M. Mullen, A.-N. Spiess, and B. Bolker. *minpack.lm: R Interface to the Levenberg-Marquardt Nonlinear Least-Squares Algorithm Found in MINPACK, Plus Support for Bounds*, 2016. URL `https://CRAN.R-project.org/package=minpack.lm`. R package version 1.2-1.

[8] R. S. Fukushima and M. S. Kerley. Use of Lignin Extracted from Different Plant Sources as Standards in the Spectrophotometric Acetyl Bromide Lignin Method. *Journal of Agricultural and Food Chemistry*, 59(8):3505–3509, Apr. 2011. ISSN 0021-8561. doi: 10.1021/jf104826n.

[9] S. Garnier. *viridis: Default Color Maps from 'matplotlib'*, 2018. URL `https://CRAN.R-project.org/package=viridis`. R package version 0.5.1.

[10] R. Hatfield and R. S. Fukushima. Can Lignin Be Accurately Measured? *Crop Science*, 45(3):832, 2005. ISSN 1435-0653. doi: 10.2135/cropsci2004.0238.

[11] M. Hu, Z. Chen, S. Wang, D. Guo, C. Ma, Y. Zhou, J. Chen, M. Laghari, S. Fazal, B. Xiao, B. Zhang, and S. Ma. Thermogravimetric kinetics of lignocellulosic biomass slow pyrolysis using distributed activation energy model, Fraser–Suzuki deconvolution, and iso-conversional method. *Energy Conversion and Management*, 118:1–11, June 2016. ISSN 01968904. doi: 10.1016/j.enconman.2016.03.058.

[12] S. G. Johnson. The nlopt nonlinear-optimization package. URL `http://ab-initio.mit.edu/nlopt`.

[13] J. K. Kauppinen, D. J. Moffatt, H. H. Mantsch, and D. G. Cameron. Fourier Self-Deconvolution: A Method for Resolving Intrinsically Overlapped Bands. *Applied Spectroscopy*, 35(3):271–276, May 1981. ISSN 0003-7028. doi: 10.1366/0003702814732634.

[14] G. J. McLachlan and K. E. Basford. *Mixture Models : Inference and Applications to Clustering*. Thesis, New York, N.Y. : M. Dekker, 1988.

[15] M. Müller-Hagedorn and H. Bockhorn. Pyrolytic behaviour of different biomasses (angiosperms) (maize plants, straws, and wood) in low temperature pyrolysis. *Journal of Analytical and Applied Pyrolysis*, 79(1-2):136–146, May 2007. ISSN 01652370. doi: 10.1016/j.jaap.2006.12.008.

[16] J. J. M. Órfão and J. L. Figueiredo. A simplified method for determination of lignocellulosic materials pyrolysis kinetics from isothermal thermogravimetric experiments. *Thermochimica Acta*, 380(1):67–78, Nov. 2001. ISSN 0040-6031. doi: 10.1016/S0040-6031(01)00634-7.

[17] D. Peel and G. J. McLachlan. Robust mixture modelling using the t distribution. *Statistics and Computing*, 10(4):339–348, Oct. 2000. ISSN 1573-1375. doi: 10.1023/A:1008981510081.

[18] A. Perejón, P. E. Sánchez-Jiménez, J. M. Criado, and L. A. Pérez-Maqueda. Kinetic Analysis of Complex Solid-State Reactions. A New Deconvolution Procedure. *The Journal of Physical Chemistry B*, 115(8):1780–1791, Mar. 2011. ISSN 1520-6106, 1520-5207. doi: 10.1021/jp110895z.

[19] N. Pérez-Harguindeguy, S. Díaz, E. Garnier, S. Lavorel, H. Poorter, P. Jaureguiberry, M. S. Bret-Harte, W. K. Cornwell, J. M. Craine, D. E. Gurvich, C. Urcelay, E. J. Veneklaas, P. B. Reich, L. Poorter, I. J. Wright, P. Ray, L. Enrico, J. G. Pausas, A. C. de Vos, N. Buchmann, G. Funes, F. Quétier, J. G. Hodgson, K. Thompson, H. D. Morgan, H. ter Steege, L. Sack, B. Blonder, P. Poschlod, M. V. Vaieretti, G. Conti, A. C. Staver, S. Aquino, and J. H. C. Cornelissen. New handbook for standardised measurement of plant functional traits worldwide. *Australian Journal of Botany*, 61(3):167, 2013. ISSN 0067-1924. doi: 10.1071/BT12225.

[20] M. Powell. The bobyqa algorithm for bound constrained optimization wihtout derivatives. *Department of Applied Mathematics and Theoretical Physics, Cambridge England, technical report NA2009/06*, 2009.

[21] W. Seidel, K. Mosler, and M. Alker. A Cautionary Note on Likelihood Ratio Tests in Mixture Models. *Annals of the Institute of Statistical Mathematics*, 52(3):481–487, Sept. 2000. ISSN 1572-9052. doi: 10.1023/A:1004117419204.

[22] W. Seidel, K. Mosler, and M. Alker. Likelihood ratio tests based on subglobal optimization: A power comparison in exponential mixture models. *Statistical Papers*, 41(1):85–98, Jan. 2000. ISSN 1613-9798. doi: 10.1007/BF02925678.

[23] Y. Sun, F. Bai, X. Lü, C. Jia, Q. Wang, M. Guo, Q. Li, and W. Guo. Kinetic study of Huadian oil shale combustion using a multi-stage parallel reaction model. *Energy*, 82:705–713, Mar. 2015. ISSN 03605442. doi: 10.1016/j.energy.2015.01.080.

[24] R. Svoboda and J. Málek. Applicability of Fraser–Suzuki function in kinetic analysis of complex crystallization processes. *Journal of Thermal Analysis and Calorimetry*, 111(2):1045–1056, Feb. 2013. ISSN 1388-6150, 1572-8943. doi: 10.1007/s10973-012-2445-9.

[25] S. M. Trevathan-Tackett, J. Kelleway, P. I. Macreadie, J. Beardall, P. Ralph, and A. Bellgrove. Comparison of marine macrophytes for their contributions to blue carbon sequestration. *Ecology*, 96(11):3043–3057, 2015.

[26] S. Wilhelm and M. B. G. *tmvtnorm: Truncated Multivariate Normal and Student t Distribution*, 2015. URL `http://CRAN.R-project.org/package=tmvtnorm`. R package version 1.4-10.

[27] H. Yang, R. Yan, H. Chen, C. Zheng, D. H. Lee, and D. T. Liang. In-Depth Investigation of Biomass Pyrolysis Based on Three Major Components: Hemicellulose, Cellulose and Lignin. *Energy & Fuels*, 20(1):388–393, Jan. 2006. ISSN 0887-0624, 1520-5029. doi: 10.1021/ef0580117.

5

Understanding variation in litter decomposition in a multispecies mesocosm

Abstract

The quantity and quality of plant litter are key predictors of decomposition rates worldwide. Key functional traits affect decomposition pathways among species in predictable ways and can therefore be used as easy-to-measure metrics for litter characteristics. Although the negative exponential model has traditionally been used to predict decay, it assumes constant rate of decay over time, making it problematic for estimating decay in heterogeneous litter. By modelling decomposition with the two-parameter Weibull model, we can test ecological theory about what traits of a plant community impact the total decay as well as the change in rate of decay over time. We conduct a mesocosm experiment to examine decomposition trajectories for 29 wetland plant species, for which we also measure seven traits: litter area per mass (LAM), dry matter content (DMC), litter nitrogen (N), litter total carbon (C), proportion of hemicellulose (HC), cellulose (CL), and lignin (LG). We use a series of cross-validated, non-linear Bayesian models to test (i) whether these species change their decay rate over time (thereby indicating the utility of the Weibull model framework), (ii) which of our measured traits affect decay and in what way, and (iii) how successful these models are at predicting the decomposition rate of new species. We found that decomposition rates decrease over time, directly contradicting the assumption underlying the single-pool negative exponential model. Trait models which include both nitrogen and carbon characteristics ranked among the best. However differences among trait models are marginal, suggesting that traits alone do not produce a single 'best' model for predicting to new species.

5.1 Introduction

Small proportional changes in growth and decomposition rates can have far-reaching effects on atmospheric CO_2 (Prentice et al., 2001). Complex processes regulate decomposition in diverse plant communities, including abiotic and biotic attributes of the ecosystem (Cornwell et al., 2008). Site-level studies, as well as global syntheses, highlight the importance of litter quality and chemistry on mass loss rates across diverse biomes worldwide (Zhang et al., 2008). Appropriate models are required to quantify decomposition rates and test the relative predictive abilities of traits on rates of decomposition (De Deyn, Cornelissen & Bardgett, 2008).

Observation of mass loss indicates that mass does not decay at a linear rate (Olson, 1963) but rather declines quickly initially and then slows. Although there are many different conceptualisations of the decomposition process, this basic concave shape is most commonly approximated by first order decay using the negative exponential model (Eq. 5.1; Olson, 1963).

$$M_t = M_0 e^{-\kappa t} \tag{5.1}$$

where M_t is mass remaining at time t, M_0 is initial mass of litter sample, and κ is rate. The negative exponential model assumes that the change in rate of decay is constant over time ($1/\kappa$), such that each molecule has equal chance of decaying at any point in time and the half life is a constant value ($t_{50} = -\frac{ln(2)}{k}$). Desite its widespread use, the negative exponential model has been criticised because of this assumption that the litter material is homogeneous when it is demonstrably not so (Wieder & Lang, 1982; Cheshire et al., 1988; Prescott, 2010; Adair, Hobbie & Hobbie, 2010). Even litter belonging to a single species is comprised of a variety of structures (roots, stems, leaves), which are not homogeneous in terms of chemical composition and therefore decompose at different rates at different phases of decay (Freschet, Aerts & Cornelissen, 2012a).

A range of complex, multiple parameter decomposition models exist that capture biological mechanisms of decay better than the negative exponential model because they are more flexible (Bruun, Six & Jensen, 2004; Feng, 2009; Manzoni et al., 2012). One such model is the two-parameter Weibull residence time model (Eq. 5.2). Originally described by Frechét (1927) and later developed by Weibull (1951), it performed best out of a suite of multi-parameter decay models based on AIC_c and BIC model selection approaches (Cornwell & Weedon, 2014). Although still a phenomenological model as it does not model the underlying biological mechanism of decay, it differs from the negative exponential model in that it allows for the rate of decay to change over time (derivation in Cornwell & Weedon, 2014). It can also be reparameterised to derive two important metrics: time to 50% mass and mean residence time, or average time a particle remains in the sample before decomposing (Cornwell & Weedon, 2014). It is defined as follows:

$$M_t = M_0 e^{-\frac{t}{\beta}^{\alpha}} \tag{5.2}$$

where α modifies the shape of the decay curve and β is a rate parameter determining the scale of decay over time. Variation in the Weibull shape parameter allows us to distinguish between decomposition trajectories that decay (i) relatively fast initially but slow over time ($\alpha<1$), (ii) relatively consistently and are well approximated by the negative exponential model ($\alpha \sim 1$), and (iii) slowly initially but speed up over time (a lag phase; $\alpha>1$). The four combinations of high and low α and β allow us to distinguish between fast overall decay that increases or decreases with time, and slow overall decay that increases or decreases with time.

Empirical work has concluded that a range of traits correlate with overall decomposition rate: i) carbon, nitrogen, or carbon to nitrogen ratio (Britson, Wardrop & Drohan, 2016; Cornelissen et al., 2001; Cornwell et al., 2008; Cornwell & Weedon, 2014; Freschet, Aerts & Cornelissen, 2012a), ii) lignin or lignin to nitrogen ratio (Britson, Wardrop & Drohan, 2016; Cornwell et al., 2008; Freschet, Aerts & Cornelissen, 2012a,b; Jackson, Peltzer & Wardle, 2013; Zhang et al., 2008) iii) specific leaf area or leaf mass area (Cornelissen et al., 1999; Cornwell et al., 2008), iv) and litter cellulose (Britson, Wardrop & Drohan, 2016), among others. With the exception of Cornwell & Weedon (2014), who found that nitrogen predicted Weibull α, these studies predicted trait effects on the negative exponential parameter, κ. In previous work comparing functional trait values for a range of wetland plant species, we found that litter high in carbon content was not necessarily high in complex carbon. Species tended to invest primarily in either simple carbon, such as hemicelluloses and cellulose, or in chemically complex lignin. This separation by investment strategy was not, however, necessarily parallel to the division between nutrient-rich and nutrient-poor tissue (Windecker et al., unpublished data). The two-parameter Weibull model provides us with the opportunity to test how these two investment strategies affect decomposition. We expect that nutrient-rich labile tissue, regardless of chemical complexity, would have low α, or initially fast then declining decay rates. We expect that litter high in complex carbon such as lignin would have higher β, or low rates of overall decay.

In this study, we collected mass loss data for 29 wetland species using a nine-month mesocosm decomposition experiment. We used these data to (i) compare the single-pool negative exponential model with the two-parameter Weibull residence time model, (ii) estimate the power of traits to explain species-level variation in decomposition shape and scale (Weibull α and β), and (iii) evaluate the ability of these models to predict decomposition rate in new species. This exercise was computationally expensive, so to reduce the number of models for comparison we assessed this aim in stages. We first compared the two model forms with no trait effects, then examined species-level estimates for α and β parameters, and finally compared 84 trait models. We evaluate the models by comparing the out-of-sample predictive performance of each model on data for a held-out species.

5.2 Methods

Litter collection

In late austral summer 2016, we collected plant litter derived from photosynthetic tissue of 29 wetland plant species. Since the study was designed to examine traits related to litter recalcitrance, we measured aboveground plant biomass that would contribute to litter. For graminoids, litter included the culm and leaves, but not the inflorescence. For forbs and ferns, litter included the entire body of the plant excluding the flower. For tree species, leaves and petioles, leaflets and rachis, but not seeds, flowers, or stems were included. For the purposes of examining litter quality, empirical work has found that traits are reasonably coordinated among different plant parts (for example, leaves and stem, Reich, 2014; Jackson, Peltzer & Wardle, 2013). In addition, similar decay rates have been observed for leaf and litter tissue (Cornwell et al., 2008).

We collected species at three previously surveyed sites in Victoria, Australia (sites within 60 km of -37.455, 144.985): one riverbank, one floodplain wetland, and one shallow groundwater- and surfacewater-fed herbland. The target species represented a range of functional groups classified according to the Brock & Casanova (1997) scheme. Functional groups included: terrestrial dry species (n = 5), terrestrial damp species (n = 9), amphibious fluctuation-tolerators (n = 10), and amphibious fluctuation-responders (n = 5). Litter was placed in moist plastic bags and stored in dark coolers until delivered to the lab, and then moved to a dark, refrigerated room.

Traits

We collected litter from ten robust individuals of each species for trait measurement. These individuals were located at least 5 m apart along a linear transect at a single site (Pérez-Harguindeguy et al., 2013) and were collected at the end of the growing season to avoid the effects of seasonal variation. We weighed each litter sample within 24 hours of collection. For each sample, we measured litter area mass, dry matter content, nitrogen, total carbon, and proportion of hemicellulose, cellulose, and lignin per descriptions in Chapter 3.

Litterbag and mesocosm preparation

We dried the fresh litter at 60 °C for 72 hours. Each species had a total of 18 litterbags spread across three replicate tubs. Each tub contained six litterbags, one of each which was removed successively at each sampling time (Fig. 5.1). We used 17 x 11.5 cm white, mesh, drawstring bags with aluminium labels, filled with approximately 4 g of dried litter. Individual leaves and compound leaves were placed directly into the bags, however stems of graminoid species were cut down to roughly 10 cm lengths to fit inside the litterbags.

Blue plastic tubs (432 x 324 x 127 mm; 13 L capacity) were used for the bioassay because we expected that the dark colour would limit algal photosynthesis and growth.

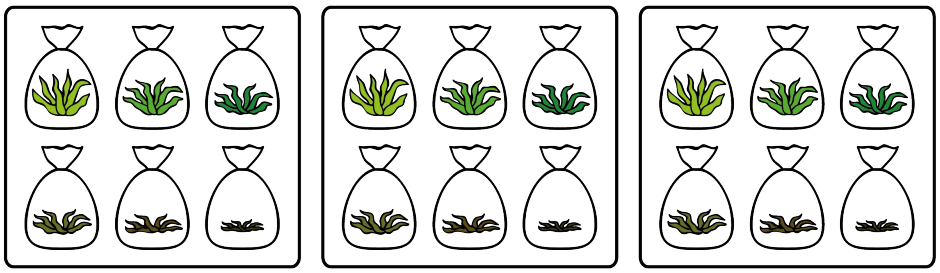

FIGURE 5.1: Mesocosm decomposition experimental design. Litter bags were removed at two, four, and six weeks, then three, six, and nine months. Each species had three replicate tubs.

Tubs were filled with 4200 mL of a 2:1 ratio of organic soil and washed sand. In addition, 90 mL of ground, homogenised soil collected from a local wetland (-37.889, 144.991) was added to the sand/soil mixture in each tub to inoculate them with local biota. The tubs were set up in 12-tub blocks in a polytunnel (University of Melbourne, Burnley campus). This polytunnel allowed in sunlight, but eliminated the effects of rain, external leaf litter, bird droppings, and any potential interference from wildlife on campus including feral foxes and reptiles (Fig. 5.2). The tunnel also buffered the ambient temperature slightly. Each species' three replicate tubs were placed randomly across the tunnel, and were re-randomised two additional times during the nine-month bioassay (after three and six months), to eliminate any effect of micro-climatic conditions in the polytunnel.

On the first day of the experiment, we placed the litterbags flat on the soil and filled the tubs with water. Overhead drip taps topped up water levels in the tubs once a week to make up for any evaporation. We conducted this experiment in flooded conditions in order to approximate the wet conditions one might expect in a wetland and to speed up decay. One litterbag was removed from each tub at two weeks, four weeks, six weeks, three months, six months, and lastly, at the end of the trial, at nine months. Bags were removed and placed directly into the oven at 60 °C for 72 hours and then weighed.

Figure 5.2: Mesocosm decomposition experiment setup. Tubs contained six litterbags for a single species that were removed one each for each sampling time. Three tubs for each species were randomly placed within the tunnel and then re-randomised twice during the duration of the study.

Null model structure

We modelled the log mass remaining for litterbag i and species j as a normal distribution with mean μ_{ij} and variance σ^2 (Eq. 5.3). We assigned a positive-truncated normal prior to σ (Eq. 5.4).

$$ln(M_{tij}) \sim N(\mu_{ij}, \sigma^2) \tag{5.3}$$

$$\sigma \sim N^{+}(0, 2) \tag{5.4}$$

μ_{ij} was described by one of two functional forms, the negative exponential (Eq. 5.5) or the Weibull residence time model (Eq. 5.6), as follows:

$$\mu_{ij} = ln(M_{0ij}) - \kappa t_{ij} \tag{5.5}$$

$$\mu_{ij} = ln(M_{0ij}) - \frac{t_{ij}}{\beta}^{\alpha} \tag{5.6}$$

$$\alpha \sim N(0, 2) \tag{5.7}$$

where M_{0ij} represents the initial mass of litterbag i and species j, and time t_{ij} is expressed in years to ensure α and β were on the same scale. When $\alpha = 1$, the two models are equivalent because $\kappa = 1/\beta$. The prior distribution for the rate parameters is given in Eq. 5.7. The remaining model variations are extensions of the Weibull

residence time model form. We use minimally informative Bayesian priors. Where we refer to α the structure is the same for the Weibull β parameter.

Weibull null hierarchical model

We model μ_{ij} as follows, where α_j and β_j for each species $j = 1, ..., 29$, are given by the sum of the global intercept (prior distribution for α is as in Eqn. 5.7) and species-level random intercept effects ϵ_j:

$$\mu_{ij} = ln(M_{0ij}) - \frac{t_{ij}}{\beta_j}^{\alpha_j} \tag{5.8}$$

$$\alpha_j = \alpha + \epsilon_j \tag{5.9}$$

$$\epsilon_j \sim N(0, \rho^2) \tag{5.10}$$

$$\rho \sim N^+(0, 2) \tag{5.11}$$

Weibull trait models

Trait variables were log-transformed, centered, and scaled by subtracting their means and dividing by twice the standard deviation. We decided for both computational and inferential reasons, that with only 29 species we could have a maximum of two traits in any given model. We therefore compared every combination of a single trait on either α or β, a single trait on both α and β, and all combinations of two traits on one parameter. This added up to 84 unique models. We modelled μ_{ij} as Eqn. 5.8, where β_j and α_j are modelled by a linear function of the global intercept (described by Eqn. 5.7) and the sum across K traits of the product of species traits (X_{kj}) and a vector of coefficients (B_{kj}):

$$\alpha_j = \alpha + \sum_{k=1}^{K} X_{kj} B_{kj} \tag{5.12}$$

$$B_{kj} \sim N(0, 2) \tag{5.13}$$

Weibull trait hierarchical model

We modelled μ_{ij} as Eqn. 5.8, where β_j and α_j are modelled by a linear function of the global intercept (described by Eqn. 5.7), the sum across K traits of the product of species traits (X_{kj}) and coefficients (B_{kj}), and a species-level random intercept effect ϵ_j:

$$\alpha_j = \alpha + \sum_{k=1}^{K} X_{kj} B_{kj} + \epsilon_j \tag{5.14}$$

Model evaluation

We compared the performance of the models using 'k-fold' cross-validation. This was achieved by splitting the dataset into a training dataset (including all but one species) and a test dataset (the held-out species). Each model was run 29 times, giving each species the opportunity to be the 'test' data. Species were used as the cross-validation grouping because we were interested in the ability of the models to predict to an entirely new species rather than to individual litterbag estimates (as in Thomas, Yen & Vesk, 2019). Model evaluation was conducted by calculating the average deviance of each model (across all folds).

$$q_j = \prod_{i=1}^{n} N(ln(M_{ij})|\mu_{ij}, \sigma^2) \tag{5.15}$$

$$D = -2\sum_{j=1}^{m} ln(q_j) \tag{5.16}$$

where q_j is the likelihood of a model for each species (the probability of observing the data given the model). Deviance D of a model is -2 times the sum across m observations j of the log likelihood of the data for each species. We have a large number of posterior samples of the parameters because we were fitting the models using Markov chain Monte Carlo (MCMC) sampling. This therefore translates into a large number of posterior samples for the deviance.

Data analysis

Our analyses were conducted within the statistical computing environment, R (R Core Team, 2013). All models were computed using the Bayesian statistical software, Stan (Carpenter et al., 2016) using the R package RStan (Stan Development Team, 2016). Stan models created for this work are contained in a R package available on Github (https://github.com/smwindecker/decaymod/).

5.3 Results

Model form

The null Weibull model outperformed the null negative exponential model across all data and for all species as determined by its lower out-of-sample deviance (Weibull deviance = 10.07, negative exponential deviance = 11.13). The difference between the deviance of the two models is not very large, likely because a simple model is not sufficient for out-of-sample prediction given the high variation of decomposition rates among species.

Posterior distributions of species-level Weibull α estimates from the null hierarchical model provide additional evidence for the strength of the Weibull model. When α = 1, the two model forms are equivalent. However, we find that roughly half of our

species have posterior distributions for α that do not intersect 1 (Fig. 5.3, Table D.1). All species except *Carex appressa* had a mean predicted α less than one and the overall mean α was around 0.6, indicating on average these species decay faster initially than would be predicted by the negative exponential model, and that the rate of decay slows down over time.

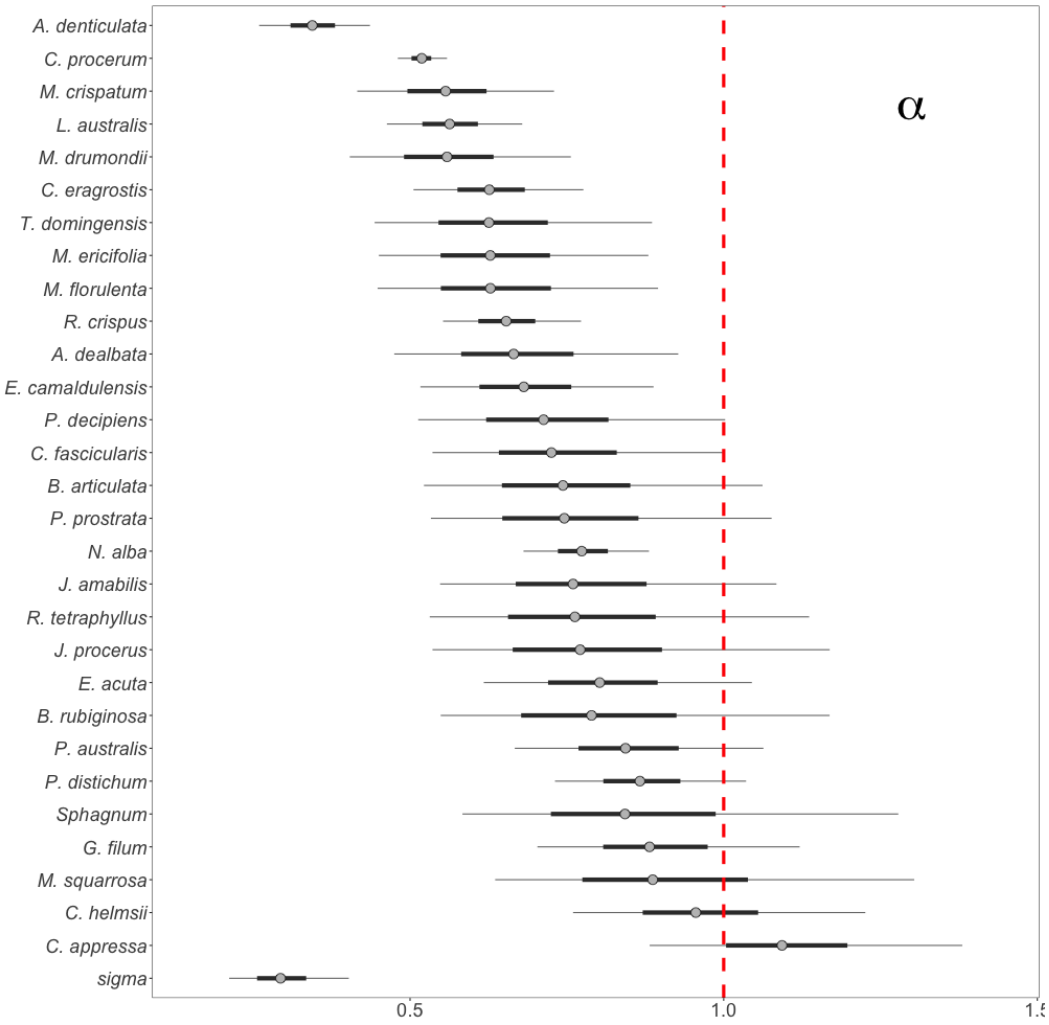

FIGURE 5.3: Posterior distributions and 95% credible intervals for parameter estimates of species-level α from the null hierarchical model. Species in descending order by median α estimate. Sigma indicates the samples drawn from the posterior for the hyperparameter of species-level standard deviation.

There is thus overall support for modelling the decomposition of these wetland plant species with the Weibull model. However, there are still some instances where one could use the negative exponential to save estimating an extra parameter, such as for species with α close to 1 (Fig 5.4a). Even for species with $\alpha<1$, the overall shape of the decay curve can be quite similar to the negative exponential, if the species decays very little (high β), such as for *Melaleuca ericifolia* (Fig. 5.4b).

Variation in the β parameter did not correlate with variation in α (r = 0.53;

Fig. D.3), suggesting the same species that decay fast initially do not necessarily decay fast overall. We therefore have evidence of species occupying both dimensions of variation in α and β: slow early stage decay with fast and slow overall decay (Fig. 5.4a–b) and early stage fast decay with high and low overall decay (Fig. 5.4c–d). All species' decay curves can be found in Fig. D.4— D.7.

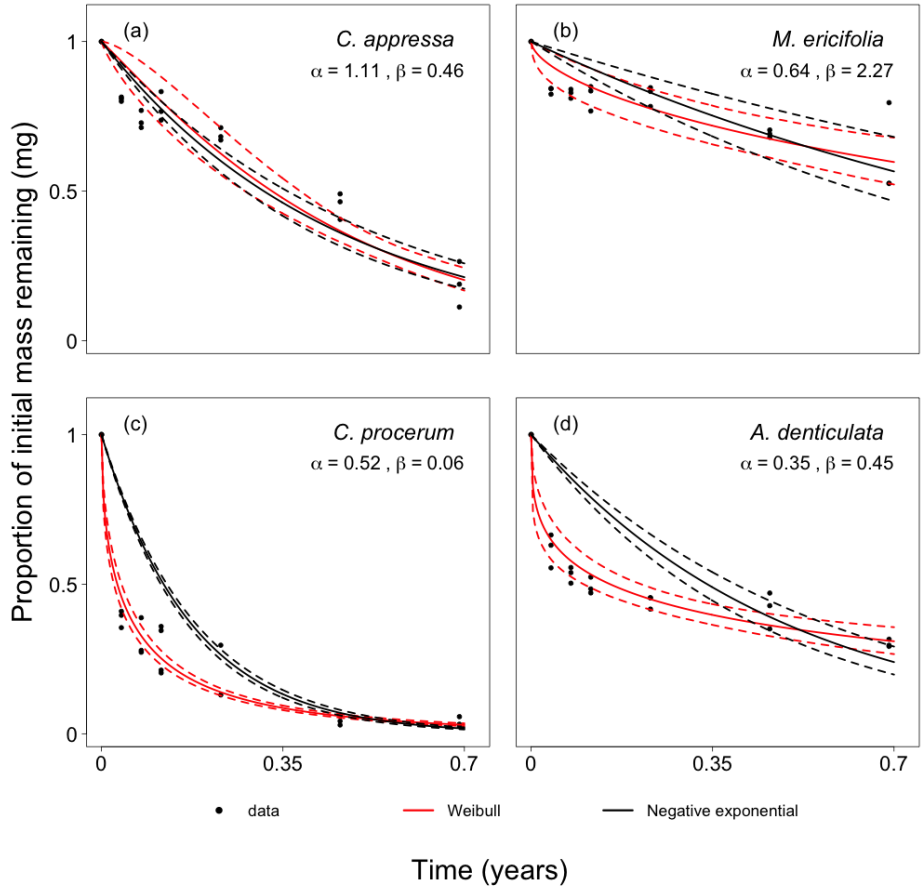

Figure 5.4: Four species' decomposition data and predictions by the negative exponential and Weibull residence time models.

Trait effects

Variation between species in β was greater and the credible interval around the estimate was wider than in α (Fig. 5.5). Models with traits on β performed the best at predicting out-of-sample species (Table 5.1). Despite variation in species-level α (Fig. 5.5), none of the top ten performing trait models (ranked by out-of-sample deviance) included traits on α (Table D.2). This suggests that despite deviation in general from the negative exponential model ($\alpha \neq 1$), traits did not necessarily predict the variation among species-level α.

The median out-of-sample deviance of the top several models did not differ greatly,

but the range of each model's deviance values varied widely, indicating that the predictive ability of any model for a given species was highly variable. This may reflect, for example, an instance where the 'test' species is at the far end of the trait spectrum, and therefore the model was unprepared for an extreme level of the variable. For this reason, we focus here on the collection of top models together rather than a single 'best' model.

TABLE 5.1: Deviance ranking with 95% credible intervals of top five Weibull models with trait fixed effects.

Formula α	Formula β	Median deviance
1	1 + N + C	-1.24[-11.7, 112]
1	1 + N + HC	1.53[-7.87, 213]
1	1 + N + LG	2.32[-10.1, 140]
1	1 + C	3.3[-1.5, 351]
1	1 + N + DMC	3.35[-8.21, 200]

Most of the top models have both nitrogen and a measure of carbon (either total carbon, hemicellulose, lignin or dry matter content) in their linear function for β. There is a strong negative correlation between β and κ (r = 0.64, p <0.001; Figs D.1, D.2). The addition of traits reduces the hyperparameter of sigma for species-level β (from 0.92 to 0.68, a 0.26% decrease), as expected, but a large amount of unexplained variation remains (Fig. 5.5).

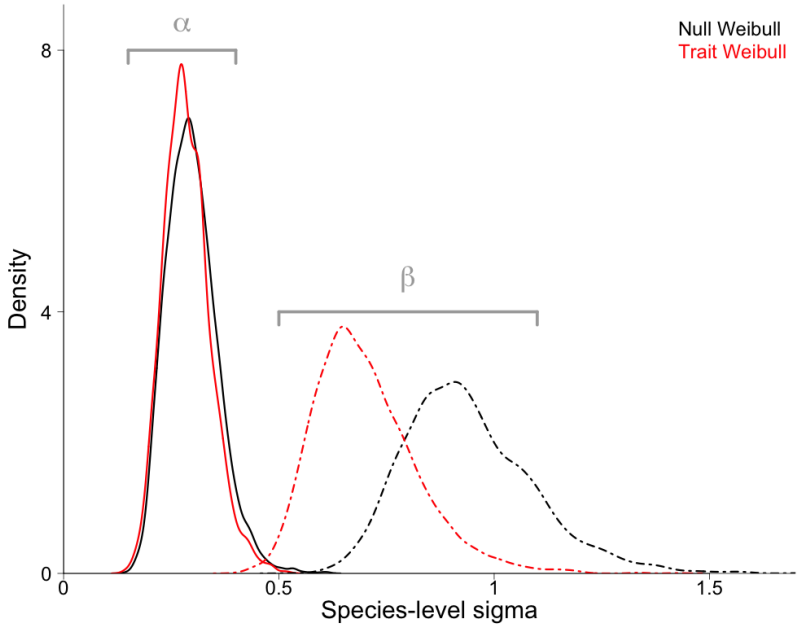

FIGURE 5.5: Density plots of posterior samples from the hyperdistribution of species-level sigma on both α and β for the null Weibull model and the lowest deviance Weibull trait model (N = 4000, bandwidth = 0.01001).

5.4 Discussion

The Bayesian framework and cross-validation used in this study revealed (i) the most predictive decomposition model was the Weibull residence time model because it captured changing rate of decay over time, (ii) despite variation in the shape (α) of decay among species, the most predictive model only included trait effects on the scale of decay, (iii) both nitrogen and some measure of carbon trait predicted the scale of decay, and finally, (iv) the overall shape (α) and scale (β) of decay varied widely between species and the most predictive trait model still explained only a fraction of this variation.

The Weibull residence time model is a useful underlying model for decomposition for our species because it allows us to model not only the overall scale of decay, but also the shape of that decay which slowed over time. This could indicate in our species the existence of a fraction of material more resistant to decay (Valiela et al., 1984). Decomposition as a function of shape and scale is important for modelling litter, which is by and large heterogeneous (Jackson, Peltzer & Wardle, 2013). Partitioning overall decomposition by shape and scale is not only more appropriate given our empirical results, but theoretically useful because it allows us to test ecological theory about which traits of a plant community impact each aspect of decay.

We found high species-level variation in both shape and overall scale of decay. We expected nutrient traits to affect decay via the shape parameter, as found in Cornwell & Weedon (2014), but none of the most predictive models included trait effects on shape. The best predictive trait models included trait effects on scale, which matches previous work documenting the influence of traits on negative exponential decomposition rate κ (Britson, Wardrop & Drohan, 2016; Prescott, 2010; Cornwell et al., 2008; Enríquez, Duarte & Sand-Jensen, 1993), because the two parameters are highly correlated. We were only measuring aboveground, non-woody litter materials, which excluded plant components such as twigs, rhizomes, and roots. Perhaps variation in Weibull shape would be more appropriately estimated with traits on these other plant parts (Jackson, Peltzer & Wardle, 2013; Silva et al., 2011; Wardle et al., 1998). Alternatively, variation in shape could be related to microbial colonisation of the litter (Glassman et al., 2018).

The models most able to predict to new species included both nitrogen and some measure of carbon on the scale parameter. Litter nitrogen can speed up decomposition by reducing the nitrogen-limitation on microbrial community growth (Cornelissen et al., 1999; Santiago, 2007; Hobbie, 2008). Chemically recalcitrant litter requires more energy to degrade (Adler et al., 2014; Lawrence, Resh & Cover, 2013), and so lignin, tannins, and polyphenols resist breakdown and reside longer in the soil (Guenet et al., 2010). Although lignin is the most chemically complex carbon (Derkacheva & Sukhov, 2008), we found total carbon and hemicellulose also performed well at predicting out-of-sample species.

The trait-based portion of this study had two phases: (i) cross-validation by species to rank predictive ability of trait models and (ii) hierarchical implementation of the best trait model to examine variance partitioning. Species-level cross-validation is

a relatively stringent metric for model selection. It asks how well a model predicts not only a species it has never seen, but also one whose trait values might well exist outside of those on which it has been trained (Gelman, 2006; Hooten & Hobbs, 2015; Mac Nally, 2000). We therefore do not expect any of these models to perform perfectly to this standard. However, this high bar is important for prediction (Falster, Duursma & FitzJohn, 2018; Mac Nally et al., 2018). It tells us not only which traits explain observed data, but how useful those traits are for predicting decomposition in a global context. Hierarchical Bayesian modelling of our trait-based models is important for inference, because by adding species-level random intercepts to our parameters we can partition inter- and intra-specific variance (Thomas, Yen & Vesk, 2019; Pollock, Morris & Vesk, 2012). We can conclude that substantial species-level variance is not explained by our 'best' trait models (as in Camac et al., 2018).

5.4.1 Conclusion

Understanding how traits predict decomposition will improve our ability to generalise about the decomposability of plant communities. In this study, we (i) provide empirical evidence for use of the Weibull residence time model, (ii) provide additional evidence that both types of litter recalcitrance traits (nutrients as well as chemical complexity) are important for predicting decay, and (iii) highlight the remaining unexplained variance of trait-based models using hierarchical modelling techniques.

5.5 Acknowledgements

The authors would like to thank volunteers Abbey Kinnish, Kelsey Johnson, Francesca Dina, Madeline Brenker, and Urtzi Enriquez Urzelai for assistance in the field and The University of Melbourne Department of Chemical and Biomolecular Engineering for training and access to the TGA-FTIR and LECO Elemental Analyser. Vegetation collection was conducted under Victorian Department of Environment, Land, Water and Planning Permit No 10007429. We thank the Australian Research Council Centre of Excellence for Environmental Decisions, the Holsworth Wildlife Research Endowment & the Ecological Society of Australia, and the Melbourne International Research Scholarship and Melbourne International Fee Remission Scholarship for support.

6
General Discussion

6.1 Overview

In this thesis I examined the role of vegetation communities in soil carbon storage across several scales. My aims were: (i) to determine the relative role of vegetation communities compared to other drivers of carbon stock at the landscape scale; (ii) to explore innovative ways to measure and quantify covariation between functional traits related to litter quality; and (iii) to empirically test the contribution of these traits to litter decomposition.

To achieve these aims I developed novel statistical models that predict soil carbon stock in freshwater wetlands and predict decomposition rate in plant species using functional traits. I parameterised these models with data collected from a state-wide field sampling protocol and a mesocosm experiment. The models greatly advance current statistical tools because (i) they are hierarchical, and therefore allow us to partition variance between sites/species and variables of interest, and because (ii) they use cross-validation for model selection, giving us insight into prediction.

This chapter synthesizes my findings and discusses their significance and implications for understanding how plants contribute to wetland soil carbon stock. I also place the statistical approaches used in this thesis into a broader context and provide details about future work.

6.2 Key insights

Carbon storage in wetlands is driven by a wide range of interacting factors. I found that carbon was highest among wetlands with intermediate levels of precipitation but in areas with infrequent permanent water cover. I also found that sites with both low and high productivity, as approximated by NDVI, had higher carbon. Possibly, these results indicate that there are a few distinct plant communities, on both extremes of the NDVI spectrum, that exist in wetlands with high carbon stock (Whitaker et al., 2015; Wang, Xu & Wan, 2016; Marín-Muñiz, Hernández & Moreno-Casasola, 2014; Ceballos, Frangi & Jobbágy, 2013).

Deposition of plant litter directly contributes to soil carbon stock. My results are consistent with others, who found that litter of different quality decomposes at different rates (Berg, 2014; Enríquez, Duarte & Sand-Jensen, 1993; Hobbie, 2008). I found that the relative contribution of biomass carbon and nutrient level of tissue combined to form the most predictive trait-based models of decomposition rate. Species can therefore decay faster either by having tissue higher in nitrogen or higher in relatively more labile forms of carbon. Other empirical decay research supports this conclusion (Britson, Wardrop & Drohan, 2016; Cornelissen et al., 2001; Cornwell et al., 2008; Cornwell & Weedon, 2014; Freschet, Aerts & Cornelissen, 2012a; Jackson, Peltzer & Wardle, 2013). My work is distinct from these previous studies because I show that these traits affect decomposition rate even when the average rate of decay is decreasing over time (Weibull residence time model α parameter <1). This is significant because I integrate trait-based hypotheses into a multi-parameter model that captures biological mechanisms of decay.

6.3 Future directions for integrated assessment of plant effects on soil carbon

My research has added to our body of knowledge about landscape- and wetland-scale influence of plant communities on soil carbon stock. However, my work still relies upon drawing indirect conclusions about how species-level recalcitrance and relative rates of decomposition affect carbon stock. I do not directly examine how species-level trait composition drives soil carbon. To address this concern I had initially planned to use species-level trait information in the wider carbon stock model (as described in Appendix A). This was beyond the scope of this thesis at the time, but is a useful direction if we hope to use community-weighted mean values of traits that affect decomposition rate to infer about carbon stock (Garnier et al., 2004).

6.4 Methodological and statistical insights and future work

Complementary to the main aims of my thesis, I came to some important insights about a handful of methodological approaches. In this section I discuss some of these insights, their implication for carbon modelling and trait-based research, and future directions.

6.4.1 Hierarchical modelling approaches

Hierarchical modelling of carbon density at depth marks an important methodological advancement for accurately estimating carbon stock. Global carbon stock comparison requires that we report stock to a consistent depth, which often requires extrapolation (Conti & Díaz, 2013; Hiraishi et al., 2014). My results confirm that it may be inaccurate to assign carbon density measured from shallower depths to deeper samples (Nahlik & Fennessy, 2016). The hierarchical approach presented in this thesis gives the model more information to extrapolate the depth profile for individual cores. The model can use variation in other cores from the same site and from the overall average, to more confidently fit a profile. This is especially important when there are few samples. In the future, researchers could build on this hierarchical framework to ask what environmental variables predict the depth profile (Adame et al., 2015; Villa & Mitsch, 2015), which has the potential to dramatically improve the accuracy of extrapolating carbon stock at depth.

By adding hierarchical effects to trait-based models of decomposition rate, I could partition inter- and intra-specific variance (Thomas, Yen & Vesk, 2019; Catford et al., 2014). The substantial species-level variance that the 'best' trait model cannot explain identifies remaining gaps in our understanding of decomposition (Camac et al., 2018). Even though this model supports other work in concluding that traits inform decomposition rate and help predict decomposition rate in new species (Cornwell et al.,

2008), it also raises questions about the remaining unexplained variance that could be examined in future work.

6.4.2 Thermogravimetry for biomass carbon trait estimation

Despite the fact that lignin is fairly resistant to chemical and biological degradation, it is not easy to accurately measure (Hatfield & Fukushima, 2005). All measurement methods must be considered estimations because they have their own sources of error and estimate some samples better than others (Dence, 1992). Compared to acid hydrolysis techniques, thermogravimetry relies on analytical pyrolysis, which avoids the need to first isolate lignin with chemical degradation (Dence, 1992). Lignin in woody species can be reliably isolated, but proteins and cutins affect the precision of this approach for estimating lignin in herbaceous species. Given there is no single perfect estimation technique, experts have concluded that the most important consideration is consistency among samples being analysed. Given my interest in multi-species comparison including not only woody species but graminoid and herbaceous species as well, thermogravimetric analysis was a reasonable choice (Órfão & Figueiredo, 2001). Considering the opportunities for rapid inter-species biomass carbon comparisons, I recommend further investigation of how we can use thermogravimetric analysis to compare to other plant structures, such as roots (Bardgett, Mommer & De Vries, 2014; Valverde-Barrantes, Smemo & Blackwood, 2015).

Use of thermogravimetry for biomass carbon estimation relies upon a second step to deconstruct a continuous multivariate curve with a mixture model. These models are notoriously difficult to fit, because many combinations of underlying curves can create the same overall curve (McLachlan & Basford, 1988). Integration under these constituent curves is the foundation for the weight estimates of the biomass carbon components. Therefore, mixture model flexibility demands careful selection of biologically reasonable starting values (Peel & McLachlan, 2000). Parameterisation of the mixture model implemented in `mixchar`, the R package we developed for this purpose, is not only based on a strong understanding of the relevant literature, but also completely transparent. Users can modify and report the starting values and other modelling choices used to prepare their component estimates. `mixchar` has already been tested for biomass carbon estimation in other multi-species comparisons (Trevathan-Tackett et al., unpublished).

More generally, writing `mixchar` encouraged me to consider how we can make all aspects of our scientific workflow more reproducible. Although many R packages exist to encourage computational reproducibility of data analysis, resources for computationally reproducible data measurement and collection steps are more rare (Fig. 6.1). In order to integrate open science principles into our entire workflow, it is my hope that resources like `mixchar` become more common.

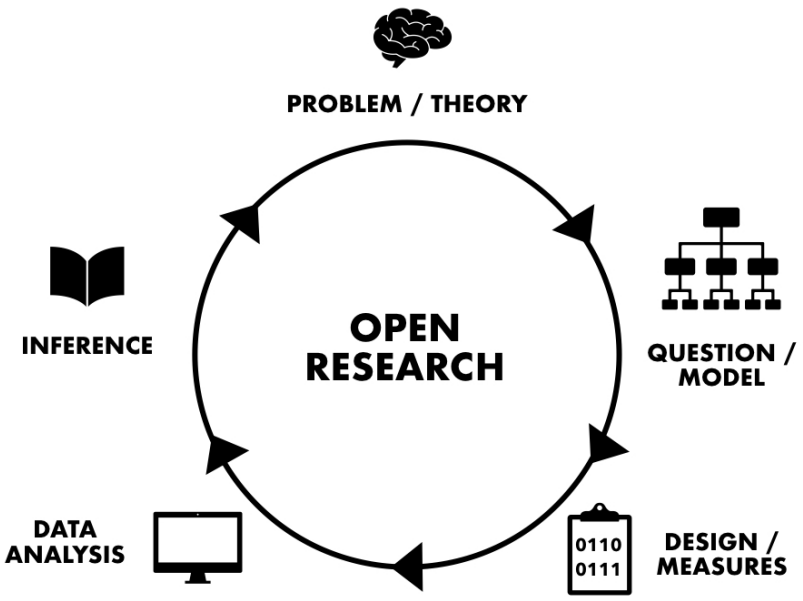

Figure 6.1: Steps for integrated open science.

6.4.3 Weibull model

I found that the Weibull residence time model predicted new species better than the negative exponential model because it allowed the rate of decay to change over time. Although multi-parameter models for decomposition are already widely discussed in the decomposition literature (Bruun, Six & Jensen, 2004; Feng, 2009; Manzoni et al., 2012), they are rarely used to test hypotheses regarding trait effects on multiple decay parameters. Markov chain Monte Carlo (MCMC) sampling made it tractable for me to fit a model with trait effects on multiple parameters (Hastings, 1970). Future decomposition research could make use of Bayesian methods to integrate biologically sensible multi-parameter decomposition models with trait hypotheses.

6.4.4 Prediction methods and implication

In both the state-wide carbon stock model and the decomposition rate model I used cross-validation to evaluate out-of-sample prediction (Gelman, 2006). This approach to model evaluation and selection improves upon information criteria approaches because it tells us not only how well a model explains observed data, but how useful that model is for predicting in a global context (Falster, Duursma & FitzJohn, 2018; Mac Nally et al., 2018). Although inference models can both guide and test ecological theory, we are often interested in using models to learn about areas that we have not sampled. In the context of global carbon storage, assessing our ability to predict to new sites is especially important. Around 64% of the world's wetlands have been lost or degraded in the last century (Davidson, 2014). As significant reservoirs for global

soil carbon storage (Bridgham et al., 2006), protection of remaining resources is especially important. Targetted conservation demands accurate prediction of soil carbon storage potential among candidate wetlands (Cartus et al., 2014).

6.5 Conclusion

This thesis quantified recalcitrance in wetland plant species, tested the impact of these measures of recalcitrance on decomposition rate of litter, and related overall vegetation productivity to landscape-scale carbon stock using innovative analytic and statistical methods. I found that carbon storage in wetlands is driven by a wide range of factors, and that neither productivity nor inundation alone could explain all the variation in wetland carbon stock among sites. I established that nutrient traits are decoupled from carbon components. Both of these trait types contributed to litter relative recalcitrance because both predicted decomposition rate. Bayesian, hierarchical modelling both made it possible to test these relationships in multi-parameter models, and revealed unexplained variance. Future work should attempt to integrate these models and explain remaining variation.

References

Adair, E.C., Hobbie, S.E. & Hobbie, R.K. (2010) Single-pool exponential decomposition models: Potential pitfalls in their use in ecological studies. *Ecology* **91**, 1225–1236.

Adame, M.F., Santini, N.S., Tovilla, C., Vázquez-Lule, A., Castro, L. & Guevara, M. (2015) Carbon stocks and soil sequestration rates of tropical riverine wetlands. *Biogeosciences* **12**, 3805–3818.

Adler, P.B., Salguero-Gómez, R., Compagnoni, A., Hsu, J.S., Ray-Mukherjee, J., Mbeau-Ache, C. & Franco, M. (2014) Functional traits explain variation in plant life history strategies. *Proceedings of the National Academy of Sciences* **111**, 740–745.

Aerts, R. & Chapin, F. (2000) The Mineral Nutrition of Wild Plants Revisited: A Re-evaluation of Processes and Patterns. *Advances in Ecological Research*, vol. 30, pp. 1–67, Elsevier.

Baldock, J.A., Hawke, B., Sanderman, J. & Macdonald, L.M. (2013) Predicting contents of carbon and its component fractions in Australian soils from diffuse reflectance mid-infrared spectra. *Soil Research* **51**, 577–595.

Barbadillo, F., Fuentes, A., Naya, S., Cao, R., Mier, J. & Artiaga, R. (2007) Evaluating the logistic mixture model on real and simulated TG curves. *Journal of thermal analysis and calorimetry* **87**, 223–227.

Bardgett, R.D., Mommer, L. & De Vries, F.T. (2014) Going underground: Root traits as drivers of ecosystem processes. *Trends in Ecology & Evolution* **29**, 692–699.

Bellon-Maurel, V., Fernandez-Ahumada, E., Palagos, B., Roger, J.M. & McBratney, A. (2010) Critical review of chemometric indicators commonly used for assessing the quality of the prediction of soil attributes by NIR spectroscopy. *TrAC Trends in Analytical Chemistry* **29**, 1073–1081.

Bengtsson, F., Rydin, H. & Hájek, T. (2018) Biochemical determinants of litter quality in 15 species of Sphagnum. *Plant and Soil* **425**, 161–176.

Berg, B. (2014) Decomposition patterns for foliar litter – A theory for influencing factors. *Soil Biology and Biochemistry* **78**, 222–232.

Bernal, B. & Mitsch, W.J. (2012) Comparing carbon sequestration in temperate freshwater wetland communities. *Global Change Biology* **18**, 1636–1647.

Bernal, B. & Mitsch, W.J. (2013) Carbon sequestration in two created riverine wetlands in the midwestern United States. *Journal of environmental quality* **42**, 1236–44.

Bridgham, S.D., Megonigal, J.P., Keller, J.K., Bliss, N.B. & Trettin, C. (2006) The carbon balance of North American wetlands. *Wetlands* **26**, 889–916.

Brinson, M.M. (1993) A hydrogeomorphic classification for wetlands. Tech. rep., U.S. Army Corpos of Engineers Waterways Experiment Station, Vicksburg, MS.

Britson, A., Wardrop, D. & Drohan, P. (2016) Plant community composition as a driver of decomposition dynamics in riparian wetlands. *Wetlands Ecology and Management* **24**, 335–346.

Brock, M.A. & Casanova, M.T. (1997) Plant life at the edge of wetlands: Ecological responses to wetting and drying patterns .

Bruun, S., Six, J. & Jensen, L.S. (2004) Estimating vital statistics and age distributions of measurable soil organic carbon fractions based on their pathway of formation and radiocarbon content. *Journal of Theoretical Biology* **230**, 241–250.

Cai, J. & Liu, R. (2007) Parametric study of the nonisothermal n th-order distributed activation energy model involved the Weibull distribution for biomass pyrolysis. *Journal of Thermal Analysis and Calorimetry* **89**, 971–975.

Camac, J.S., Condit, R., FitzJohn, R.G., McCalman, L., Steinberg, D., Westoby, M., Wright, S.J. & Falster, D.S. (2018) Partitioning mortality into growth-dependent and growth-independent hazards across 203 tropical tree species. *Proceedings of the National Academy of Sciences* **115**, 12459–12464.

Carnell, P.E., Windecker, S.M., Brenker, M., Baldock, J., Masque, P., Brunt, K. & Macreadie, P.I. (2018) Carbon stocks, sequestration, and emissions of wetlands in south eastern Australia. *Global Change Biology* **24**, 4173–4184.

Carpenter, B., Gelman, A., Hoffman, M., Lee, D., Goodrich, B., Betancourt, M., Brubaker, M.A., Guo, J., Li, P. & Riddell, A. (2016) Stan: A probabilistic programming language. *Journal of Statistical Software* **20**, 1–37.

Cartus, O., Kellndorfer, J., Walker, W., Franco, C., Bishop, J., Santos, L. & Fuentes, J.M.M. (2014) A National, Detailed Map of Forest Aboveground Carbon Stocks in Mexico. *Remote Sensing* **6**, 5559–5588.

Catford, J.A., Downes, B.J., Gippel, C.J. & Vesk, P.A. (2011) Flow regulation reduces native plant cover and facilitates exotic invasion in riparian wetlands. *Journal of Applied Ecology* **48**, 432–442.

Catford, J.A. & Jansson, R. (2014) Drowned, buried and carried away: Effects of plant traits on the distribution of native and alien species in riparian ecosystems. *New Phytologist* **204**, 19–36.

Catford, J.A., Morris, W.K., Vesk, P.A., Gippel, C.J. & Downes, B.J. (2014) Species and environmental characteristics point to flow regulation and drought as drivers of riparian plant invasion. *Diversity and Distributions* **20**, 1084–1096.

Ceballos, D.S., Frangi, J. & Jobbágy, E.G. (2013) Soil volume and carbon storage shifts in drained and afforested wetlands of the Paraná River Delta. *Biogeochemistry* **112**, 359–372.

Chanlabut, U., Gomontean, B. & Srifa, A. (2019) Soil Organic Carbon Stocks across Hydrologic Schemes in Freshwater Wetlands of the Chi River Basin, Northeast Thailand. *Wetlands* .

Chave, J., Coomes, D., Jansen, S., Lewis, S.L., Swenson, N.G. & Zanne, A.E. (2009) Towards a worldwide wood economics spectrum. *Ecology Letters* **12**, 351–366.

Chen, C., Miao, W., Zhou, C. & Wu, H. (2017) Thermogravimetric pyrolysis kinetics of bamboo waste via Asymmetric Double Sigmoidal (Asym2sig) function deconvolution. *Bioresource Technology* **225**, 48–57.

Chen, Z., Hu, M., Zhu, X., Guo, D., Liu, S., Hu, Z., Xiao, B., Wang, J. & Laghari, M. (2015) Characteristics and kinetic study on pyrolysis of five lignocellulosic biomass via thermogravimetric analysis. *Bioresource Technology* **192**, 441–450.

Cheng, Z., Wu, W., Ji, P., Zhou, X., Liu, R. & Cai, J. (2015) Applicability of Fraser–Suzuki function in kinetic analysis of DAEM processes and lignocellulosic biomass pyrolysis processes. *Journal of Thermal Analysis and Calorimetry* **119**, 1429–1438.

Cheshire, M.V., Inkson, R.H.E., Mundie, C.M. & Sparling, G.P. (1988) Studies on the rate of decomposition of plant residues in soil by following the changes in sugar components. *Journal of Soil Science* **39**, 227–236.

Chiariello, N.R., Mooney, H.A. & Williams, K. (1989) Growth, carbon allocation and cost of plant tissues. *Plant Physiological Ecology: Field Methods and Instrumentation* (eds. R.W. Pearcy, J.R. Ehleringer, H.A. Mooney & P.W. Rundel), pp. 327–365, Springer Netherlands, Dordrecht.

Chmura, G.L., Anisfeld, S.C., Cahoon, D.R. & Lynch, J.C. (2003) Global carbon sequestration in tidal, saline wetland soils. *Global Biogeochemical Cycles* **17**, n/a–n/a.

Conti, G. & Díaz, S. (2013) Plant functional diversity and carbon storage - an empirical test in semi-arid forest ecosystems. *Journal of Ecology* **101**, 18–28.

Cornelissen, J., Aerts, R., Cerabolini, B., Werger, M. & van der Heijden, M. (2001) Carbon cycling traits of plant species are linked with mycorrhizal strategy. *Oecologia* **129**, 611–619.

Cornelissen, J.H.C., Perez-Harguindeguy, N., Diaz, S., Grime, J.P., Marzano, B., Cabido, M., Vendramini, F. & Cerabolini, B. (1999) Leaf structure and defence control litter decomposition rate across species and life forms in regional floras on two continents. *New Phytologist* **143**, 191–200.

Cornwell, W.K., Cornelissen, J.H.C., Amatangelo, K., Dorrepaal, E., Eviner, V.T., Godoy, O., Hobbie, S.E., Hoorens, B., Kurokawa, H., Pérez-Harguindeguy, N., Quested, H.M., Santiago, L.S., Wardle, D.A., Wright, I.J., Aerts, R., Allison, S.D., van Bodegom, P., Brovkin, V., Chatain, A., Callaghan, T.V., Díaz, S., Garnier, E., Gurvich, D.E., Kazakou, E., Klein, J.A., Read, J., Reich, P.B., Soudzilovskaia, N.A., Vaieretti, M.V. & Westoby, M. (2008) Plant species traits are the predominant control on litter decomposition rates within biomes worldwide. *Ecology Letters* **11**, 1065–1071.

Cornwell, W.K. & Weedon, J.T. (2014) Decomposition trajectories of diverse litter types: A model selection analysis. *Methods in Ecology and Evolution* **5**, 173–182.

Corrick, A. & Norman, F. (1980) Wetlands of Victoria I. *Wetlands and Waterbirds of the Snowy River and Gippsland Lakes Catchment*, 91, pp. 1–15, Royal Society of Victoria.

Cowardin, L.M., Carter, V., Golet, F.C. & Laroe, E.T. (1979) Classification of Wetlands and Deepwater Habitats of the United States. *Water Encyclopedia* (eds. J.H. Lehr & J. Keeley), John Wiley & Sons, Inc., Hoboken, NJ, USA.

Davidson, N.C. (2014) How much wetland has the world lost? Long-term and recent trends in global wetland area. *Marine and Freshwater Research* **65**, 934.

de Bello, F., Lavorel, S., Díaz, S., Harrington, R., Cornelissen, J.H.C., Bardgett, R.D., Berg, M.P., Cipriotti, P., Feld, C.K., Hering, D., Martins da Silva, P., Potts, S.G., Sandin, L., Sousa, J.P., Storkey, J., Wardle, D.A. & Harrison, P.A. (2010) Towards an assessment of multiple ecosystem processes and services via functional traits. *Biodiversity and Conservation* **19**, 2873–2893.

De Deyn, G.B., Cornelissen, J.H.C. & Bardgett, R.D. (2008) Plant functional traits and soil carbon sequestration in contrasting biomes. *Ecology Letters* **11**, 516–531.

de Vries, F.T., Manning, P., Tallowin, J.R.B., Mortimer, S.R., Pilgrim, E.S., Harrison, K.A., Hobbs, P.J., Quirk, H., Shipley, B., Cornelissen, J.H.C., Kattge, J. & Bardgett, R.D. (2012) Abiotic drivers and plant traits explain landscape-scale patterns in soil microbial communities. *Ecology Letters* **15**, 1230–1239.

Dence, C.W. (1992) The Determination of Lignin. *Methods in Lignin Chemistry* (eds. S.Y. Lin & C.W. Dence), Springer Series in Wood Science, pp. 33–61, Springer Berlin Heidelberg, Berlin, Heidelberg.

Derkacheva, O. & Sukhov, D. (2008) Investigation of Lignins by FTIR Spectroscopy. *Macromolecular Symposia* **265**, 61–68.

Diaz, S., Hodgson, J.G., Thompson, K., Cabido, M., Cornelissen, J.H.C., Jalili, A., Montserrat-Martí, G., Grime, J.P., Zarrinkamar, F., Asri, Y., Band, S.R., Basconcelo, S., Castro-Díez, P., Funes, G., Hamzehee, B., Khoshnevi, M., Pérez-Harguindeguy, N., Pérez-Rontomé, M.C., Shirvany, F.A., Vendramini, F., Yazdani, S., Abbas-Azimi, R., Bogaard, A., Boustani, S., Charles, M., Dehghan, M., de Torres-Espuny, L., Falczuk, V., Guerrero-Campo, J., Hynd, A., Jones, G., Kowsary, E., Kazemi-Saeed, F., Maestro-Martínez, M., Romo-Díez, A., Shaw, S., Siavash, B., Villar-Salvador, P. & Zak, M.R. (2004) The plant traits that drive ecosystems: Evidence from three continents. *Journal of Vegetation Science* **15**, 295–304.

Díaz, S., Lavorel, S., de Bello, F., Quétier, F., Grigulis, K. & Robson, T.M. (2007) Incorporating plant functional diversity effects in ecosystem service assessments. *Proceedings of the National Academy of Sciences* **104**, 20684–20689.

Dorrepaal, E. (2007) Are plant growth-form-based classifications useful in predicting northern ecosystem carbon cycling feedbacks to climate change? *Journal of Ecology* **95**, 1167–1180.

Dorrepaal, E., Cornelissen, J.H.C., Aerts, R., Wallén, B. & Logtestijn, R.S.P.V. (2005) Are growth forms consistent predictors of leaf litter quality and decomposability across peatlands along a latitudinal gradient? *Journal of Ecology* **93**, 817–828.

Elliott, M.J., Knerr, N.J. & Schmidt-Lebuhn, A.N. (2018) Choice between phylogram and chronogram can have a dramatic impact on the location of phylogenetic diversity hotspots. *Journal of Biogeography* **45**, 2190–2201.

Elzhov, T.V., Mullen, K.M., Spiess, A.N. & Bolker, B. (2016) *minpack.lm: R Interface to the Levenberg-Marquardt Nonlinear Least-Squares Algorithm Found in MINPACK, Plus Support for Bounds*. R package version 1.2-1.

Enríquez, S., Duarte, C.M. & Sand-Jensen, K.A.J. (1993) Patterns in decomposition rates among photosynthetic organisms: The importance of detritus C: N: P content. *Oecologia* **94**, 457–471.

Eviner, V.T. (2004) Plant traits that influence ecosystem processes vary independently among species. *Ecology* **85**, 2215–2229.

Ewers Lewis, C.J., Carnell, P.E., Sanderman, J., Baldock, J.A. & Macreadie, P.I. (2018) Variability and Vulnerability of Coastal 'Blue Carbon' Stocks: A Case Study from Southeast Australia. *Ecosystems* **21**, 263–279.

Falster, D.S., Duursma, R.A. & FitzJohn, R.G. (2018) How functional traits influence plant growth and shade tolerance across the life cycle. *Proceedings of the National Academy of Sciences of the United States of America* **115**, E6789–E6798, wOS:000438892600017.

Feng, Y. (2009) K-Model-A Continuous Model of Soil Organic Carbon Dynamics: Theory. *Soil Science* **174**, 482–493.

FitzJohn, R. (2015) *remake: Make-like build management*. R package version 0.2.0.

Fornara, D.A. & Tilman, D. (2008) Plant functional composition influences rates of soil carbon and nitrogen accumulation. *Journal of Ecology* **96**, 314–322.

Fornara, D.A. & Tilman, D. (2012) Soil carbon sequestration in prairie grasslands increased by chronic nitrogen addition. *Ecology* **93**, 2030–2036.

Frechét, M... (1927) Sur la loi de probabilité de l'écart maximum. *Annales de la Société Polonaise de Mathématique* **6**.

Freschet, G.T., Aerts, R. & Cornelissen, J.H.C. (2012a) Multiple mechanisms for trait effects on litter decomposition: Moving beyond home-field advantage with a new hypothesis. *Journal of Ecology* **100**, 619–630.

Freschet, G.T., Aerts, R. & Cornelissen, J.H.C. (2012b) A plant economics spectrum of litter decomposability: *Afterlife effects of the plant economics spectrum. Functional Ecology* **26**, 56–65.

Gallant, J.C. & Dowling, T.I. (2003) A multiresolution index of valley bottom flatness for mapping depositional areas. *Water Resources Research* **39**.

Garnier, E., Cortez, J., Billès, G., Navas, M.L., Roumet, C., Debussche, M., Laurent, G., Blanchard, A., Aubry, D. & Bellmann, A. (2004) Plant functional markers capture ecosystem properties during secondary succession. *Ecology* **85**, 2630–2637.

Gelman, A. (2006) Prior distributions for variance parameters in hierarchical models(Comment on an Article by Browne and Draper). *Bayesian Analysis* **1**, 515–533, wOS:000207447000014.

Glassman, S.I., Weihe, C., Li, J., Albright, M.B.N., Looby, C.I., Martiny, A.C., Treseder, K.K., Allison, S.D. & Martiny, J.B.H. (2018) Decomposition responses to climate depend on microbial community composition. *Proceedings of the National Academy of Sciences* **115**, 11994–11999.

Godshalk, G.L. & Wetzel, R.G. (1978) Decomposition of aquatic angiosperms. II. Particulate components. *Aquatic Botany* **5**, 301–327.

Grigulis, K., Lavorel, S., Krainer, U., Legay, N., Baxendale, C., Dumont, M., Kastl, E., Arnoldi, C., Bardgett, R.D., Poly, F., Pommier, T., Schloter, M., Tappeiner,

U., Bahn, M. & Clément, J.C. (2013) Relative contributions of plant traits and soil microbial properties to mountain grassland ecosystem services. *Journal of Ecology* **101**, 47–57.

Grover, S.P.P., Baldock, J.A. & Jacobsen, G.E. (2012) Accumulation and attrition of peat soils in the Australian Alps: Isotopic dating evidence: ACCUMULATION AND ATTRITION OF PEAT. *Austral Ecology* **37**, 510–517.

Guenet, B., Danger, M., Abbadie, L. & Lacroix, G. (2010) Priming effect: Bridging the gap between terrestrial and aquatic ecology. *Ecology* **91**, 2850–2861.

Hastings, W.K. (1970) Monte Carlo sampling methods using Markov chains and their applications. *Biometrika* **57**, 97–109.

Hatfield, R. & Fukushima, R.S. (2005) Can Lignin Be Accurately Measured? *Crop Science* **45**, 832.

Herndon, E.M., Mann, B.F., Chowdhury, T.R., Yang, Z., Wullschleger, S.D., Graham, D., Liang, L. & Gu, B. (2015) Pathways of anaerobic organic matter decomposition in tundra soils from Barrow, Alaska. *Journal of Geophysical Research: Biogeosciences* **120**, 2345–2359.

Hijmans, R.J. (2019) *raster: Geographic Data Analysis and Modeling*. R package version 2.8-19.

Hiraishi, T., Krug, T., Tanabe, K., Srivastava, N., Baasansuren, J., Fukuda, M. & Troxler, T. (2014) IPCC 2014, 2013 Supplement to the 2006 IPCC Guidelines for National Greenhouse Gas Inventories: Wetlands. Tech. rep., IPCC, Switzerland.

Hobbie, S.E. (2008) Nitrogen Effects on Decomposition: A Five-Year Experiment in Eight Temperate Sites. *Ecology* **89**, 2633–2644.

Hooten, M.B. & Hobbs, N.T. (2015) A guide to Bayesian model selection for ecologists. *Ecological Monographs* **85**, 3–28, wOS:000349389800002.

Hu, M., Chen, Z., Wang, S., Guo, D., Ma, C., Zhou, Y., Chen, J., Laghari, M., Fazal, S., Xiao, B., Zhang, B. & Ma, S. (2016) Thermogravimetric kinetics of lignocellulosic biomass slow pyrolysis using distributed activation energy model, Fraser–Suzuki deconvolution, and iso-conversional method. *Energy Conversion and Management* **118**, 1–11.

Ives, A.R., Midford, P.E. & Garland, T. (2007) Within-species variation and measurement error in phylogenetic comparative methods. *Systematic Biology* **56**, 252–270.

Jackson, B.G., Peltzer, D.A. & Wardle, D.A. (2013) Are functional traits and litter decomposability coordinated across leaves, twigs and wood? A test using temperate rainforest tree species. *Oikos* **122**, 1131–1142.

Katoh, K. & Standley, D.M. (2013) MAFFT Multiple Sequence Alignment Software Version 7: Improvements in Performance and Usability. *Molecular Biology and Evolution* **30**, 772–780.

Kearse, M., Moir, R., Wilson, A., Stones-Havas, S., Cheung, M., Sturrock, S., Buxton, S., Cooper, A., Markowitz, S., Duran, C., Thierer, T., Ashton, B., Meintjes, P. & Drummond, A. (2012) Geneious Basic: An integrated and extendable desktop software platform for the organization and analysis of sequence data. *Bioinformatics* **28**, 1647–1649.

Keddy, P.A. (2010) *Wetland Ecology: Principles and Conservation*. Cambridge University Press.

Kennard, R.W. & Stone, L.A. (1969) Computer Aided Design of Experiments. *Technometrics* **11**, 137–148.

Kramer-Walter, K.R., Bellingham, P.J., Millar, T.R., Smissen, R.D., Richardson, S.J. & Laughlin, D.C. (2016) Root traits are multidimensional: Specific root length is independent from root tissue density and the plant economic spectrum. *Journal of Ecology* **104**, 1299–1310.

Kremer, C., Pettolino, F., Bacic, A. & Drinnan, A. (2004) Distribution of cell wall components in Sphagnum hyaline cells and in liverwort and hornwort elaters. *Planta* **219**, 1023–1035.

Krull, E.S., Baldock, J.A. & Skjemstad, J.O. (2003) Importance of mechanisms and processes of the stabilisation of soil organic matter for modelling carbon turnover. *Functional Plant Biology* **30**, 207–222.

Lal, R. (2004) Soil carbon sequestration to mitigate climate change. *Geoderma* **123**, 1–22.

Lal, R. (2007) Carbon sequestration. *Philosophical Transactions of the Royal Society B: Biological Sciences* **363**, 815–830.

Lang, S.I., Cornelissen, J.H.C., Klahn, T., van Logtestijn, R.S.P., Broekman, R., Schweikert, W. & Aerts, R. (2009) An experimental comparison of chemical traits and litter decomposition rates in a diverse range of subarctic bryophyte, lichen and vascular plant species. *Journal of Ecology* **97**, 886–900.

Lavorel, S. & Garnier, E. (2002) Predicting changes in community composition and ecosystem functioning from plant traits: Revisiting the Holy Grail. *Functional Ecology* **16**, 545–556.

Lawrence, J.E., Resh, V.H. & Cover, M.R. (2013) Large-Wood Loading from Natural and Engineered Processes at the Watershed Scale. *River Research and Applications* **29**, 1030–1041.

Liao, C., Peng, R., Luo, Y., Zhou, X., Wu, X., Fang, C., Chen, J. & Li, B. (2008) Altered ecosystem carbon and nitrogen cycles by plant invasion: A meta-analysis. *New Phytologist* **177**, 706–714.

López-Mondéjar, R., Zühlke, D., Becher, D., Riedel, K. & Baldrian, P. (2016) Cellulose and hemicellulose decomposition by forest soil bacteria proceeds by the action of structurally variable enzymatic systems. *Scientific Reports* **6**.

Ma, K., Liu, J., Zhang, Y., Parry, L.E., Holden, J. & Ciais, P. (2015) Refining soil organic carbon stock estimates for China's palustrine wetlands. *Environmental Research Letters* **10**, 124016.

Mac Nally, R. (2000) Regression and model-building in conservation biology, biogeography and ecology: The distinction between and reconciliation of 'predictive' and 'explanatory' models. *Biodiversity and Conservation* **9**, 655–671, wOS:000087051000005.

Mac Nally, R., Duncan, R.P., Thomson, J.R. & Yen, J.D.L. (2018) Model selection using information criteria, but is the "best" model any good? *Journal of Applied Ecology* **55**, 1441–1444, wOS:000430059500037.

Macreadie, P.I., Ollivier, Q.R., Kelleway, J.J., Serrano, O., Carnell, P.E., Ewers Lewis, C.J., Atwood, T.B., Sanderman, J., Baldock, J., Connolly, R.M., Duarte, C.M., Lavery, P.S., Steven, A. & Lovelock, C.E. (2017) Carbon sequestration by Australian tidal marshes. *Scientific Reports* **7**.

Maire, V., Gross, N., Hill, D., Martin, R., Wirth, C., Wright, I.J. & Soussana, J.F. (2013) Disentangling Coordination among Functional Traits Using an Individual-Centred Model: Impact on Plant Performance at Intra- and Inter-Specific Levels. *PLoS ONE* **8**, 1–1.

Makkonen, M., Berg, M.P., Handa, I.T., Hättenschwiler, S., van Ruijven, J., van Bodegom, P.M. & Aerts, R. (2012) Highly consistent effects of plant litter identity and functional traits on decomposition across a latitudinal gradient. *Ecology Letters* **15**, 1033–1041.

Manning, P., de Vries, F.T., Tallowin, J.R.B., Smith, R., Mortimer, S.R., Pilgrim, E.S., Harrison, K.A., Wright, D.G., Quirk, H., Benson, J., Shipley, B., Cornelissen, J.H.C., Kattge, J., Bönisch, G., Wirth, C. & Bardgett, R.D. (2015) Simple measures of climate, soil properties and plant traits predict national-scale grassland soil carbon stocks. *Journal of Applied Ecology* **52**, 1188–1196.

Mantel, N. (1967) The detection of disease clustering and a generalized regression approach. *Cancer Research* **27**, 209–220.

Manzoni, S., Piñeiro, G., Jackson, R.B., Jobbágy, E.G., Kim, J.H. & Porporato, A. (2012) Analytical models of soil and litter decomposition: Solutions for mass loss and time-dependent decay rates. *Soil Biology and Biochemistry* **50**, 66–76.

Marín-Muñiz, J.L., Hernández, M.E. & Moreno-Casasola, P. (2014) Comparing soil carbon sequestration in coastal freshwater wetlands with various geomorphic features and plant communities in Veracruz, Mexico. *Plant and Soil* **378**, 189–203.

Marion, Z.H., Fordyce, J.A. & Fitzpatrick, B.M. (2018) A hierarchical Bayesian model to incorporate uncertainty into methods for diversity partitioning. *Ecology* **99**, 947–956.

Marra, G. & Wood, S.N. (2011) Practical variable selection for generalized additive models. *Computational Statistics & Data Analysis* **55**, 2372–2387.

McLachlan, G.J. & Basford, K.E. (1988) *Mixture Models : Inference and Applications to Clustering*. Thesis, New York, N.Y. : M. Dekker.

Mcleod, E., Chmura, G.L., Bouillon, S., Salm, R., Björk, M., Duarte, C.M., Lovelock, C.E., Schlesinger, W.H. & Silliman, B.R. (2011) A blueprint for blue carbon: Toward an improved understanding of the role of vegetated coastal habitats in sequestering CO $_2$. *Frontiers in Ecology and the Environment* **9**, 552–560.

Mitra, S., Wassmann, R. & Vlek, P.L.G. (2005) An appraisal of global wetland area and its organic carbon stock. *Current Science* **88**, 25–35.

Mitsch, W.J. & Gosselink, J.G. (2007) *Wetlands*. Wiley, 4 edn.

Moor, H., Rydin, H., Hylander, K., Nilsson, M.B., Lindborg, R. & Norberg, J. (2017) Towards a trait-based ecology of wetland vegetation. *Journal of Ecology* **105**, 1623–1635.

Moorhead, D., Lashermes, G., Recous, S. & Bertrand, I. (2014) Interacting Microbe and Litter Quality Controls on Litter Decomposition: A Modeling Analysis. *PLOS ONE* **9**, e108769.

Moreno-Casasola, P., Hernández, M.E. & C, A.C. (2017) Hydrology, Soil Carbon Sequestration and Water Retention along a Coastal Wetland Gradient in the Alvarado Lagoon System, Veracruz, Mexico. *Journal of Coastal Research* **77**, 104–115.

Müller-Hagedorn, M. & Bockhorn, H. (2007) Pyrolytic behaviour of different biomasses (angiosperms) (maize plants, straws, and wood) in low temperature pyrolysis. *Journal of Analytical and Applied Pyrolysis* **79**, 136–146.

Nahlik, A.M. & Fennessy, M.S. (2016) Carbon storage in US wetlands. *Nature Communications* **7**, 13835.

Olson, J.S. (1963) Energy Storage and the Balance of Producers and Decomposers in Ecological Systems. *Ecology* **44**, 322–331.

Órfão, J.J.M. & Figueiredo, J.L. (2001) A simplified method for determination of lignocellulosic materials pyrolysis kinetics from isothermal thermogravimetric experiments. *Thermochimica Acta* **380**, 67–78.

Orwin, K.H., Buckland, S.M., Johnson, D., Turner, B.L., Smart, S., Oakley, S. & Bardgett, R.D. (2010) Linkages of plant traits to soil properties and the functioning of temperate grassland. *Journal of Ecology* **98**, 1074–1083.

Park, H., Kwon, O. & Ryu, K. (2015) Thermal stability and degradation kinetics of polyphenols and polyphenylenediamines enzymatically synthesized by horseradish peroxidase. *Korean Journal of Chemical Engineering* **32**, 1847–1852.

Pearse, A.L., Barton, J.L., Lester, R.E., Zawadzki, A. & Macreadie, P.I. (2018) Soil organic carbon variability in Australian temperate freshwater wetlands: Temperate wetland soil organic carbon variability. *Limnology and Oceanography* **63**, S254–S266.

Peel, D. & McLachlan, G.J. (2000) Robust mixture modelling using the t distribution. *Statistics and Computing* **10**, 339–348.

Peregon, A., Maksyutov, S., Kosykh, N.P. & Mironycheva-Tokareva, N.P. (2008) Map-based inventory of wetland biomass and net primary production in western Siberia. *Journal of Geophysical Research: Biogeosciences* **113**.

Perejón, A., Sánchez-Jiménez, P.E., Criado, J.M. & Pérez-Maqueda, L.A. (2011) Kinetic Analysis of Complex Solid-State Reactions. A New Deconvolution Procedure. *The Journal of Physical Chemistry B* **115**, 1780–1791.

Pérez-Harguindeguy, N., Díaz, S., Garnier, E., Lavorel, S., Poorter, H., Jaureguiberry, P., Bret-Harte, M.S., Cornwell, W.K., Craine, J.M., Gurvich, D.E., Urcelay, C., Veneklaas, E.J., Reich, P.B., Poorter, L., Wright, I.J., Ray, P., Enrico, L., Pausas, J.G., de Vos, A.C., Buchmann, N., Funes, G., Quétier, F., Hodgson, J.G., Thompson, K., Morgan, H.D., ter Steege, H., Sack, L., Blonder, B., Poschlod, P., Vaieretti, M.V., Conti, G., Staver, A.C., Aquino, S. & Cornelissen, J.H.C. (2013) New handbook for standardised measurement of plant functional traits worldwide. *Australian Journal of Botany* **61**, 167.

Pollock, L.J., Morris, W.K. & Vesk, P.A. (2012) The role of functional traits in species distributions revealed through a hierarchical model. *Ecography* **35**, 716–725, wOS:000305892300005.

Prentice, I.C., Farquhar, G.D., Fasham, M.J.R., Goulden, M.L., Heimann, M., Jaramillo, V.J., Kheshgi, H.S., LeQuéré, C., Scholes, R.J. & Wallace, D.W.R. (2001) The Carbon Cycle and Atmospheric Carbon Dioxide. *Climate Change 2001: The Scientific Basis. Contributions of Working Group I to the Third Assessment Report of the Intergovernmental Panel on Climate Change* (eds. J.T. Houghton, Y. Ding, D.J. Griggs, M. Noguer, P.J. van der Linden, X. Dai, K. Maskell & C.A. Johnson), pp. 185–237, Cambridge University Press, Cambridge, UK.

Prescott, C.E. (2010) Litter decomposition: What controls it and how can we alter it to sequester more carbon in forest soils? *Biogeochemistry* **101**, 133–149.

R Core Team (2013) *R: A Language and Environment for Statistical Computing*. R Foundation for Statistical Computing, Vienna, Austria.

Reich, P.B. (2014) The world-wide 'fast-slow' plant economics spectrum: A traits manifesto. *Journal of Ecology* **102**, 275–301.

Rejmánková, E. & Houdková, K. (2006) Wetland plant decomposition under different nutrient conditions: What is more important, litter quality or site quality? *Biogeochemistry* **80**, 245–262.

Ricker, M.C. & Lockaby, B.G. (2015) Soil Organic Carbon Stocks in a Large Eutrophic Floodplain Forest of the Southeastern Atlantic Coastal Plain, USA. *Wetlands* **35**, 291–301.

Ronquist, F., Teslenko, M., van der Mark, P., Ayres, D.L., Darling, A., Höhna, S., Larget, B., Liu, L., Suchard, M.A. & Huelsenbeck, J.P. (2012) MrBayes 3.2: Efficient Bayesian Phylogenetic Inference and Model Choice Across a Large Model Space. *Systematic Biology* **61**, 539–542.

Rose, C. & Crumpton, W.G. (1996) Effects of emergent macrophytes on dissolved oxygen dynamics in a prairie pothole wetland. *Wetlands* **16**, 495–502.

Roumet, C., Birouste, M., Picon-Cochard, C., Ghestem, M., Osman, N., Vrignon-Brenas, S., Cao, K.f. & Stokes, A. (2016) Root structure–function relationships in 74 species: Evidence of a root economics spectrum related to carbon economy. *New Phytologist* **210**, 815–826.

Sanderman, J., Hengl, T., Fiske, G., Solvik, K., Adame, M.F., Benson, L., Bukoski, J.J., Carnell, P., Cifuentes-Jara, M., Donato, D., Duncan, C., Eid, E.M., zu Ermgassen, P., Lewis, C.J.E., Macreadie, P.I., Glass, L., Gress, S., Jardine, S.L., Jones, T.G., Nsombo, E.N., Rahman, M.M., Sanders, C.J., Spalding, M. & Landis, E. (2018) A global map of mangrove forest soil carbon at 30 m spatial resolution. *Environmental Research Letters* **13**, 055002.

Santiago, L.S. (2007) Extending the Leaf Economics Spectrum to Decomposition: Evidence from a Tropical Forest. *Ecology* **88**, 1126–1131.

Scharpenseel, H.W. & Becker-Heidmann, P. (1992/ed) Twenty-Five Years of Radiocarbon Dating Soils: Paradigm of Erring and Learning. *Radiocarbon* **34**, 541–549.

Silva, D.S., Cunha-Santino, M.B., Marques, E.E. & Bianchini, I. (2011) The decomposition of aquatic macrophytes: Bioassays versus in situ experiments. *Hydrobiologia* **665**, 219–227.

Stan Development Team (2016) RStan: the R interface to Stan. R package version 2.14.1.

Suding, K.N., Lavorel, S., Chapin, F.S., Cornelissen, J.H.C., DíAz, S., Garnier, E., Goldberg, D., Hooper, D.U., Jackson, S.T. & Navas, M.L. (2008) Scaling environmental change through the community-level: A trait-based response-and-effect framework for plants. *Global Change Biology* **14**, 1125–1140.

Sun, Y., Bai, F., Lü, X., Jia, C., Wang, Q., Guo, M., Li, Q. & Guo, W. (2015) Kinetic study of Huadian oil shale combustion using a multi-stage parallel reaction model. *Energy* **82**, 705–713.

Svoboda, R. & Málek, J. (2013) Applicability of Fraser–Suzuki function in kinetic analysis of complex crystallization processes. *Journal of Thermal Analysis and Calorimetry* **111**, 1045–1056.

Talbot, J.M. & Treseder, K.K. (2012) Interactions among lignin, cellulose, and nitrogen drive litter chemistry–decay relationships. https://esajournals.onlinelibrary.wiley.com/doi/abs/10.1890/11-0843.1.

Thomas, F.M., Yen, J.D.L. & Vesk, P.A. (2019) Using functional traits to predict species growth trajectories, and cross-validation to evaluate these models for ecological prediction. *Ecology and Evolution* **9**, 1554–1566.

Tootchi, A., Jost, A. & Ducharne, A. (2019) Multi-source global wetland maps combining surface water imagery and groundwater constraints. *Earth System Science Data* **11**, 189–220.

Trevathan-Tackett, S.M., Kelleway, J., Macreadie, P.I., Beardall, J., Ralph, P. & Bellgrove, A. (2015) Comparison of marine macrophytes for their contributions to blue carbon sequestration. *Ecology* **96**, 3043–3057.

Valéry, L., Bouchard, V. & Lefeuvre, J.C. (2004) Impact of the invasive native species Elymus athericus on carbon pools in a salt marsh. *Wetlands* **24**, 268–276.

Valiela, I., Wilson, J., Buchsbaum, R., Rietsma, C., Bryant, D., Foreman, K. & Teal, J. (1984) Importance of chemical composition of salt marsh litter on decay rates and feeding by detritivores. *Bulletin of Marine science* **35**, 261–269.

Valverde-Barrantes, O.J., Smemo, K.A. & Blackwood, C.B. (2015) Fine root morphology is phylogenetically structured, but nitrogen is related to the plant economics spectrum in temperate trees. *Functional Ecology* **29**, 796–807.

Vaughan, E., Matos, M., Ríos, S., Santiago, C. & Marín-Spiotta, E. (2019) Clay and climate are poor predictors of regional-scale soil carbon storage in the US Caribbean. *Geoderma* **354**, 113841.

Villa, J.A. & Mitsch, W.J. (2015) Carbon sequestration in different wetland plant communities in the Big Cypress Swamp region of southwest Florida. *International Journal of Biodiversity Science, Ecosystem Services & Management* **11**, 17–28.

Violle, C., Navas, M.L., Vile, D., Kazakou, E., Fortunel, C., Hummel, I. & Garnier, E. (2007) Let the concept of trait be functional! *Oikos* **116**, 882–892.

Wang, X., Xu, L. & Wan, R. (2016) Comparison on soil organic carbon within two typical wetland areas along the vegetation gradient of Poyang Lake, China. *Hydrology Research* **47**, 261–277.

Wardle, D.A., Barker, G.M., Bonner, K.I. & Nicholson, K.S. (1998) Can comparative approaches based on plant ecophysiological traits predict the nature of biotic interactions and individual plant species effects in ecosystems? *Journal of Ecology* **86**, 405–420.

Weibull, W. (1951) A Statistical Distribution Function of Wide Applicability p. 7.

Weng, Q. & Fu, P. (2014) Modeling annual parameters of clear-sky land surface temperature variations and evaluating the impact of cloud cover using time series of Landsat TIR data. *Remote Sensing of Environment* **140**, 267–278.

Westoby, M. & Wright, I.J. (2006) Land-plant ecology on the basis of functional traits. *Trends in Ecology & Evolution* **21**, 261–268.

Whitaker, K., Rogers, K., Saintilan, N., Mazumder, D., Wen, L. & Morrison, R.J. (2015) Vegetation persistence and carbon storage: Implications for environmental water management for *P hragmites australis*: *P. AUSTRALIS* BIOMASS, PRODUCTIVITY, AND BELOWGROUND CARBON STORE. *Water Resources Research* **51**, 5284–5300.

Wieder, R.K. & Lang, G.E. (1982) A Critique of the Analytical Methods Used in Examining Decomposition Data Obtained From Litter Bags. *Ecology* **63**, 1636–1642.

Wilhelm, S. & G, M.B. (2015) *tmvtnorm: Truncated Multivariate Normal and Student t Distribution*. R package version 1.4-10.

Windecker, S.M. & Golding, N. (2018) mixchar. https://github.com/smwindecker/mixchar.

Wood, S. (2017) *Generalized Additive Models: An Introduction with R*. Chapman and Hall/CRC, 2 edn.

Wright, I.J., Reich, P.B., Cornelissen, J.H.C., Falster, D.S., Garnier, E., Hikosaka, K., Lamont, B.B., Lee, W., Oleksyn, J., Osada, N., Poorter, H., Villar, R., Warton, D.I. & Westoby, M. (2005) Assessing the generality of global leaf trait relationships. *New Phytologist* **166**, 485–496.

Wright, I.J., Reich, P.B., Westoby, M., Ackerly, D.D., Baruch, Z., Bongers, F., Cavender-Bares, J., Chapin, T., Cornelissen, J.H. & Diemer, M. (2004) The worldwide leaf economics spectrum. *Nature* **428**, 821–827.

Xu, T., Kesteven, J. & Hutchinson, M. (2018) ANUClimate collection.

Yang, H., Yan, R., Chen, H., Zheng, C., Lee, D.H. & Liang, D.T. (2006) In-Depth Investigation of Biomass Pyrolysis Based on Three Major Components: Hemicellulose, Cellulose and Lignin. *Energy & Fuels* **20**, 388–393.

Zhang, D., Hui, D., Luo, Y. & Zhou, G. (2008) Rates of litter decomposition in terrestrial ecosystems: Global patterns and controlling factors. *Journal of Plant Ecology* **1**, 85–93.

Zhong, Z., Chen, Z., Xu, Y., Ren, C., Yang, G., Han, X., Ren, G. & Feng, Y. (2018) Relationship between Soil Organic Carbon Stocks and Clay Content under Different Climatic Conditions in Central China. *Forests* **9**, 598.

Appendix A: Supplementary material for Chapter 2

A.1 Carbon analysis protocol

As described in Carnell et al. (2018).

Based on the protocols of Baldock et al. (2013), a Thermo Nicolet 6700 FTIR spectrometer equipped with a Pike AutoDiff automated diffuse reflectance accessory was used to obtain diffuse reflectance Fourier-transform MIR spectra for all samples across a spectral range of 8000–400 cm^{-1} with a spectral resolution of 8 cm^{-1}. Using Unscrambler X version 10.3 software (CAMO softare, Olso, Norway), a principle component analysis (PCA) was used to visualize spectral variability across the set of 1672 samples included in this study. A Kennard-Stone Algorithm (Kennard & Stone, 1969) was used to identify 286 samples that were most representative of the spectral variability exhibited across the dataset.

The total carbon (TC), total organic carbon (TOC), total nitrogen (TN), and inorganic carbon (IC) content of all 286 samples was determined by analysing approximately 0.80 g of the dried and ground soil. High temperature (1350 °C) oxidative combustion on a LECO Trumac CN analyzer was used to estimate TC and TN using lance oxygen flows and an extended purge to ensure complete combustion of carbonates. Non-calcareous samples identified based on MIR spectra (absence of reflectance peak at 2500 cm^{-1}) had no further analysis (TC = TOC).

Fifty-two were identified to contain inorganic carbon by the presence of a reflectance peak at 2500 cm^{-1} and were labelled as calcareous. The calcaeous soils were pre-treated by addition of 1 ml of 1 M HCl to a known mass of dried and ground soil, shaken and centrifuged with the supernatant being retained for each sample. The HCl pretreatment was repeated until no further effervescence was detected. The soils were then washed three times with 50 ml of deionised water with centrifuging and collection of the supernatent between washes. After the last wash the soils were frozen, freeze dried and analysed again on the LECO trumac CN analyser. All supernatants (after 1 M HCl treatment and water washes) were accumulated for each sample and the amount of dissolved organic carbon present in the bulk supernatant was determined using a Thermalox DOC analyser. The C_{org} content of the calcareous soils was determined as the total carbon measured by the LECO on the freeze dried HCl pretreated soil plus the organic carbon present in the accumulated supernatents corrected back to the orginial mass of soil that was pretreated.

The C_{org} content of all 286 samples were combined with their respective MIR spectra and a partial least squares regression (PLSR) analysis was used to develop an algorithm capable of predicting C_{org} content from MIR spectra. A square root tranformation was applied to the C_{org} contents to correct for nonlinearity and an inhomogeneity of variance in the resultant model. A full cross validation process was used to validate the PLSR prediction algorithm derived for the square root of C_{org} content. The PLSR prediction algorithm was then applied to the MIR spectra derived for all 1672 samples and the values derived for the square root of C_{org} content were squared to provide values for C_{org} content of the samples per Bellon-Maurel et al. (2010).

A.2 Supplementary figures and tables

Table A.1: Carbon stock generalised addivie model output.

A. parametric coefficients	Estimate	Std. Error	t-value	p-value
(Intercept)	5.0586	0.0571	88.5380	< 0.0001
B. smooth terms	edf	Ref.df	F-value	p-value
s(annprecip)	3.8586	4.0000	25.5978	< 0.0001
s(ndvi)	2.6752	4.0000	5.8327	< 0.0001
s(twi)	3.5916	4.0000	4.8657	0.0003
s(mvbf)	2.8760	4.0000	7.4906	< 0.0001
s(VGAM::yeo.johnson(water_obs, 0.2))	2.2435	4.0000	12.6167	< 0.0001
s(log(catchment_area))	3.3023	4.0000	10.6531	< 0.0001
s(natveg_prop)	0.7358	4.0000	0.7208	0.0461

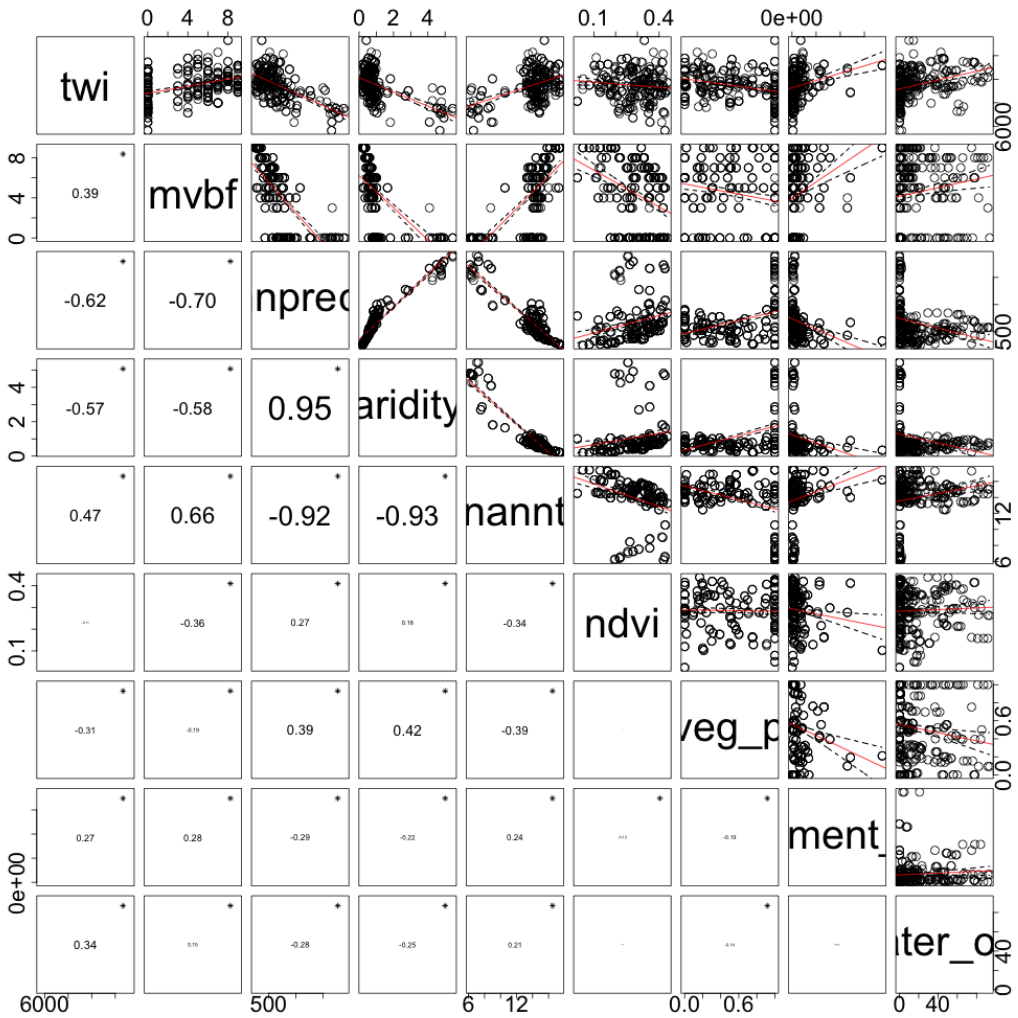

FIGURE A.1: Correlations between spatial environmental variables. Size of R^2 listed on bottom panel proportional to weight of relationship, with star to indicate significance at P <0.05.

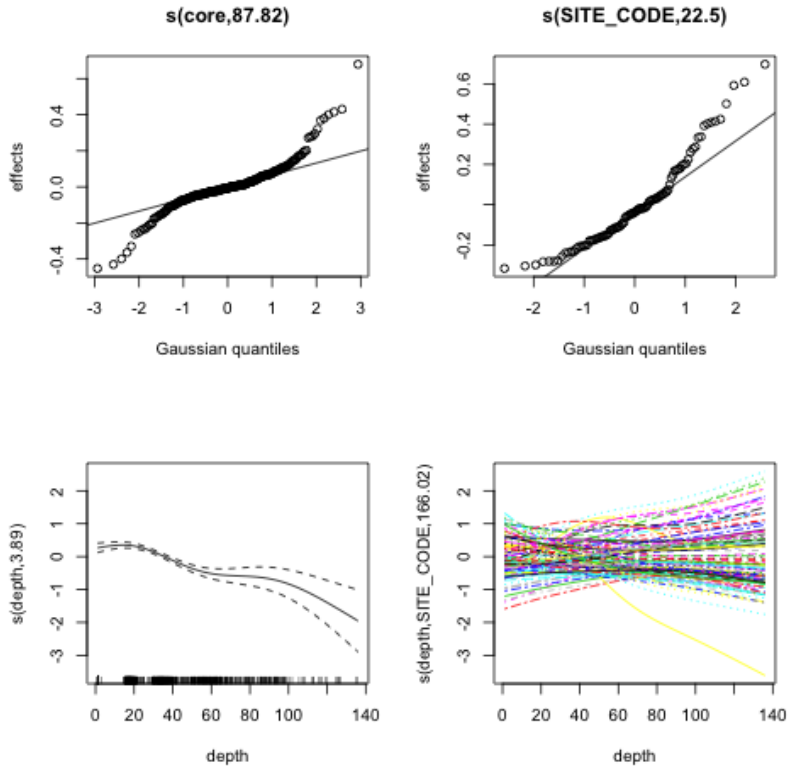

Figure A.2: Model evaluation plots for organic carbon density model.

A.3 Plant species composition methodology

In addition to the methods described in the chapter, I also conducted vegetation quadrat surveys at each core location. My aim was to incorporate local community-level plant structure and function into the model of carbon stock. Due to time limitations, I was unable to analyse this data to incorporate it into this study. I describe those methods here, as my future work to extend and improve this model will incorporate this data.

At each of the 5 cores collected per site, I laid down a 1 m^2 quadrat to estimate bare ground and species percent cover. I placed the quadrat with the core in the center, in order to reduce subjectivity in quadrat placement around the core. I could not identify most species in the field, both due to time restrictions at each site and the sheer number of species we encountered. I therefore attached a sample to an herbarium notebook and assigned a unique identifier to it. I took pictures of each quadrat from above in case the notes were lost. Although I did my best to uncover and identify submerged species, I undoubtedly missed species in sites with deep water. In many dry sites, on the other hand, we found extremely dessicated individuals that were difficult to identify.

To identify the plant samples, I used region-specific plant identification books. In many cases, though, we also had a local land guide with us on site, for example, the property manager or a Catchment Management Authority representative, who could also assist in identifying individual species. I was able to identify confidently 86 species, which covered a range of water tolerance positions in the landscape. These species corresponded to 151 of 441 unique ID's that were given to specimens in the field, as many were collected multiple times if a previous collection ID for that species was not on hand. 295 ID's remain unresolved. Although this is likely substantially fewer than 295 species, it still represented a high burden. It is likely many of these species will not be able to be identified at all, due to insufficient collection of plant parts, mispreservation of samples, or lack of available expertise, for example in the case of the wide assortment of *Juncus* species we found.

Appendix B: Supplementary material for Chapter 3

B.1 Supplementary figures and tables for Ch. 3

TABLE B.1: GenBank Accession codes.

Species	rbcl	matK
Acacia dealbata	NC_034985.1	NC_034985.1
Alternanthera pungens	AY514795.1	AY270054.1
Baumea articulata		AM999787.1
Baumea rubiginosa		AY725940.1
Carex nigra	FN668463.1	GQ469838.1
Crassula falcata	AF115594.1	
Crassula helmsii		KM360736.1
Cycnogeton procerum	KF632824.1	U80713.1
Cyperus eragrostis	KX369451.1	HM849936.1
Eleocharis acuta		AM999820.1
Eleocharis marginulata	KC123404.1	
Eucalyptus camaldulensis	NC_022398	NC_022398.1
Gahnia aspera		AB369962.1
Juncus maritimus	JN894909.1	AY216629.1
Lycopus rubellus	KJ772924.1	KJ773662.1
Marsilea crenata	KC536646	
Marsilea drummondii		DQ643299.1
Melaleuca leucadendra		KX527090.1
Melaleuca viridiflora	AF184708.1	
Muehlenbeckia australis		FM883618.1
Myriophyllum exalbescens		L11195.2
Myriophyllum sibiricum	EF178980.1	
Nymphaea alba	AJ627251	AJ627251
Paspalum distichum	FN908063.1	FN870399.1
Persicaria decipiens	KR734365.1	FM883624.1
Phragmites australis	MF035995	MF035995
Restio tetraphyllus	AF164379.1	AF206816.1
Rumex crispus	EU840458.1	JX848510.1
Sphagnum australe	KU725452	KU725452.1
Typha domingensis	HM850522.1	KJ773961.1

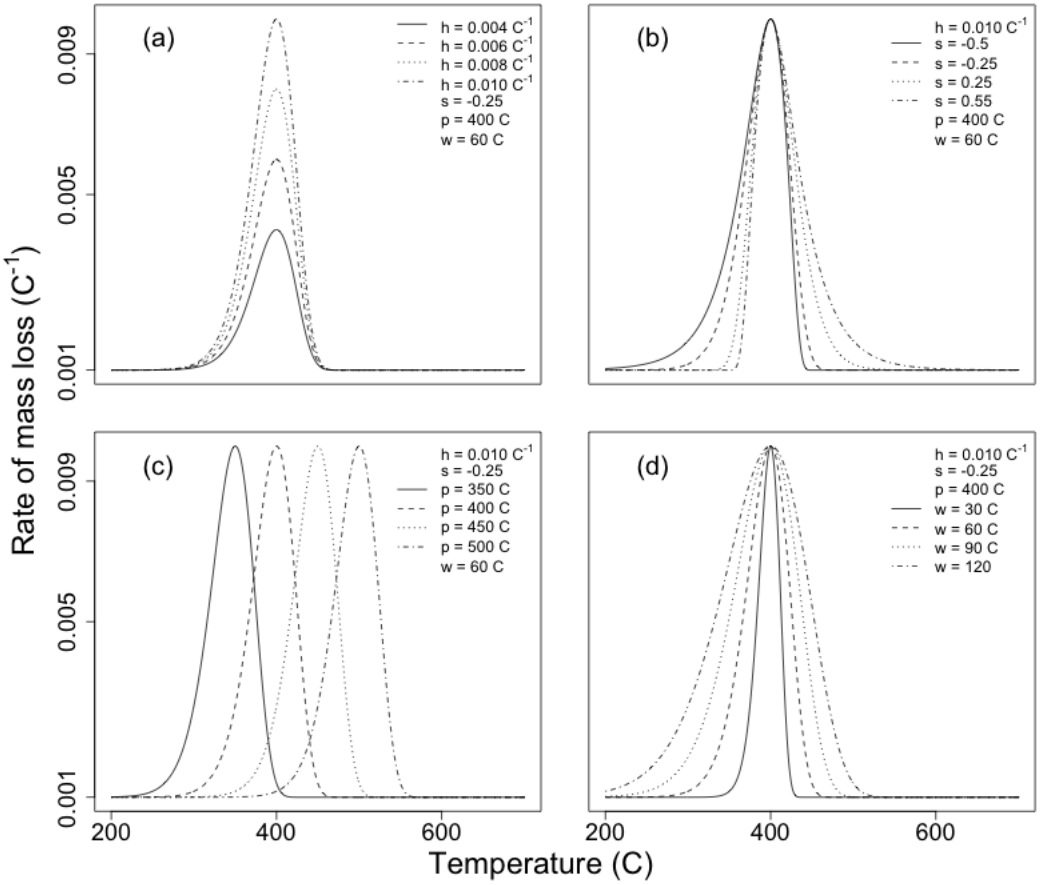

Figure B.1: Parametric study of the Fraser-Suzuki function for deconvolution of derivative thermogravimetric biomass curves: (a) Effect of modifying height; (b) skew; (c) position; and (d) width.

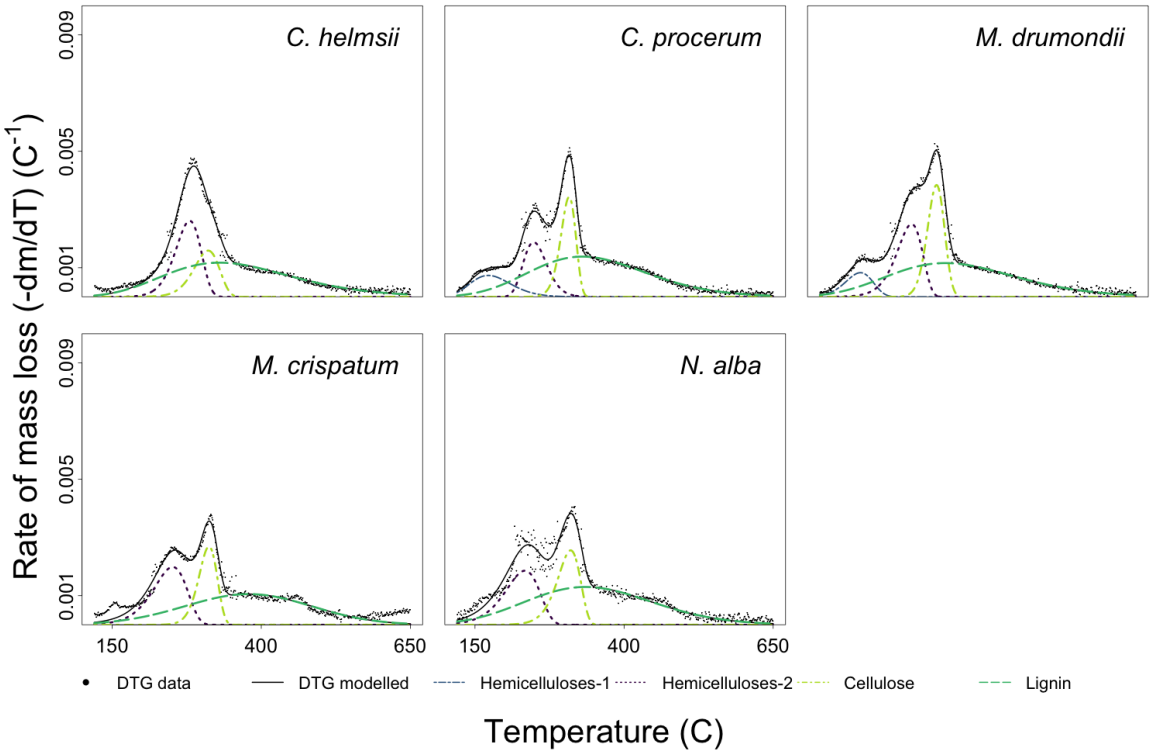

FIGURE B.2: First derivative thermogravimetric (DTG) deconvolution for amphibious fluctuation-responders (AR; n = 5).

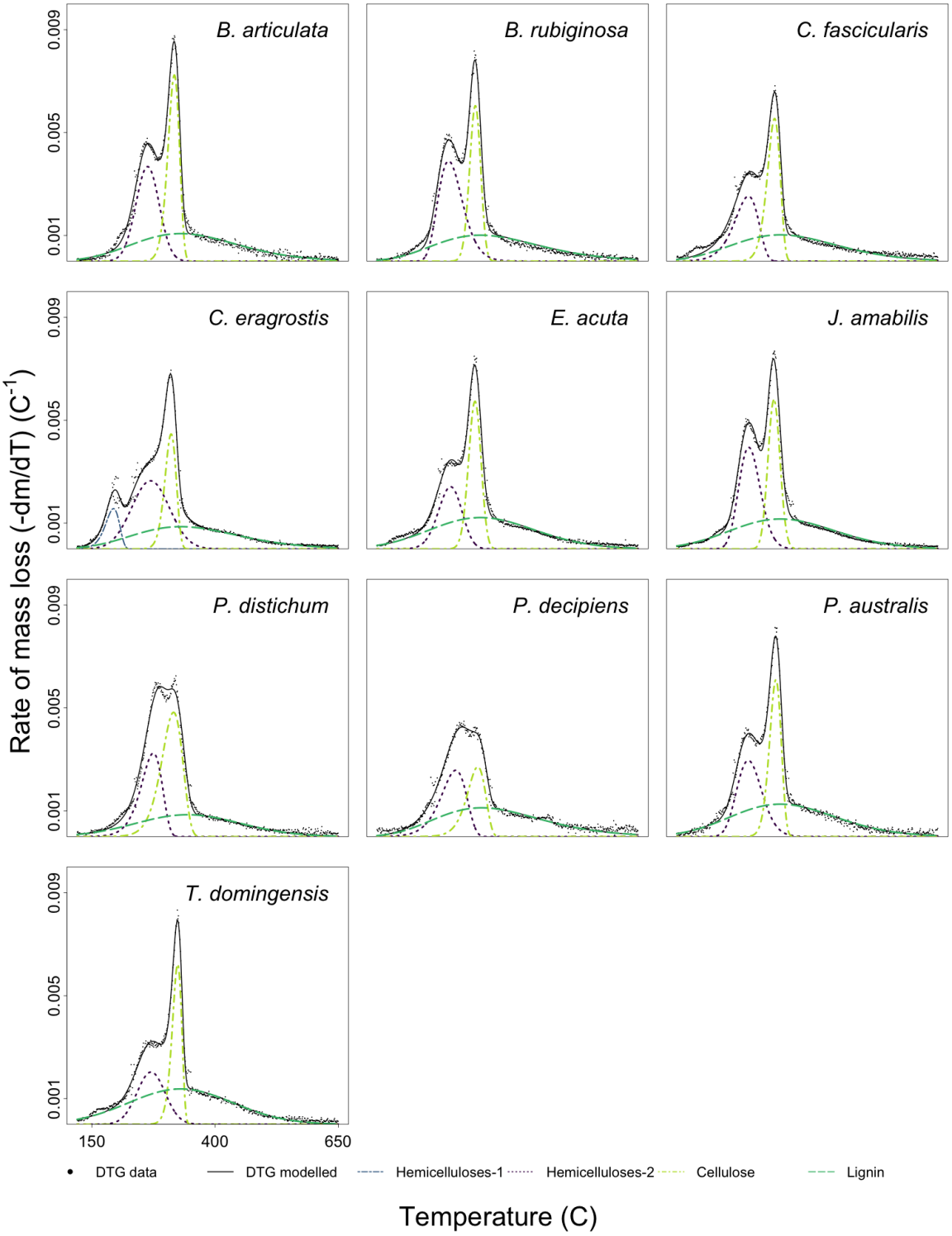

Figure B.3: First derivative thermogravimetric (DTG) deconvolution for amphibious fluctuation-tolerators (AT; n = 11).

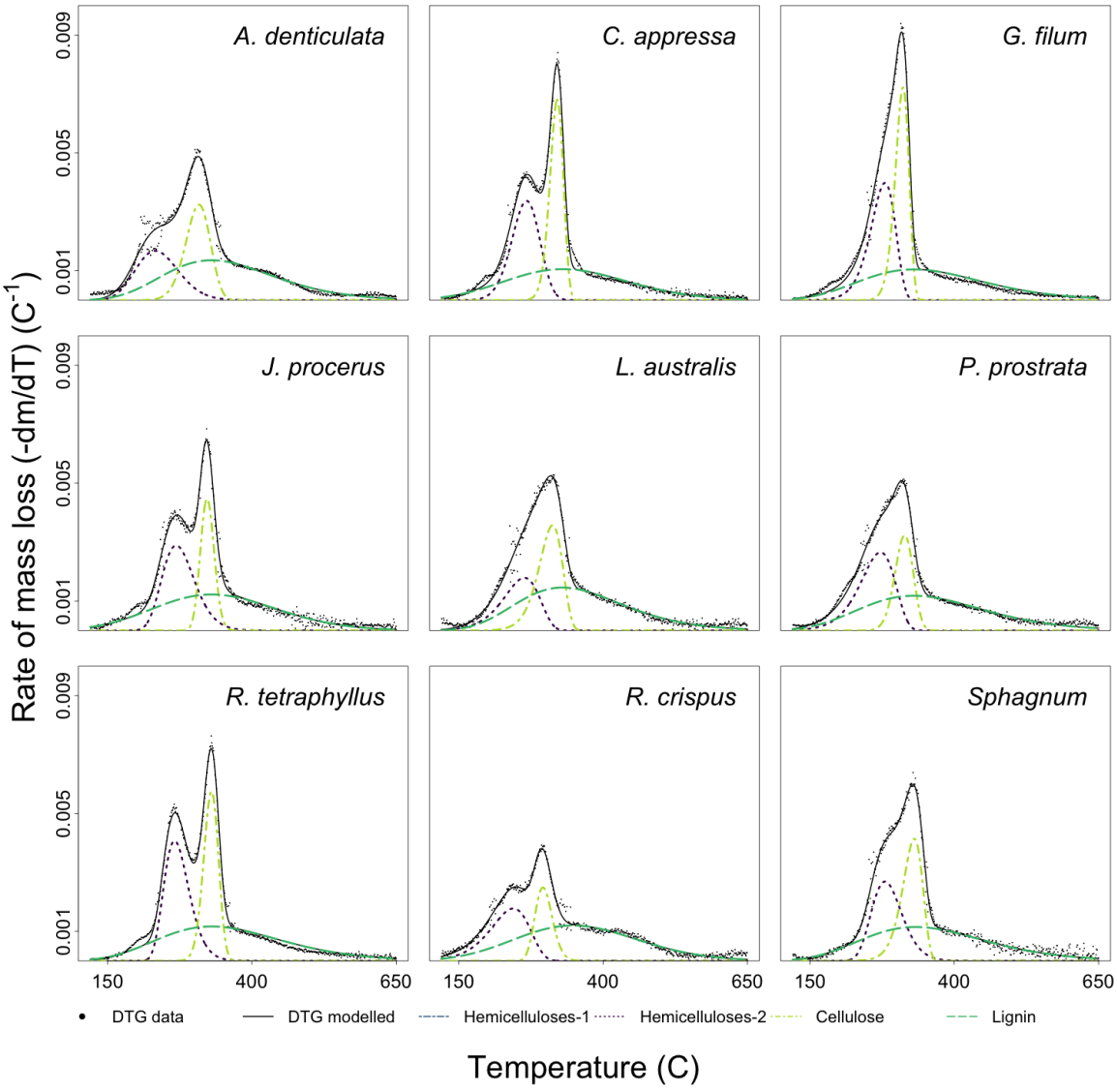

FIGURE B.4: First derivative thermogravimetric (DTG) deconvolution for terrestrial damp species (Tda; n = 8).

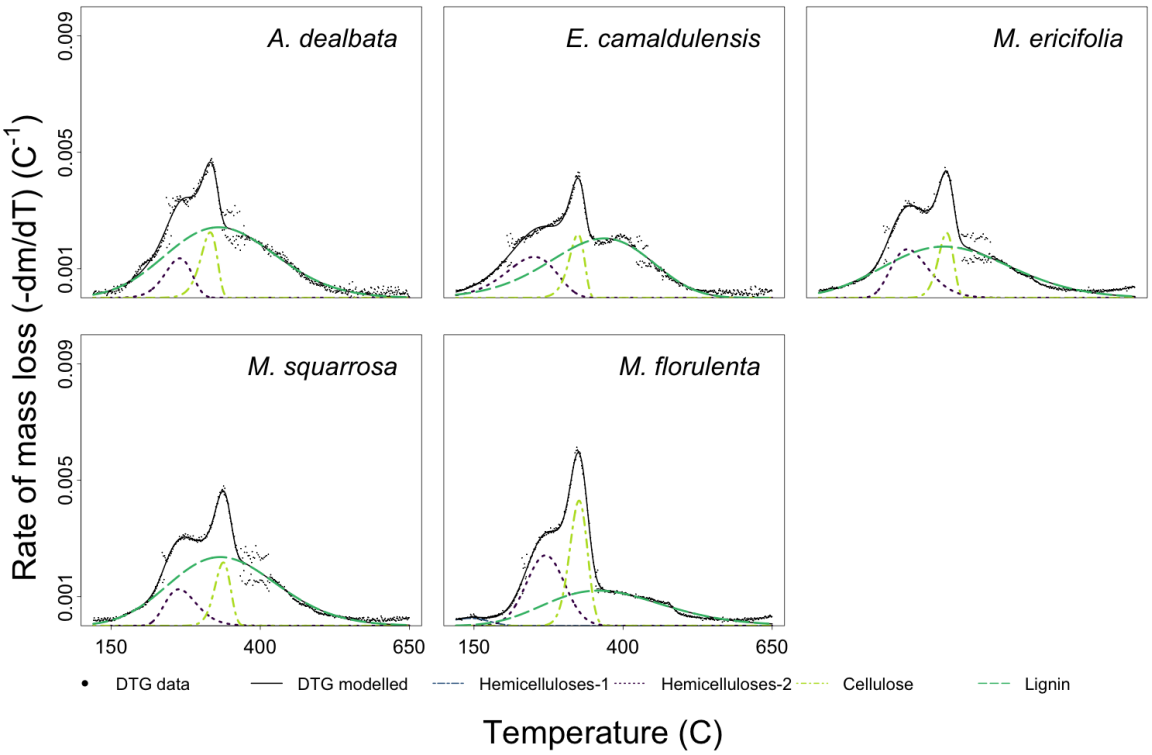

Figure B.5: First derivative thermogravimetric (DTG) deconvolution for terrestrial dry species (Tdr; n = 5).

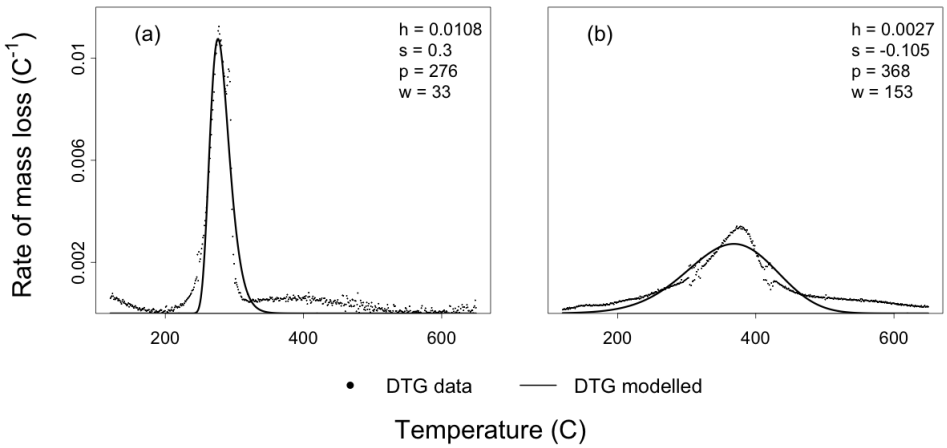

Figure B.6: Predicted negative derivative thermogravimetric for raw biomass samples: (a) carboxy-methyl cellulose; (b) alkali lignin.

Table B.2: Fraser-Suzuki mixture model parameter estimates for each species.

	Height				Position				Skew				Width			
Species	HC-1	HC-2	CL	LG	HC-1	HC-2	CL	LG	HC-1	HC-2	CL	LG	HC-1	HC-2	CL	LG
Acacia dealbata		0.0014	0.0023	0.0024		265	316	330		-0.216	-0.330	0.085		53	32	217
Alternanthera denticulata		0.0017	0.0032	0.0014		233	308	330		0.134	-0.138	0.250		87	50	224
Baumea articulata		0.0037	0.0072	0.0011		263	317	330		-0.015	-0.226	0.172		55	27	250
Baumea rubiginosa		0.0039	0.0060	0.0010		266	320	330		0.250	-0.071	0.250		58	26	250
Carex appressa		0.0034	0.0068	0.0011		268	321	330		-0.115	-0.169	0.112		57	27	250
Carex fascicularis		0.0025	0.0055	0.0010		265	319	330		-0.330	-0.270	0.176		57	31	250
Crassula helmsii		0.0026	0.0016	0.0012		280	311	330		-0.249	-0.255	0.250		50	50	250
Cycnogeton procerum	0.0007	0.0019	0.0034	0.0014	172	248	308	330	0.200	0.200	-0.228	0.177	80	46	29	229
Cyperus eragrostis	0.0016	0.0026	0.0045	0.0009	194	269	311	330	-0.323	0.002	-0.202	0.200	33	90	27	250
Eleocharis acuta		0.0024	0.0057	0.0012		270	319	330		-0.079	-0.061	0.072		56	30	250
Eucalyptus camaldulensis		0.0014	0.0022	0.0020		251	324	369		-0.275	-0.330	-0.165		100	30	203
Gahnia filum		0.0040	0.0072	0.0010		280	311	330		-0.303	-0.238	0.250		50	28	250
Juncus amabilis		0.0039	0.0058	0.0012		266	317	330		0.125	0.014	0.094		51	29	250
Juncus procerus		0.0029	0.0045	0.0012		269	322	330		0.219	0.054	0.100		66	28	250
Lycopus australis		0.0018	0.0036	0.0015		264	312	330		-0.330	-0.304	0.250		73	48	217
Marsilea drummondii	0.0008	0.0025	0.0038	0.0012	188	274	316	330	-0.201	-0.330	-0.141	0.200	54	50	34	250
Melaleuca ericifolia		0.0017	0.0022	0.0018		268	334	330		0.250	-0.227	0.101		73	30	250
Melaleuca squarrosa		0.0013	0.0022	0.0024		264	338	333		0.250	-0.195	0.109		62	31	212
Meuhlenbeckia florulenta	0.0003	0.0024	0.0043	0.0012	143	270	326	358	-0.162	-0.007	-0.122	0.200	80	75	35	230
Myriophyllum crispatum		0.0020	0.0027	0.0011		251	312	379		-0.330	-0.234	-0.017		66	36	250
Nymphaea alba		0.0019	0.0026	0.0013		234	310	335		-0.330	-0.330	0.104		68	45	250
Paspalum distichum		0.0032	0.0048	0.0008		275	316	344		-0.330	-0.287	0.029		50	50	250
Persicaria decipiens		0.0026	0.0027	0.0011		280	325	332		-0.330	-0.330	0.250		60	43	250
Persicaria prostrata		0.0027	0.0032	0.0012		272	314	330		-0.330	-0.107	0.250		70	37	250
Phragmites australis		0.0030	0.0061	0.0013		265	321	330		0.143	-0.183	0.112		59	28	250
Restio tetraphyllus		0.0041	0.0058	0.0012		266	330	330		0.250	-0.103	0.250		51	30	250
Rumex crispus		0.0018	0.0025	0.0012		244	296	347		-0.330	0.128	0.102		79	35	250
Sphagnum sp		0.0027	0.0041	0.0011		280	331	333		0.203	-0.312	0.250		62	40	250
Typha domingensis		0.0020	0.0062	0.0014		270	324	330		-0.006	-0.285	0.008		67	23	250

Table B.3: Mantel test for the correlation between branch length distance and functional trait distances between the seven traits. Litter area per mass is bold to indicate significant correlation.

Trait	Mantel Test observation	*P*-value
Litter area per mass	**0.42**	**0.01**
Litter dry matter content	0.06	0.27
Litter nitrogen	-0.1	0.72
Litter carbon	-0.13	0.86
Litter hemicelluloses	-0.07	0.59
Litter cellulose	-0.02	0.48
Litter lignin	-0.13	0.83

Table B.4: Principal Component Analysis axis loadings.

Trait	Axis 1	Axis 2
Litter area per mass	0.34	0.38
Litter dry matter content	-0.23	-0.56
Litter nitrogen	0.45	0.14
Litter carbon	0.07	-0.59
Litter hemicelluloses	-0.47	0.17
Litter cellulose	-0.46	0.07
Litter lignin	0.44	-0.37

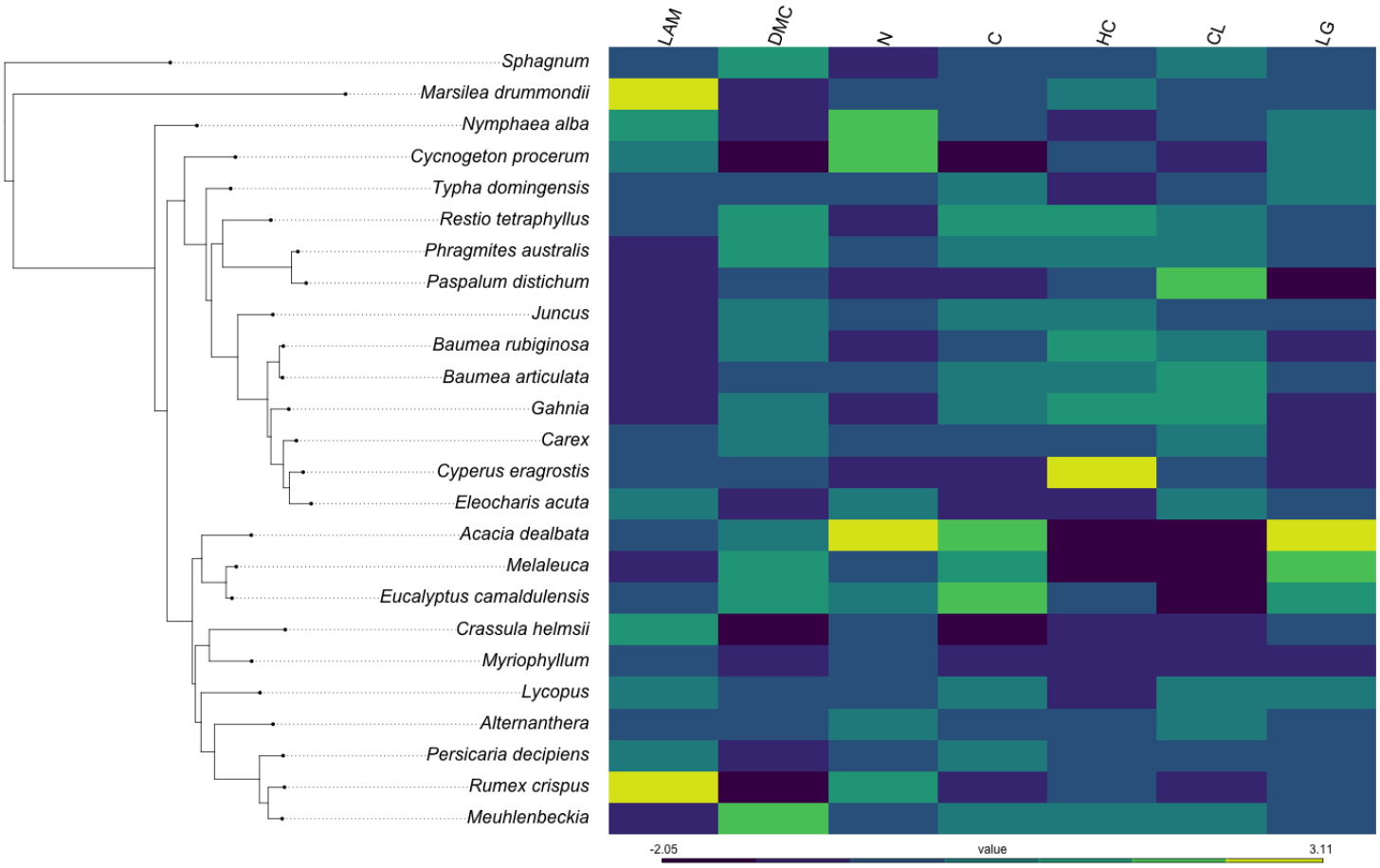

FIGURE B.7: Phylogenetic tree of species with traits. Tree at genus level where species level sequences for rcbL gene unavailable. If the branch represents more than one species, the trait value was averaged among species in that genus.

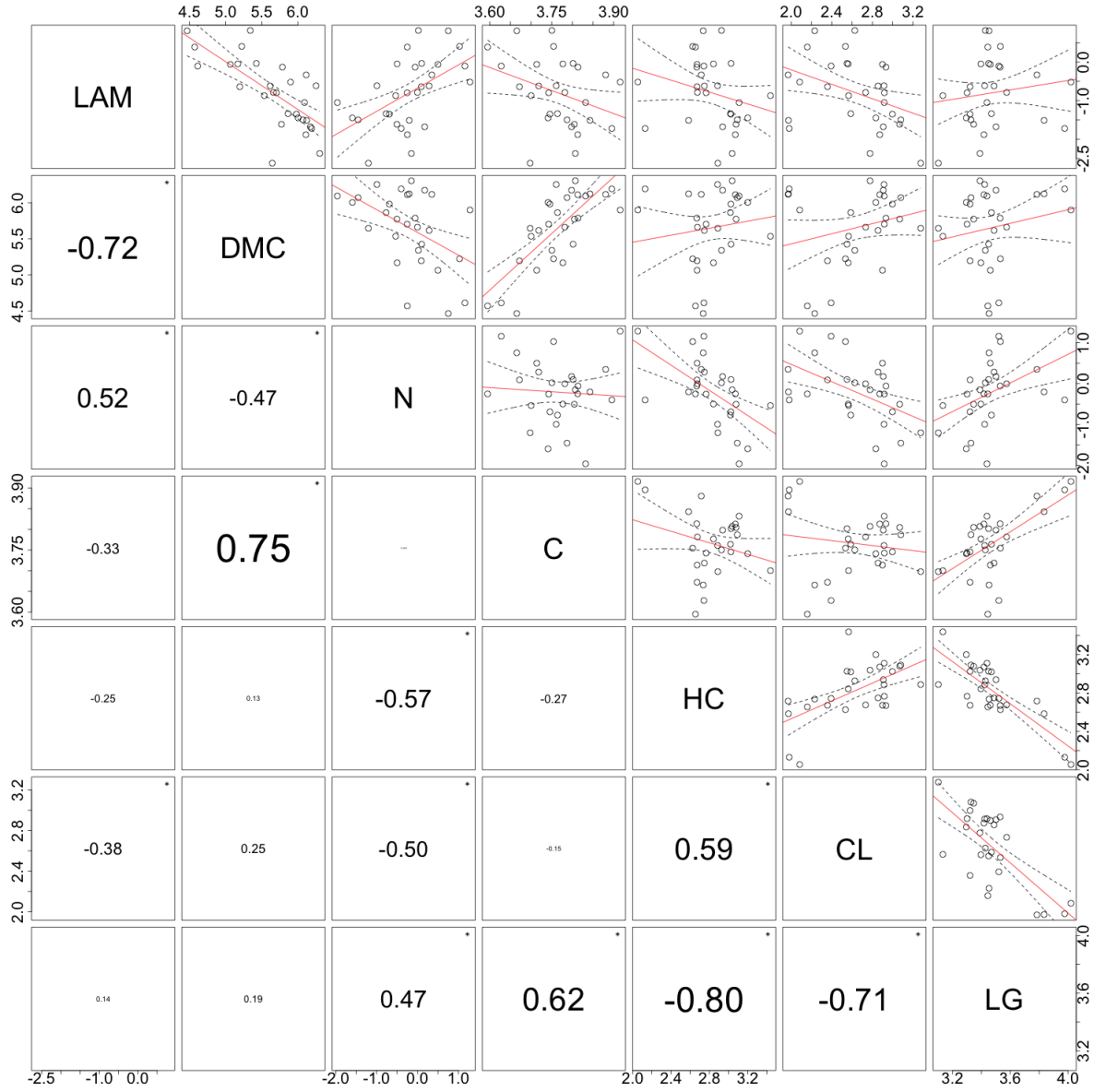

Figure B.8: Correlations between traits. Size of R^2 listed on bottom panel proportional to weight of relationship, with star to indicate significance at P $<$0.05.

Appendix C: Supplementary material for Chapter 4

C.1 Vignette: Workflow for thermal decay deconvolution with mixchar

The following is the contents of the instructional how-to vignette that accompanies the mixchar R package. It can be found at https://smwindecker.github.io/mixchar/articles/mixchar.html.

1. Load data

The first step is to load the data derived from the thermogravimetric analysis into R. This step will vary depending on the format of your exported data. Two of many options for reading data in R are `read.csv()` for .csv files and `read.table()` for .txt files. Both of these functions also have a `skip` argument, in which you can tell R to begin reading data from a certain line, useful if the exported data has several lines of metadata at the top. You may also then have to assign column names. For example:

```
my_data <- read.csv('your_file_path_here.csv', header = FALSE, skip = 15)
colnames(c('temperature_C', 'mass_mg'))
```

More information about reading data into R can be found at http://www.sthda.com/english/wiki/rea
data-from-txt-csv-files-r-base-functions.

This package was developed using data from a Netzsch TGA-FTIR thermogravimetric analyser. We have included two example datasets in this package, called `juncus` and `marsilea`, that we will use for this demonstration. The `juncus` dataset contains theromogravimetric data for a sample of the freshwater reed, *Juncus amabilis*, and `marsilea` contains data for the freshwater fern, *Marsilea drumondii*.

```
library(mixchar)
head(juncus)

##   temp_C mass_loss
## 1 31.453 -0.000931
## 2 31.452 -0.001340
## 3 31.450 -0.001350
## 4 31.450 -0.001660
## 5 31.450 -0.001680
## 6 31.450 -0.001800
```

2. Process data

After we've loaded our data, can use the function `process()` to take the derivative of this data, resulting in rate of mass loss over temperature data. This produces the multi-peaked rate of decay curve that we will apply the mixture model to. The `process` function needs the dataset, the initial mass of sample, the name of the temperature data column, and the name of your mass column (mg). Mass might be recorded in your exported dataset in different ways:

- If you have **mass loss of sample**, such as in the `juncus` dataset, you can specify the column name using the `mass_loss` argument.
- If you have **mass remaining of sample**, you specify the column name using the `mass` argument.
- **You only need to specify one of these columns** for the `process` function. But make sure the argument matches the kind of data!

The function defaults to temperature data in Celsius, but you can also modify to indicate the data is provided in Kelvin, by specifying the argument `temp_units = 'K'`.

```
deriv_juncus <- process(juncus,                    # dataframe name
                        init_mass = 18.96,
                        temp = 'temp_C',           # column name for temperature
                        mass_loss = 'mass_loss')  # column name for mass loss data
deriv_juncus

## Derivative thermogravimetry data (DTG) calculated for
##  768 datapoints from 31.5 to 798.52 degrees C.
```

```
deriv_marsilea <- process(marsilea,
                          init_mass = 15.29,
                          temp = 'temp_C',
                          mass_loss = 'mass_loss')
deriv_marsilea

## Derivative thermogravimetry data (DTG) calculated for
##  768 datapoints from 31.5 to 798.51 degrees C.
```

3. Plot mass loss and rate of mass loss curves

At this point we can take a look at what we've done so far using the default plotting option for the processed data. If you `plot()` the output of the `process` function, you will get two curves: the mass of sample across time and the rate of mass loss curve. If you're only interested in one plot, you can specify `plot_type = 'mass'` or `plot_type = 'rate'`. You can also specify a size factor using `cex`.

The rate of mass loss curve helps us to visualise the three stages of mass loss:

(i) A short period of dehydration, up until approximately 120 °C.

(ii) A wide mid-range of high mass loss, caused by devolatilisation of primary biomass carbon components, between approximately 120–650 °C.

(iii) A final period of little mass loss when carbonaceous material associated with the inorganic fraction decomposes, after approximately 650 °C.

In the next step we will crop the data to include only phase 2, so visualising your own data is important to check that the default temperature bounds will be suitable, in case for example the dehydration phase extends past 120 °C or ends earlier. Comparing the plots for the two species we can see similarities in the shape and location of the peaks of the overall rate of mass loss curve, but also subtle differences. It is these characteristics we will tease apart using the nonlinear mixture model in the next step.

```
plot(deriv_juncus, cex = 0.8)
```

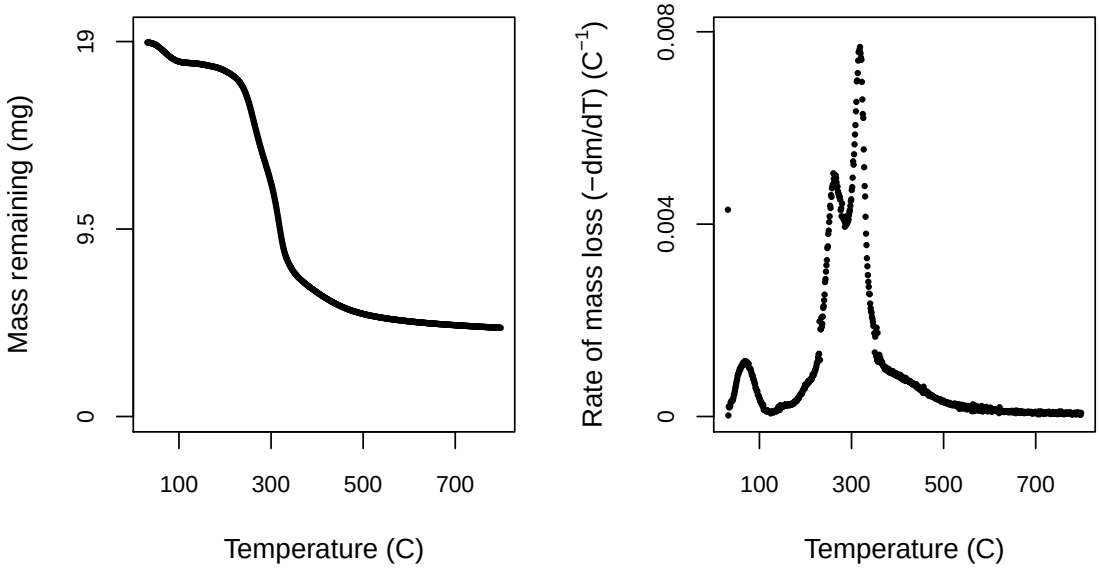


```
plot(deriv_marsilea, cex = 0.8)
```

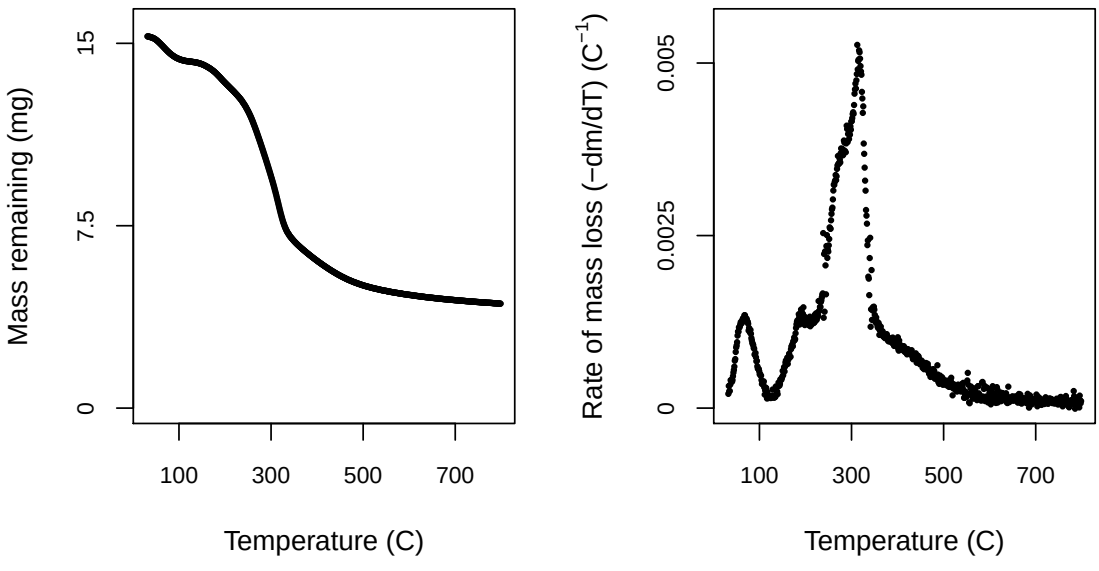

4. Deconvolve data

The `decovolve` function takes care of modelling the rate of mass loss data with the nonlinear mixture model. To do so it first crops to the second phase, as mentioned above, to default temperature bounds of 120 °C and 700 °C. These can be modified with the `lower_temp` and `upper_temp` arguments. Although most biomass samples have only three main components (corresponding to hemicellulose, cellulose, and lignin), some have a second hemicellulose peak in the low temperature range. `deconvolve` will decide whether three or four peaks are best using an internal function that determines if there is a peak below 220 °C. Upon inspection of your curve you can override this by modifying the `n_peaks` argument. The function also has built in starting values for the nonlinear optimisation. These values were tested on litter from 30 plant species, encompassing herbaceous, graminoid, as well as woody species. However, if they do not work for your sample, or you would like to play with the effect of changing them, you can do so with the `start_vec`, `lower_vec`, and `upper_vec` arguments.

```
output_juncus <- deconvolve(deriv_juncus)
output_juncus

## Deconvolution by 4-part Fraser-Suzuki mixture model fitted to
## 580 datapoints from 120 to 700 degrees C.
```

```
# here's an example of specifying your starting vector.
# the order of values is height, skew, position, then width

my_starting_vec <- c(height_0 = 0.002, skew_0 = -0.15,
                     position_0 = 210, width_0 = 50,
                     height_1 = 0.003, skew_1 = -0.15,
                     position_1 = 250, width_1 = 50,
                     height_2 = 0.006, skew_2 = -0.15,
                     position_2 = 320, width_2 = 30,
                     height_3 = 0.001, skew_3 = -0.15,
                     position_3 = 390, width_3 = 200)

output_marsilea <- deconvolve(deriv_marsilea,
                              n_peaks = 4,
                              start_vec = my_starting_vec)

output_marsilea

## Deconvolution by 4-part Fraser-Suzuki mixture model fitted to
## 580 datapoints from 120 to 700 degrees C.
```

5. Examine outputs

`deconvolve` results in a few different outputs that you can retrieve with accessor functions.

- `rate_data()` will show you the processed dataset that results from the `process` function, useful if you want to play around with other modelling approaches or plotting options:

```
juncus_rate <- rate_data(output_juncus)
head(juncus_rate)

##       temp_C        deriv   mass_T
## 5325 120.514 9.570652e-05 17.91630
## 5384 121.501 9.885901e-05 17.91445
## 5445 122.515 1.003878e-04 17.91252
## 5505 123.514 9.133606e-05 17.91079
## 5565 124.513 6.493836e-05 17.90956
## 5625 125.509 8.578618e-05 17.90794
```

- `temp_bounds()` will print the temperature values at which the data were cropped for analysis:

```
temp_bounds(output_juncus)

## [1] 120 700
```

- `model_fit()` will show you the output of the mixture model and estimated parameter values for height, skew, position, and width for each peak. Peak 1 is hemicellulose, peak 2 is cellulose, and peak 3 is lignin. If present, the optional fourth peak located at the lowest temperature interval will be listed as peak 0:

```
model_fit(output_juncus)
```

```
## Nonlinear regression model
##   model: deriv ~ fs_mixture(temp_C, height_1, skew_1, position_1,
##     width_1, height_2, skew_2, position_2, width_2, height_3,
##     skew_3, position_3, width_3)
##   data: dataframe
##   height_1   skew_1     position_1 width_1    height_2   skew_2
##   3.944e-03  1.258e-01  2.662e+02  5.106e+01  5.793e-03  1.344e-02
##   position_2 width_2    height_3   skew_3     position_3 width_3
##   3.173e+02  2.866e+01  1.163e-03  1.085e-01  3.300e+02  2.500e+02
##   residual sum-of-squares: 9.299e-06
##
## Number of iterations to convergence: 23
## Achieved convergence tolerance: 1.49e-08
```

- `component_weights()` will display the mean, 2.5% and 97.5% estimates, median, and standard deviation of the weight of each component:

```
component_weights(output_juncus)
```

```
##           HC         CL         LG value_type
## 1 21.5600422 17.6748693 30.6629891       mean
## 2 20.4327310 16.6433643 29.5201899       2.5%
## 3 21.5980403 17.6367428 30.6535159        50%
## 4 22.7575067 18.6700545 31.8302178      97.5%
## 5  0.5978226  0.5128315  0.5914671         sd
```

```
component_weights(output_marsilea)
```

```
##       HC_1      HC_2        CL        LG value_type
## 1 4.625424 16.281262 11.601421 31.009216       mean
## 2 2.664669  9.124992  3.885895 24.840610       2.5%
## 3 4.555857 16.317491 11.763705 31.052827        50%
## 4 6.922566 27.118052 22.561005 36.140567      97.5%
## 5 1.114594  4.434647  4.829687  3.013464         sd
```

6. Plot deconvolved curves

The default plotting function for the output of the `deconvolve` function shows you your raw mass data, the estimated full curve from the mixture model, and also plots the individual component peaks using their parameter estimates from the model. The default plot is in black and white, but you can plot a colour version that uses colour-blind friendly viridis colours by specifying `bw = FALSE`.

Take a look at your plot. Do the estimates seem reasonable?

```
plot(output_juncus, bw = FALSE)
```

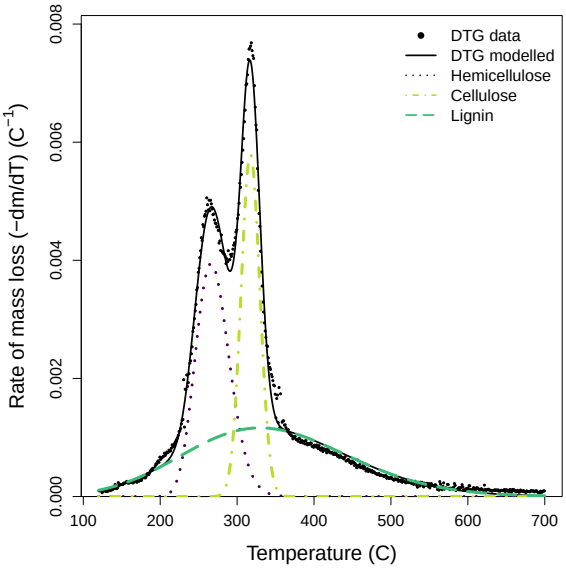


```
plot(output_marsilea, bw = FALSE)
```

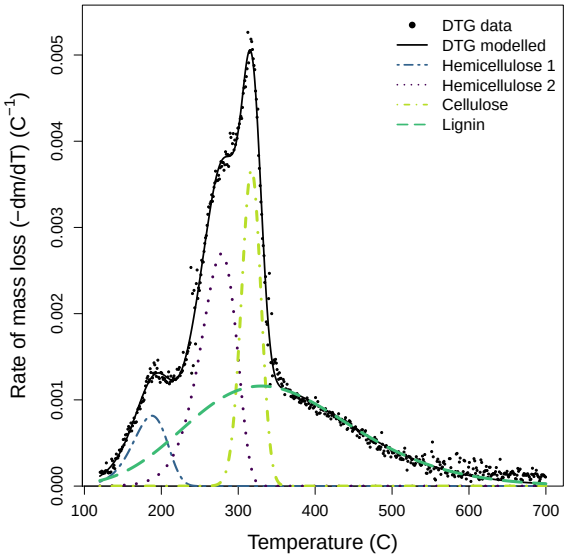

If the estimated peaks do not match your data well, it may be that your sample is a bit different than those used to develop the package. That's not a problem, but you may need to try the deconvolution again with different starting values. If you aren't managing to produce reasonable estimates, get in touch with us via the issues page at http://www.github.com/smwindecker/mixchar/issues.

If you want to modify the aesthetics of this plot for your own work, then you can access the parameter estimates as follows:

```
juncus_parameters <- model_parameters(output_juncus)
```

and use `fs_function()` to plot individual component peaks, and `fs_mixture` function to plot the overall mixture curve.

More information

To read more about the methodology, check out the Detailed Methodology article at http://smwindecker.github.io/mixchar/articles/Background.html.

Appendix D: Supplementary material for Chapter 5

D.1 Supplementary figures and tables for Ch. 5

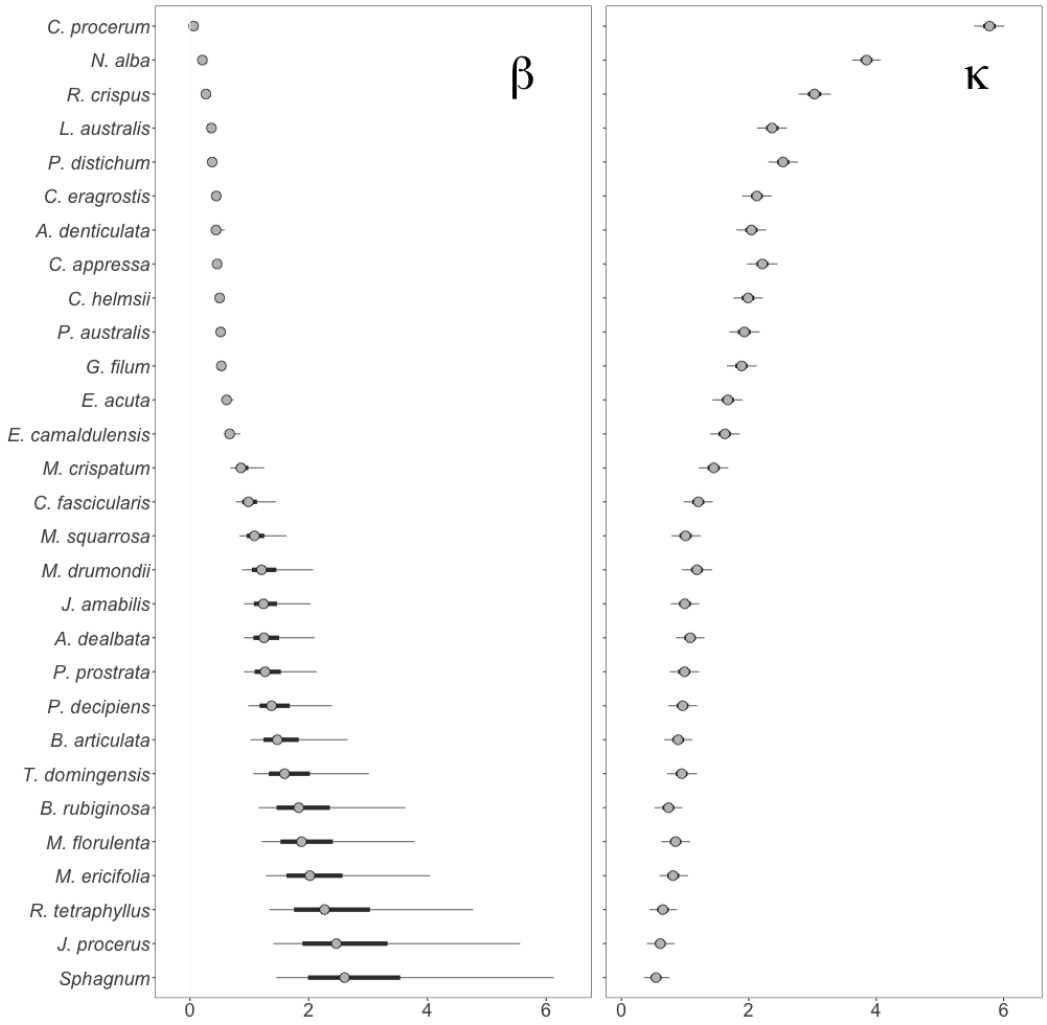

FIGURE D.1: Posterior distributions and 95% credible intervals for parameter estimates of species-level β and κ from the null hierarchical model. Species in descending order by median β estimate. Sigma indicates the posterior draws for the hyperparameter of species-level standard deviation.

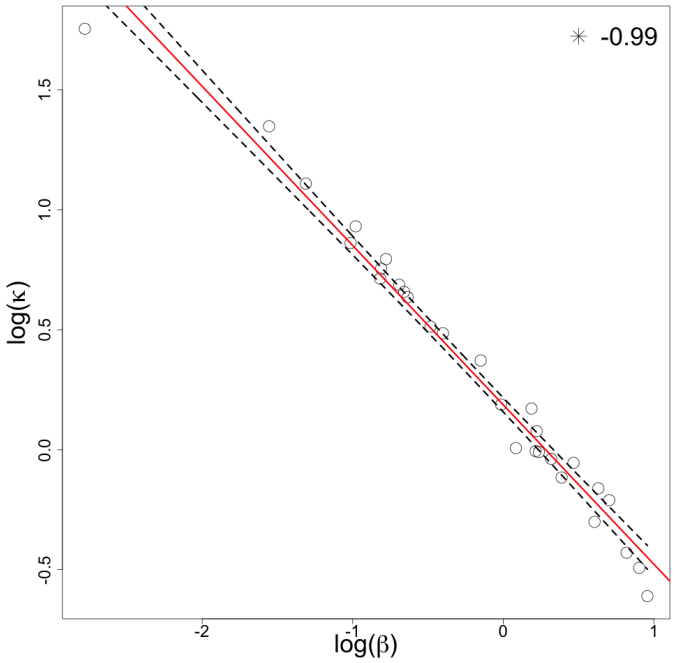

Figure D.2: Correlation between β and κ parameter estimates per species (p<0.5).

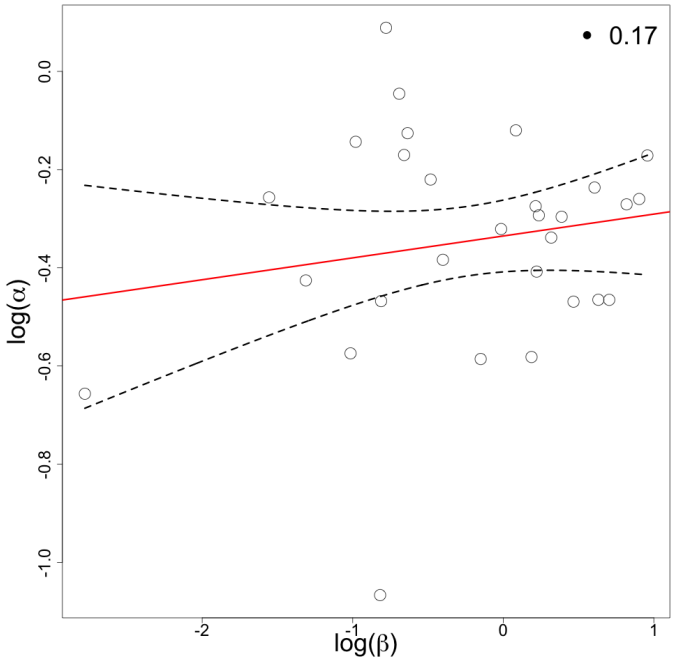

Figure D.3: Correlation between α and β parameter estimates per species (p>0.5).

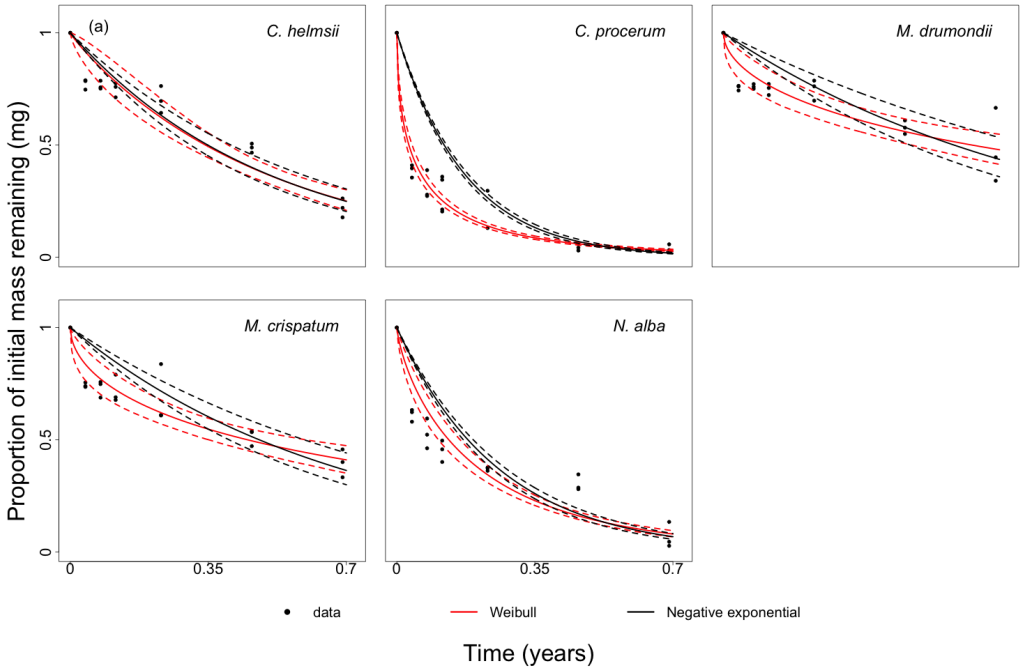

FIGURE D.4: Decomposition data and predictions by the negative exponential and Weibull residence time models for amphibious fluctuation-responder species (n = 5).

TABLE D.1: Parameter estimates for κ, α, and β for all species. Presented with lower and upper 95% confidence intervals of estimates in brackets.

Family	Species	Functional group	Growth form	κ	α	β	t_{50}	Mean residence time
Amaranthaceae	*Alternanthera denticulata*	Tda	Forb	2.04[1.76, 2.31]	0.35[0.24, 0.45]	0.45[0.34, 0.63]	0.16	2.38
Crassulaceae	*Crassula helmsii*	AR	Forb	1.99[1.70, 2.27]	0.97[0.73, 1.29]	0.50[0.44, 0.56]	0.34	0.51
Cyperaceae	*Baumea articulata*	AT	Graminoid	0.89[0.63, 1.15]	0.76[0.49, 1.15]	1.62[0.96, 3.10]	1.00	1.90
Cyperaceae	*Baumea rubiginosa*	AT	Graminoid	0.74[0.48, 1.01]	0.82[0.51, 1.27]	2.04[1.10, 4.32]	1.30	2.28
Cyperaceae	*Carex appressa*	Tda	Graminoid	2.21[1.93, 2.50]	1.11[0.84, 1.44]	0.46[0.41, 0.51]	0.33	0.44
Cyperaceae	*Carex fascicularis*	AT	Graminoid	1.21[0.93, 1.49]	0.74[0.49, 1.07]	1.03[0.74, 1.59]	0.63	1.24
Cyperaceae	*Cyperus eragrostis*	AT	Graminoid	2.13[1.86, 2.41]	0.63[0.48, 0.81]	0.45[0.38, 0.53]	0.25	0.63
Cyperaceae	*Eleocharis acuta*	AT	Graminoid	1.67[1.39, 1.95]	0.81[0.59, 1.10]	0.62[0.53, 0.77]	0.40	0.70
Cyperaceae	*Gahnia filum*	Tda	Graminoid	1.89[1.61, 2.17]	0.90[0.67, 1.18]	0.53[0.47, 0.62]	0.35	0.56
Fabaceae	*Acacia dealbata*	Tdr	Tree	1.08[0.82, 1.35]	0.68[0.44, 0.99]	1.35[0.86, 2.40]	0.78	1.76
Haloragaceae	*Myriophyllum crispatum*	AR	Forb	1.45[1.17, 1.72]	0.56[0.39, 0.77]	0.90[0.65, 1.37]	0.47	1.48
Juncaceae	*Juncus amabilis*	AT	Graminoid	1.00[0.73, 1.26]	0.78[0.52, 1.17]	1.33[0.87, 2.31]	0.83	1.53
Juncaceae	*Juncus procerus*	Tda	Graminoid	0.61[0.36, 0.87]	0.80[0.50, 1.29]	2.86[1.28, 6.66]	1.81	3.24
Juncaginaceae	*Cycnogeton procerum*	AR	Graminoid	5.78[5.49, 6.06]	0.52[0.47, 0.57]	0.06[0.05, 0.07]	0.03	0.12
Lamiaceae	*Lycopus australis*	AT	Forb	2.37[2.09, 2.64]	0.57[0.45, 0.71]	0.36[0.31, 0.43]	0.19	0.59
Marsileaceae	*Marsilea drummondii*	AR	Forb	1.19[0.90, 1.46]	0.57[0.38, 0.80]	1.31[0.84, 2.33]	0.68	2.12
Myrtaceae	*Eucalyptus camaldulensis*	Tdr	Tree	1.62[1.35, 1.90]	0.69[0.49, 0.94]	0.68[0.56, 0.90]	0.40	0.88
Myrtaceae	*Melaleuca ericifolia*	Tdr	Tree	0.81[0.55, 1.09]	0.64[0.42, 0.94]	2.27[1.20, 4.79]	1.28	3.13
Myrtaceae	*Melaleuca squarrosa*	Tdr	Tree	1.01[0.74, 1.29]	0.92[0.60, 1.41]	1.14[0.80, 1.87]	0.77	1.19
Nymphaeaceae	*Nymphaea alba*	AR	Forb	3.85[3.58, 4.11]	0.78[0.67, 0.90]	0.21[0.18, 0.24]	0.13	0.24
Poaceae	*Paspalum distichum*	AT	Graminoid	2.54[2.26, 2.81]	0.87[0.71, 1.07]	0.38[0.33, 0.42]	0.25	0.40
Poaceae	*Phragmites australis*	AT	Graminoid	1.93[1.65, 2.22]	0.85[0.63, 1.11]	0.52[0.45, 0.61]	0.34	0.56
Polygonaceae	*Meuhlenbeckia florulenta*	Tdr	Shrub	0.85[0.59, 1.12]	0.65[0.42, 0.97]	2.10[1.13, 4.59]	1.19	2.90
Polygonaceae	*Persicaria decipiens*	AT	Forb	0.96[0.69, 1.23]	0.73[0.48, 1.08]	1.50[0.93, 2.78]	0.90	1.82
Polygonaceae	*Persicaria prostrata*	Tda	Forb	0.99[0.72, 1.27]	0.77[0.50, 1.16]	1.37[0.87, 2.46]	0.85	1.60
Polygonaceae	*Rumex crispus*	Tda	Forb	3.03[2.73, 3.34]	0.66[0.53, 0.80]	0.27[0.23, 0.31]	0.15	0.36
Restionaceae	*Restio tetraphyllus*	Tda	Graminoid	0.65[0.41, 0.91]	0.79[0.50, 1.24]	2.58[1.24, 5.70]	1.62	2.95
Sphagnaceae	*Sphagnum sp*	Tda	Non-vascular	0.55[0.31, 0.80]	0.88[0.55, 1.40]	3.06[1.34, 7.49]	2.02	3.27
Typhaceae	*Typha domingensis*	AT	Graminoid	0.95[0.67, 1.24]	0.64[0.41, 0.94]	1.77[1.01, 3.60]	1.00	2.46

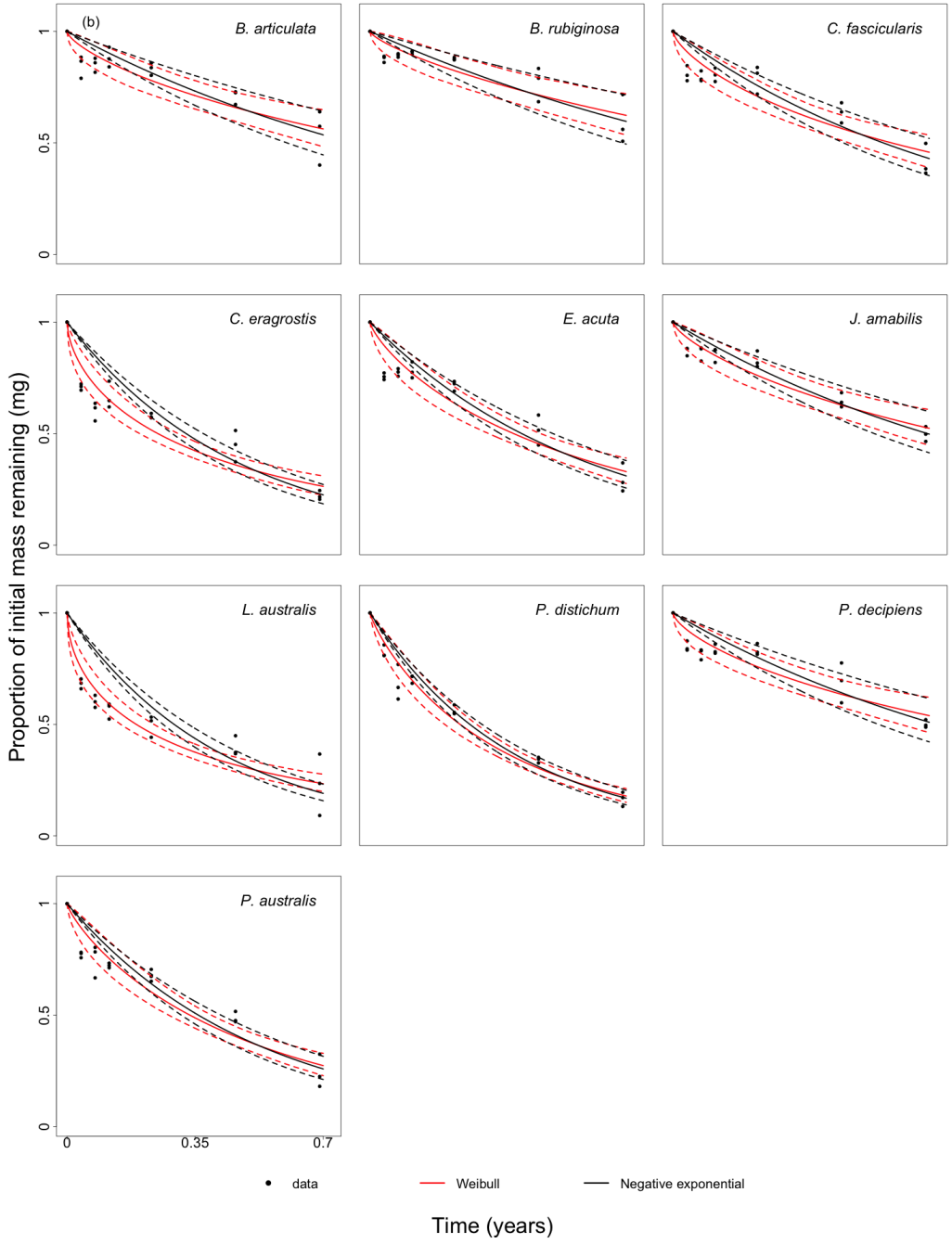

Figure D.5: Decomposition data and predictions by the negative exponential and Weibull residence time models for amphibious fluctuation-tolerator species (n = 11).

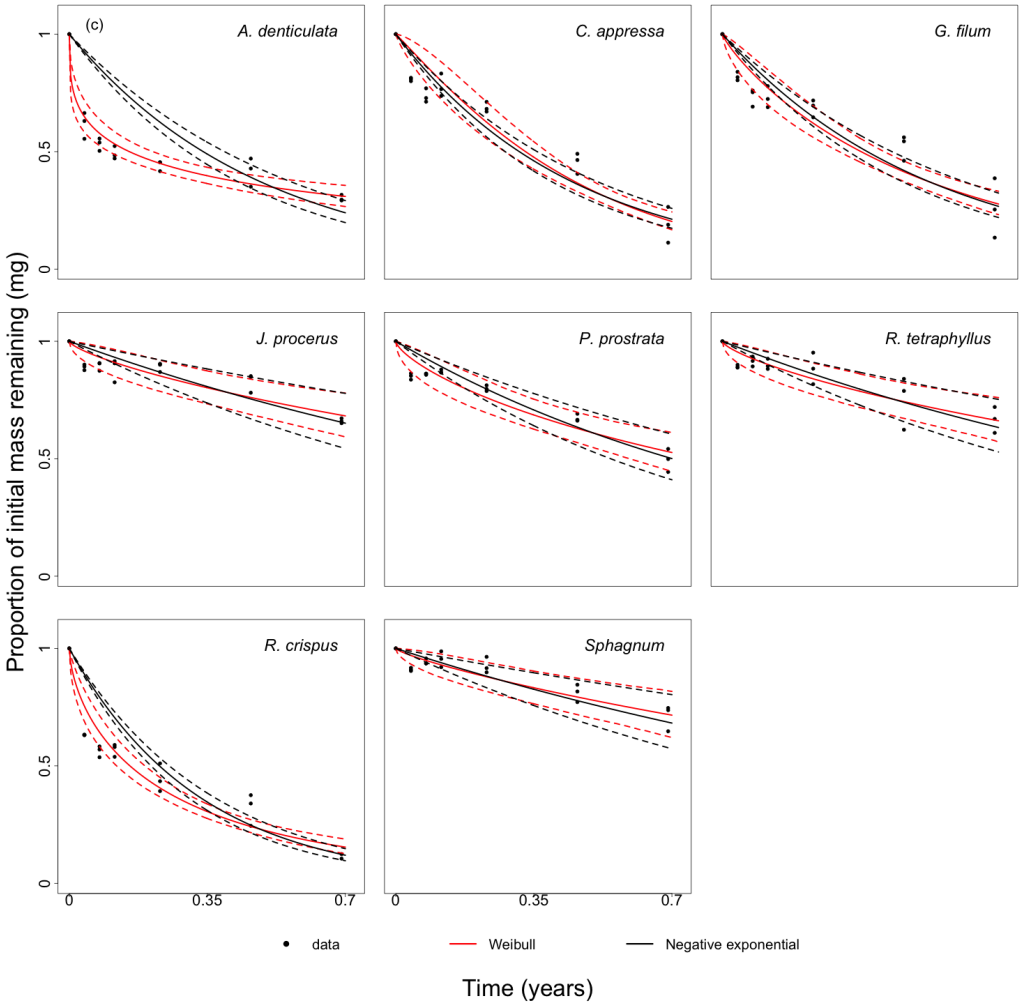

FIGURE D.6: Decomposition data and predictions by the negative exponential and Weibull residence time models for terrestrial damp species (n = 8).

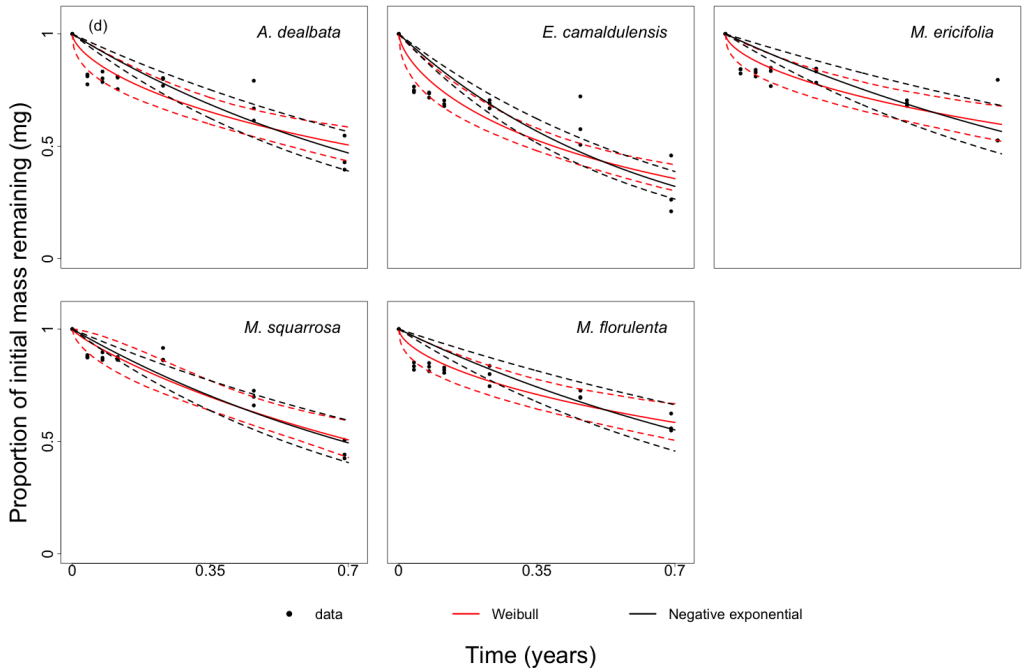

Figure D.7: Decomposition data and predictions by the negative exponential and Weibull residence time models for terrestrial dry species (n = 5).

TABLE D.2: Deviance ranking of all Weibull models with trait fixed effects.

Formula α	Formula β	Median deviance
1	1 + N + C	-1.24[-11.7, 112]
1	1 + N + HC	1.53[-7.87, 213]
1	1 + N + LG	2.32[-10.1, 140]
1	1 + C	3.3[-1.5, 351]
1	1 + N + DMC	3.35[-8.21, 200]
1	1 + N + LAM	3.71[-3.38, 422]
1	1 + N + CL	4.86[-3.89, 371]
1	1 + C + CL	4.91[-1.39, 366]
1	1 + C + HC	4.93[-2.38, 375]
1	1 + N	5.42[-2.81, 396]
1 + LAM	1 + N	5.6[-3.31, 1020000]
1	1 + C + LAM	6.02[-1.9, 371]
1	1 + C + DMC	6.18[-4.03, 298]
1	1 + LAM + DMC	6.48[-3.71, 227]
1	1 + C + LG	6.86[-2.91, 407]
1	1 + DMC	7.35[-3.85, 182]
1 + DMC	1 + N	7.37[-4.71, 7.08e+13]
1	1 + DMC + LG	7.5[-4, 187]
1 + CL	1 + N	7.53[-2.8, 1.32e+29]
1	1 + DMC + HC	7.97[-3.9, 185]
1 + C	1	8.19[2.18, 1.94e+09]
1 + DMC	1	8.44[1.59, 2.17e+12]
1	1 + DMC + CL	8.52[-4.53, 188]
1 + CL	1 + DMC	8.66[-3.79, 9.81e+56]
1 + N + DMC	1	8.93[1.55, 8.19e+37]
1 + DMC	1 + HC	9.03[2.33, 229]
1	1 + LAM	9.19[1.37, 199]
1 + CL	1 + LAM	9.69[1.22, 176]
1 + N	1	9.87[3.92, 4.74e+25]
1	1 + LAM + LG	9.89[1.52, 210]
1	1 + LAM + CL	9.99[1.43, 205]
1 + LG	1 + N	10.1[-1.97, 146000]
1 + C + LG	1	10.2[2.04, 2.14e+09]
1	1 + LG	10.2[4.62, 228]
1 + HC	1 + N	10.3[-2.98, 5.33e+15]
1	1 + HC + LG	10.5[4, 236]
1 + CL + LG	1	10.5[5.05, 211]
1 + LAM	1	10.6[4.1, 3490]
1	1 + CL	10.9[4.73, 221]
1	1 + CL + LG	11[4.96, 226]
1	1 + LAM + HC	11[1.19, 198]
1 + DMC	1 + LG	11.1[-0.426, 468]
1 + C	1 + LAM	11.1[0.11, 1.3e+26]
1 + CL	1	11.1[4.44, 88100]
1 + N + CL	1	11.2[1.24, 2.09e+182]
1 + N	1 + N	11.3[-2.4, 1330000]
1 + C + LAM	1	11.4[3, 3.07e+107]
1 + DMC	1 + DMC	11.4[-3.06, 6.85e+50]
1 + C + CL	1	11.6[3.38, 1.17e+23]
1 + C + DMC	1	11.6[2.72, 2.47e+86]
1 + DMC + LG	1	12[1.95, 8.99e+37]
1 + LAM + HC	1	12.1[5.26, 191000]
1 + N + HC	1	12.4[1.66, 3.26e+11]
1 + CL	1 + LG	12.4[4.67, 1.2e+104]
1 + LAM	1 + LAM	12.5[1.51, 6.02e+16]
1	1 + HC	12.6[4.59, 217]
1	1 + HC + CL	12.7[4.71, 225]
1 + DMC + HC	1	12.7[2.31, 9.82e+73]
1 + HC	1 + LG	12.8[4.89, 7.87e+09]
1 + LAM + LG	1	12.9[4.06, 3.27e+15]
1 + LG	1 + LG	13.1[7.08, 1.29e+13]
1 + HC + LG	1	13.2[5.88, 1.1e+169]
1 + LG	1	13.2[4.61, 3.56e+15]
1 + C	1 + CL	13.3[2.66, 8.76e+10]
1 + C + HC	1	13.6[2.54, 3.6e+07]
1 + LAM + CL	1	13.8[4.8, 2.1e+13]
1 + C	1 + LG	13.9[0.306, 147000]
1 + HC	1 + LAM	13.9[2.19, 894]
1 + DMC + CL	1	14.2[2.42, 2.68e+54]
1 + HC	1	14.4[4.69, 7390]
1 + LAM	1 + LG	14.8[3.66, 7.88e+42]
1 + CL	1 + CL	14.8[4.62, 5.51e+166]
1 + CL	1 + HC	14.9[5.45, 1.82e+23]
1 + C	1 + DMC	14.9[-2.22, 1.79e+43]
1 + DMC	1 + LAM	15.8[1.6, 2.29e+16]
1 + N + C	1	15.8[1.38, 3.12e+24]
1 + C	1 + HC	16.1[2.01, 1.29e+37]
1 + HC	1 + HC	16.3[4.71, 2.54e+11]
1 + N + LG	1	16.5[2.06, 2.84e+24]
1 + N + LAM	1	17.1[3.26, 2.76e+18]
1 + C	1 + C	17.2[-2.37, 5660]
1 + C	1 + N	17.9[-1.05, 5.87e+29]
1 + HC + CL	1	17.9[5.93, 1.07e+305]
1 + LAM + DMC	1	19.9[2.27, 2.46e+52]

D.2 Stan code

Stan code for negative exponential model with cross validation

```
functions {
#include /functions/neg_exp_functions.stan
#include /functions/param_functions.stan
}

data {
  int<lower=1> N;                          // number of data points
  int<lower=1> N_test;
  vector[N] mT;                            // logged mass at time T
  vector[N_test] mT_test;
  vector[N] m0;                            // logged initial mass
  vector[N_test] m0_test;
  vector<lower=0>[N] time;                 // time
  vector<lower=0>[N_test] time_test;
  int<lower=1> P;                          // no fixefs
  int<lower=1> J;                          // number of species
  matrix[J, P] X;                          // design matrix for alpha effects
  matrix[1, P] X_test;
  int<lower=1, upper=J> sp[N];             // species id
}

parameters {
  vector[P] b;
  real<lower=0> sigma_obs;                 // observation sd
}

model {
  vector[J] k;

  // priors
  sigma_obs ~ normal(0, 2);
  b ~ normal(0, 2);

  // likelihood
  k = param(b, X, P, J);
  mT ~ normal(m0 - k[sp] .* time, sigma_obs);
}

generated quantities {

  real neg_loglik;
  vector[N_test] mT_pred;

  {
  real k_pred;

  k_pred = param_pred(b, X_test, P);
  mT_pred = negexp_pred_rng(N_test, m0_test, time_test, k_pred, sigma_obs);
  neg_loglik = negexp_negloglik(mT_test, m0_test, time_test, k_pred, sigma_obs, N_
      test);
  }
}
```

Stan model for negative exponential model with random effects by species

```
functions {
```

```
#include /functions/neg_exp_functions.stan
#include /functions/param_functions.stan
}

data {
  int<lower=1> N;                          // number of data points
  vector[N] mT;                            // logged mass at time T
  vector[N] m0;                            // logged initial mass
  vector<lower=0>[N] time;                 // time
  int<lower=1> P;                          // no fixefs
  int<lower=1> J;                          // number of species
  matrix[J, P] X;                          // design matrix for alpha effects
  int<lower=1, upper=J> sp[N];             // species id

  int<lower=1> N_sim;                      // number of data points
  vector[N_sim] m0_sim;
  vector<lower=0>[N_sim] time_sim;         // time
  int<lower=1, upper=J> sp_sim[N_sim];     // species id
}

parameters {
  vector[P] b;
  vector[J] a;                             // species intercepts on alpha
  real<lower=0> sigma_obs;                 // observation sd
  real<lower=0> sigma_sp;                  // species sp
}

model {
  vector[J] k;

  // priors
  a ~ normal(0, sigma_sp);                 // species random effects on alpha
  sigma_sp ~ normal(0, 2);
  sigma_obs ~ normal(0, 2);
  b ~ normal(0, 2);

  // likelihood
  k = param_re(b, X, P, J, a);
  mT ~ normal(m0 - k[sp] .* time, sigma_obs);
}

generated quantities {

  vector[N_sim] mT_sim;
  vector[J] k_fit;

  k_fit = param_re(b, X, P, J, a);
  mT_sim = negexp_sim_rng(N_sim, m0_sim, time_sim, k_fit, sp_sim);

}
```

Stan model for Weibull residence time model with cross validation

```
functions {
#include /functions/weibull_functions.stan
#include /functions/param_functions.stan
}

data {
  int<lower=1> N;                          // number of data points
  int<lower=1> N_test;
  vector[N] mT;                            // logged mass at time T
```

```
  vector[N_test] mT_test;
  vector[N] m0;                          // logged initial mass
  vector[N_test] m0_test;
  vector<lower=0>[N] time;               // time
  vector<lower=0>[N_test] time_test;
  int<lower=1> P_alpha;                  // num fixefs
  int<lower=1> P_beta;                   // num fixefs
  int<lower=1> J;                        // number of species
  matrix[J, P_alpha] X_alpha;            // design matrix for alpha effects
  matrix[1, P_alpha] X_alpha_test;       // design matrix for alpha effects
  matrix[J, P_beta] X_beta;              // design matrix for alpha effects
  matrix[1, P_beta] X_beta_test;
  int<lower=1, upper=J> sp[N];           // species id
}

parameters {
  vector[P_alpha] b_alpha;
  vector[P_beta] b_beta;
  real<lower=0> sigma_obs;               // observation sd
}

model {
  vector[J] alpha;
  vector[J] beta;
  vector[N] mu;

  // priors
  sigma_obs ~ normal(0, 2);
  b_alpha ~ normal(0, 2);
  b_beta ~ normal(0, 2);

  // likelihood
  alpha = param(b_alpha, X_alpha, P_alpha, J);
  beta = param(b_beta, X_beta, P_beta, J);
  mu = weibull(N, m0, time, beta, alpha, sp, sigma_obs);
  mT ~ normal(mu, sigma_obs);
}

generated quantities {

  real neg_loglik;
  vector[N_test] mT_pred;

  {
  real alpha_pred;
  real beta_pred;

  alpha_pred = param_pred(b_alpha, X_alpha_test, P_alpha);
  beta_pred = param_pred(b_beta, X_beta_test, P_beta);
  mT_pred = weibull_pred_rng(N_test, m0_test, time_test, beta_pred, alpha_pred, sigma
      _obs);
  neg_loglik = weibull_negloglik(mT_test, m0_test, time_test, beta_pred, alpha_pred,
      sigma_obs, N_test);
  }
}
```

Stan model for Weibull residence time model with random effects by species

```
functions {
#include /functions/weibull_functions.stan
#include /functions/param_functions.stan
}
```

```
5
6  data {
7    int<lower=1> N;                          // number of data points
8    vector[N] mT;                            // logged mass at time T
9    vector[N] m0;                            // logged initial mass
10   vector<lower=0>[N] time;                 // time
11   int<lower=1> P_alpha;                    // no fixefs
12   int<lower=1> P_beta;                     // no fixefs
13   int<lower=1> J;                          // number of species
14   matrix[J, P_alpha] X_alpha;              // design matrix for alpha effects
15   matrix[J, P_beta] X_beta;                // design matrix for alpha effects
16   int<lower=1, upper=J> sp[N];             // species id
17
18   int<lower=1> N_sim;                      // number of data points
19   vector[N_sim] m0_sim;
20   vector<lower=0>[N_sim] time_sim;         // time
21   int<lower=1, upper=J> sp_sim[N_sim];     // species id
22 }
23
24 parameters {
25   vector[P_alpha] b_alpha;
26   vector[P_beta] b_beta;
27   vector[J] a_sp_alpha;                    // species intercepts on alpha
28   vector[J] a_sp_beta;                     // species intercepts on beta
29   real<lower=0> sigma_obs;                 // observation sd
30   real<lower=0> sigma_sp_alpha;            // species sd
31   real<lower=0> sigma_sp_beta;
32 }
33
34 model {
35   vector[J] alpha;
36   vector[J] beta;
37   vector[N] mu;
38
39   // priors
40   a_sp_alpha ~ normal(0, sigma_sp_alpha);     // species random effects on alpha
41   a_sp_beta ~ normal(0, sigma_sp_beta);       // species random effects on beta
42   sigma_sp_alpha ~ normal(0, 2);
43   sigma_sp_beta ~ normal(0, 2);
44   sigma_obs ~ normal(0, 2);
45   b_alpha ~ normal(0, 2);
46   b_beta ~ normal(0, 2);
47
48   // likelihood
49   alpha = param_re(b_alpha, X_alpha, P_alpha, J, a_sp_alpha);
50   beta = param_re(b_beta, X_beta, P_beta, J, a_sp_beta);
51   mu = weibull(N, m0, time, beta, alpha, sp, sigma_obs);
52   mT ~ normal(mu, sigma_obs);
53 }
54
55 generated quantities {
56
57   vector[N_sim] mT_sim;
58   vector[J] alpha_fit;
59   vector[J] beta_fit;
60
61   alpha_fit = param_re(b_alpha, X_alpha, P_alpha, J, a_sp_alpha);
62   beta_fit = param_re(b_beta, X_beta, P_beta, J, a_sp_beta);
63   mT_sim = weibull_sim_rng(N_sim, m0_sim, time_sim, beta_fit, alpha_fit, sp_sim);
64
65 }
```

Extra stan code

```
/**
  * Create negative exponential fit for data
  *
  * @param N number of data
  * @param m0 initial mass of data
  * @param time time of data
  * @param k_fit fit k
  * @param sp species number
  * @param sigma_obs datapoint error
  * @return A vector of parameter estimates
  */
vector negexp_fit_rng(int N, vector m0, vector time, vector k_fit, int[] sp, real
    sigma_obs) {

  vector[N] mT_fit;

  for (i in 1:N) {
    mT_fit[i] = normal_rng(m0[i] - (k_fit[sp[i]] * time[i]), sigma_obs);
  }

  return mT_fit;
}

/**
  * Create negative exponential fit for simulated data
  *
  * @param N_sim number of simulated data
  * @param m0_sim simulated m0
  * @param time_sim simulated time data
  * @param k_fit fit k
  * @param sp_sim species number
  * @return A vector of parameter estimates
  */
vector negexp_sim_rng(int N_sim, vector m0_sim, vector time_sim, vector k_fit, int[]
    sp_sim) {

  vector[N_sim] mT_sim;

  for (i in 1:N_sim) {
    mT_sim[i] = m0_sim[i] - (k_fit[sp_sim[i]] * time_sim[i]);
  }

  return mT_sim;
}

/**
  * Create negative exponential predictions for test datapoints
  *
  * @param N_test number of test data
  * @param m0_test initial mass of test data
  * @param time_test time of test data
  * @param k_pred predicted k
  * @param sigma_obs datapoint error
  * @return A vector of parameter estimates
  */
vector negexp_pred_rng(int N_test, vector m0_test, vector time_test, real k_pred,
    real sigma_obs) {

  vector[N_test] mT_pred;

  for (i in 1:N_test) {
    mT_pred[i] = normal_rng(m0_test[i] - (k_pred * time_test[i]), sigma_obs);
  }

  return mT_pred;
}

```

```
65 /**
66   * Calculate negative logliklihood for negative exponential
67   *
68   * @param mT_test true mass at time T of test data
69   * @param m0_test initial mass of test data
70   * @param time_test time of test data
71   * @param k_pred predicted k
72   * @param sigma_obs datapoint error
73   * @param N_test number of test data
74   * @return A vector of parameter estimates
75   */
76 real negexp_negloglik(vector mT_test, vector m0_test, vector time_test, real k_pred,
       real sigma_obs, int N_test) {
77
78   vector[N_test] loglik;
79   real neg_loglik;
80
81   for (i in 1:N_test) {
82     loglik[i] = normal_lpdf(mT_test[i] | m0_test[i] - (k_pred * time_test[i]), sigma_
         obs);
83   }
84
85   neg_loglik = -1 * sum(loglik);
86   return neg_loglik;
87 }
88
89 /**
90   * Create weibull model for data
91   *
92   * @param N number of test data
93   * @param m0 initial mass of test data
94   * @param time time of test data
95   * @param beta predicted beta
96   * @param sp list of species numbers
97   * @param alpha predicted alpha
98   * @param sigma_obs datapoint error
99   * @return mu
100  */
101 vector weibull(int N, vector m0, vector time, vector beta, vector alpha, int[] sp,
       real sigma_obs) {
102
103   vector[N] mu;
104
105   for (i in 1:N) {
106     mu[i] = m0[i] - (time[i] / beta[sp[i]])^alpha[sp[i]];
107   }
108
109   return mu;
110 }
111
112 /**
113   * Create weibull fit for data
114   *
115   * @param N number of data
116   * @param m0 initial mass of data
117   * @param time time of data
118   * @param beta_fit fit beta
119   * @param alpha_fit fit alpha
120   * @param sp species number
121   * @param sigma_obs datapoint error
122   * @return A vector of parameter estimates
123   */
124 vector weibull_fit_rng(int N, vector m0, vector time, vector beta_fit, vector alpha_
       fit, int[] sp, real sigma_obs) {
125
126   vector[N] mT_fit;
127
```

```
128   for (i in 1:N) {
129     mT_fit[i] = normal_rng(m0[i] - (time[i] / beta_fit[sp[i]])^alpha_fit[sp[i]],
          sigma_obs);
130   }
131
132   return mT_fit;
133 }
134
135 /**
136   * Create weibull predictions for simulated data
137   *
138   * @param N_sim number of simulated data
139   * @param m0_sim simulated m0
140   * @param time_sim simulated time data
141   * @param beta_fit fit beta
142   * @param alpha_fit fit alpha
143   * @param sp_sim species number in simulated dataset
144   * @return A vector of parameter estimates
145   */
146 vector weibull_sim_rng(int N_sim, vector m0_sim, vector time_sim, vector beta_fit,
      vector alpha_fit, int[] sp_sim) {
147
148   vector[N_sim] mT_sim;
149
150   for (i in 1:N_sim) {
151     mT_sim[i] = m0_sim[i] - (time_sim[i] / beta_fit[sp_sim[i]])^alpha_fit[sp_sim[i]];
152   }
153
154   return mT_sim;
155 }
156
157 /**
158   * Create weibull predictions for test datapoints
159   *
160   * @param N_test number of test data
161   * @param m0_test initial mass of test data
162   * @param time_test time of test data
163   * @param beta_pred predicted beta
164   * @param alpha_pred predicted alpha
165   * @param sigma_obs datapoint error
166   * @return A vector of parameter estimates
167   */
168 vector weibull_pred_rng(int N_test, vector m0_test, vector time_test, real beta_pred,
      real alpha_pred, real sigma_obs) {
169
170   vector[N_test] mT_pred;
171
172   for (i in 1:N_test) {
173     mT_pred[i] = normal_rng(m0_test[i] - (time_test[i] / beta_pred)^alpha_pred, sigma
          _obs);
174   }
175
176   return mT_pred;
177 }
178
179 /**
180   * Calculate negative loglikelihood
181   *
182   * @param mT_test true mass at time T of test data
183   * @param m0_test initial mass of test data
184   * @param time_test time of test data
185   * @param beta_pred predicted beta
186   * @param alpha_pred predicted alpha
187   * @param sigma_obs datapoint error
188   * @param N_test number of test data
189   * @return A vector of parameter estimates
190   */
```

```
real weibull_negloglik(vector mT_test, vector m0_test, vector time_test, real beta_
    pred, real alpha_pred, real sigma_obs, int N_test) {

  vector[N_test] loglik;
  real neg_loglik;

  for (i in 1:N_test) {
    loglik[i] = normal_lpdf(mT_test[i] | m0_test[i] - (time_test[i] / beta_pred)^
        alpha_pred, sigma_obs);
  }

  neg_loglik = -1 * sum(loglik);
  return neg_loglik;
}

/**
  * Create weibull predictions for simulated data - sim traits, single time
  *
  * @param N_sim number of simulated data
  * @param m0_sim simulated m0
  * @param time_sim simulated time data
  * @param beta_fit fit beta
  * @param alpha_fit fit alpha
  * @param sp_sim species number in simulated dataset
  * @return A vector of parameter estimates
  */
vector weibull_best_sim_rng(int N_sim, real m0_sim, real time_sim, vector beta_fit,
    vector alpha_fit, int[] sp_sim) {

  vector[N_sim] mT_sim;

  for (i in 1:N_sim) {
    mT_sim[i] = m0_sim - (time_sim / beta_fit[sp_sim[i]])^alpha_fit[sp_sim[i]];
  }

  return mT_sim;
}

/**
  * Create weibull predictions for simulated data - sim traits, across time
  *
  * @param N_sim number of simulated data
  * @param m0_sim simulated m0
  * @param time_sim simulated time data
  * @param beta_fit fit beta
  * @param alpha_fit fit alpha
  * @param sp_sim species number in simulated dataset
  * @return A vector of parameter estimates
  */
vector weibull_sim_traits_rng(int N_sim, real m0_sim, vector time_sim, vector beta_
    fit, vector alpha_fit, int[] sp_sim) {

  vector[N_sim] mT_sim;

  for (i in 1:N_sim) {
    mT_sim[i] = m0_sim - (time_sim[i] / beta_fit[sp_sim[i]])^alpha_fit[sp_sim[i]];
  }

  return mT_sim;
}

/**
  * Create likelihoods for parameter with random effects
  *
  * @param b effects vector of parameters
  * @param X model matrix of effect values
  * @param P number of effects
```

```
254   * @param J number of species
255   * @param a random effect
256   * @return A vector of parameter estimates
257   */
258   vector param_re(vector b, matrix X, int P, int J, vector a) {
259
260     vector[J] param_ln;
261     vector[J] param_vector;
262
263     for (j in 1:J) {
264
265       param_ln[j] = a[j];
266
267       for (p in 1:P) {
268         param_ln[j] = param_ln[j] + b[p] * X[j, p];
269       }
270
271       param_vector[j] = exp(param_ln[j]);
272     }
273
274     return param_vector;
275   }
276
277 /**
278   * Create likelihoods for parameter without random effects
279   *
280   * @param b effects vector of parameters
281   * @param X model matrix of effect values
282   * @param P number of effects
283   * @param J number of species
284   * @return A vector of parameter estimates
285   */
286   vector param(vector b, matrix X, int P, int J) {
287
288     vector[J] param_ln;
289     vector[J] param_vector;
290
291     for (j in 1:J) {
292
293       param_ln[j] = 0;
294
295       for (p in 1:P) {
296         param_ln[j] = param_ln[j] + b[p] * X[j, p];
297       }
298
299       param_vector[j] = exp(param_ln[j]);
300     }
301
302     return param_vector;
303   }
304
305 /**
306   * Create prediction for parameter
307   *
308   * @param b effects vector of parameters
309   * @param X model matrix of effect values
310   * @param P number of effects
311   * @return A vector of parameter estimates
312   */
313   real param_pred(vector b, matrix X, int P) {
314
315     real param_ln;
316     real param_value;
317
318     param_ln = 0;
319
320     for (p in 1:P) {
```

```
321       param_ln = param_ln + b[p] * X[1, p];
322     }
323
324     param_value = exp(param_ln);
325     return param_value;
326   }
```

Appendix E: Published works

E.1 Carbon stocks, sequestration, and emission of wetlands in south eastern Australia

Carnell PE, **Windecker SM**, Brenker M, Baldock J, Maque P, Brunt K, & Macreadie PI. 2018. Carbon stocks, sequestration, and emission of wetlands in south eastern Australia. Global Change Biol. 2018;00:1–12.

E.2 Australian Vegetation

Catford JA, Roberts J, Capon SJ, Froend RH, **Windecker SM**, & Douglas MM. 2017. Wetland vegetation of inland Australia. *Australian Vegetation* (ed. D.A. Keith), 3rd edition. Cambridge University Press, p. 490-515.